PETROLEUM RESEARCH JOURNAL

TECHNICAL PAPERS

ENGINEERING

The thermodynamics of enhanced oil recovery processes, ... *D.B. Robinson and H. Kalra.* 3

Advanced reservoir management aspects of enhanced oil recovery, ... *G.L. Chierici.* 13

Rheological properties of Sarir crude oil, ... *M. Elgarni, H.H. Beck, S.M. Debbah and N.A. Faruqi.* 21

EXPLORATION

Acoustic properties as function of depth in the Gulf of Suez, Egypt, ... *Adel A.A. Othman and G.H. Hamada.* 27

Petrography and diagenesis of the Lidam Formation (Carbonate Units): From selected wells in Sirt Basin, Libya, ... *M. El Bakai.* 35

Diagenetic history of Early-Middle Eocene Jdeir Formation, Farwah Group, Northwestern Libyan offshore, ... *I.Y. Mriheel.* 44

CHEMISTRY

The comparative catalytic activities of tungstate and molybdate ions in the epoxidation of maleic anhydride by hydrogen peroxide .... *I. Ahmad, M.Degam and A. Labib.* 53

SHORT NOTES

Sensitivity of pipe-line steels to hydrogen induced cracking, ... *A. Mazur, T. Militti and K. Abosowa.* 57

The atmospheric corrosion of austenitic stainless steel pneumatic tubing system in an offshore environment, ... *M. Mehta and K. Abosowa.* 63

DISCUSSION

On: "Hydrocarbon habitat in Sirt Basin" .... and reply by author. 68

ABSTRACTS

Of papers presented at the 1st Technical Symposium of EOR in Libya, Tripoli, May, 1 & 2, 1990. 73

VOLUME 3-1991

Petroleum Research Centre
P.O. Box 6431 Tripoli
Great Socialist People's Libyan Arab Jamahiriya

PRJ, Vol. 3 (January 1991); P. 3–12, 14 FIGS, 5 TABLES.

THE THERMODYNAMICS OF ENHANCED OIL RECOVERY PROCESSES

D.B. Robinson* and H. Kalra*

الميكانيكية الحرارية في عمليات الإسترداد الإضافي

روبنسن د. ب ، كالرا هـ .

تراجع هذه الورقة العلمية الطور السلوكي لخلائط مذيبات الزيت وعلاقتها بعمليات الإسترداد الإضافي . وتقدم الورقة أيضاً نموذجاً لحجب الطور لخليط الهيدروكربونات الشطرية وخلائط الزيت مع المذيبات الهيدروكربونية وغاز ثاني أكسيد الكربون .

المعلومات المدرجة في هذه الورقة جمعت من تجارب دراسات الإسترداد الإضافي لموائع مكمن جنوب شرق حقل الناصر مع دراسات مذيب الغاز الطبيعي المسيل/والغاز الجاف وثاني أكسيد الكربون . اختبارات الإنتفاخ ، قياسات إتزان الطور، وإختبارات الأنابيب الدقيقة أجريت باستخدام كلا من المذيبين .

وخلاصتاً وجد أن كلا من الحد الأدنى لمحتوى الإمتزاجية للغاز الطبيعي المسيل في المذيب والحد الأدنى لضغط الإمتزاجية عند إستعمال غاز ثاني أكسيد الكربون تقع في نفس الظروف التي عندها نتائج التوقعات النظرية في الحقيقة تدل على حدوث إمتزاج .

وبالرغم من هذا ، كل المؤشرات تقترح حدوث إزاحات بكفاءة عالية . نتائج الملاحظات المرئية (البصرية) والحسابات الممثلة ببيانات للمركب الثلاثي تدل على أن إزاحة الهيدروكربونات حدث كنتيجة لنوع من الميكانيكية الموحدة للبخر المكثف .

تفصيل طبيعة ميكانيكية الإزاحة في وجود غاز ثاني أكسيد الكربون تبدو أنها معتمدة على الكمية النسبية للمركبات الخفيفة مقارنة بالمركبات الثقيلة للزيت الأصلي .

ABSTRACT

The phase behavior of solvent-oil mixtures as it relates to enhanced oil recovery operations is reviewed. Typical phase envelopes for a model binary hydrocarbon mixture and for a model binary hydrocarbon mixture and for mixtures of an oil with a hydrocarbon solvent and with CO_2 are presented.

Experimental data were obtained for an enhanced oil recovery study of the South East Nasser reservoir fluid with a NGL/Dry Gas solvent and with CO_2. Swelling tests, phase equilibrium measurements and slim tube runs were conducted with both solvents.

It is concluded that the minimum miscibility content of NGL in the solvent and the minimum miscibility pressure when using CO_2 both occur at conditions where theoretical predictions would suggest that miscibility has in fact not been achieved. Nevertheless, all key indicators would suggest very efficient displacements supported also with high displacement efficiencies.

A combination of visual observations and calculations represented on a pseudo ternary component diagram suggest that the hydrocarbon displacements correspond to a combined condensing-vaporising type mechanism.

The detailed nature of the displacement mechanism in the presence of carbon dioxide is shown to depend on the relative amount of the lighter compared to the heavier components in the parent oil.

*D.B. Robinson & Associates Ltd., Edmonton, Alberta, Canada.

INTRODUCTION

The successful evaluation of the potential for enhanced oil recovery from a conventional reservoir relies on the development of appropriate tools for

predicting future reservoir performance. The development of these tools requires specific information relating to the reservoir rock characteristics, the reservoir fluid and injection fluid properties and the interaction between these variables. The interaction between the injection solvent and the reservoir fluid is usually quantified through experimental laboratory measurements.

The development of a suitable program of study and the interpretation of the results requires that certain assumptions be made with respect to the nature of the solvent-oil interactions and of the subsequent oil displacement. Two of the more widely assumed mechanisms are the condensing drive and the vaporizing drive. These have been discussed in detail by several authors [1, 2, 3, 4, 5, 6, 7, 8, 9].

Recently, considerable discussion has also been given to combined condensing-vaporizing [1, 10, 11] drive mechanisms.

Traditionally, enriched hydrocarbon solvent injection fluids have been thought to result in a condensing drive mechanism and carbon dioxide has been considered to result in a vaporizing drive mechanism. The essential distinguishing feature of these different modes of contact is the behavior of the intermediate (C2–C5) fraction at the point of contact between the solvent and the oil. In a vaporizing drive, there is a net gain in intermediate fraction components in the vapor phase relative to the solvent and in the condensing drive, there is a net gain of intermediate components in the liquid phase relative to the oil. In either case, the equilibrium vapor phase is assumed to move preferentially through the formation. Precise definition of the contacting mechanism has remained elusive because of the lack of experimental evidence on the in-situ nature of the transition zone between the solvent and the oil within the reservoir. We believe the results we are reporting in this paper shed some light on the problem.

The basis for our discussion rests primarily on an extensive enhanced oil recovery study recently carried out on the South East Nasser reservoir oil using both enriched hydrocarbons and carbon dioxide as solvents.

DISPLACEMENT WITH HYDROCARBON SOLVENTS

Fluids

The compositions of the enriched hydrocarbon solvent and the reservoir oil are given in Table 1. However, before examining the swelling and slim tube tests conducted with these fluids, it may be instructive to examine the phase behavior of solvent-oil mixtures.

Table 1. Injection Solvent and Oil Composition

Component	Concentration, Mole% Solvent	Reservoir Oil
CO_2	2.17	1.41
H2S	0.45	1.16
N2	1.10	0.47
C1	53.58	18.99
C2	11.92	9.04
C3	13.07	5.08
IC4	5.54	1.76
NC4	11.26	2.34
IC5	0.45	2.35
NC5	0.46	1.34
C6		4.83
C7–9		14.46
C10–14		15.97
C15–20		9.56
C21–29		6.36
C30+		4.88

Thermodynamic Behavior

For illustrative purposes we could consider a very simple binary system consisting of ethane as the solvent and n-heptane as the oil.

Thermodinamically, the behavior of this system can be represented in three dimensional space in pressure-temperature-composition coordinates. However, it can also be represented in two dimensional space on pressure-temperature coordinates if all composition variables are projected onto the plane. This has been done for selected mixtures of ethane and n-heptane in Fig. 1. Figure 1 shows how the pure solvent (ethane) and the pure oil (n-heptane) are represented by their vapor pressure curves, whereas any mixtures of the solvent and oil are represented by a phase envelope consisting of a bubble point locus, a critical point and a dew point locus.

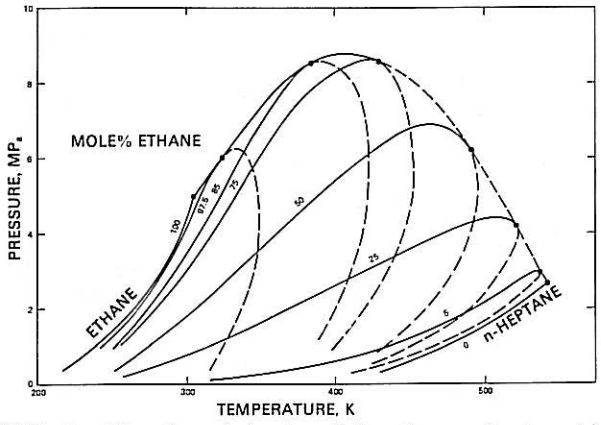


FIG. 1. The phase behavior of the ethane-n-heptane binary system.

A swelling curve for ethane in n-heptane can be envisaged by looking at the points of intersection of

an isothermal plane, for example at 350K, with the bubble point locus or the retrograde dew point locus for mixtures successively more rich in ethane. Such a swelling curve is shown in Fig. 2. It will also be noted that there will be one mixture, i.e. one solvent-oil composition that will have its critical temperature at the temperature in question.

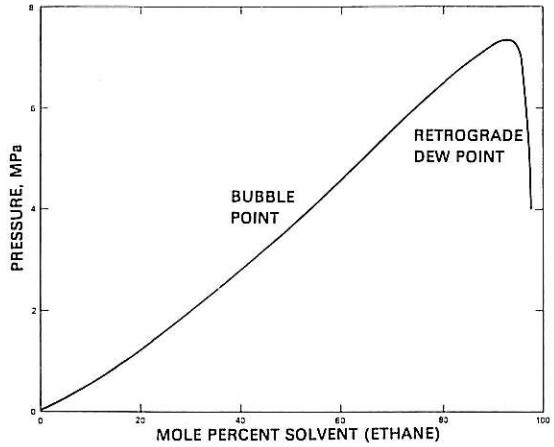


FIG. 2. A simulated swelling curve for a solvent (ethane) in an oil (n-heptane) at 350K.

The thermodynamics of the solvent-SE Nasser oil system can also be viewed in the same way in two-dimensional space. Here the solvent and the oil are multicomponent mixtures each having its own phase envelope and critical point rather than a vapor pressure curve with its critical point. These phase envelopes are shown in Fig. 3 together with phase envelopes for representative mixtures of the solvent and oil. Again, the points of intersection of an isothermal plane at 350K with the bubble point or retrograde dew point loci would represent a typical swelling curve for this system on pressure-solvent concentration coordinates. Such a curve for this system is shown later.

It may also be seen from Fig. 3 that there will be one mixture of solvent and oil which will have its critical point at 350K. By interpolation, this would be a mixture containing about 78 mole% solvent and 22 mole% oil.

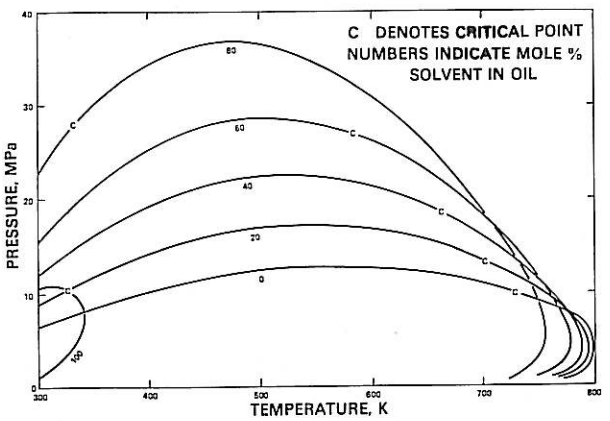


FIG. 3. The influence of hydrocarbon solvent content on the phase behavior of SE Nasser reservoir fluid.

Swelling Test

A conventional swelling test was conducted using the solvent and SE Nasser oil defined in Table 1 at a temperature of 350K. The solvent concentrations examined were 15.0, 30.0, 45.6, 62.0 and 8.0 mole%. One of the primary objectives in conducting the swelling test is to obtain data which can be used to characterize the fluids. Thus any phase behavior package such as our EQUI-PHASE [12] phase behavior package can be tuned so that it can be used to predict the behavior of the solvent-oil system. The reason for including the one very high solvent concentration was to make sure some data would be available in the retrograde region. This was considered important because somewhere during the displacement process the solvent concentration was expected to be in the range where retrograde fluids would exist. This condition would normally be encountered in the trailing end of the transition zone.

In addition to the saturation pressure being determined at each solvent concentration, the 62 mole% mixture was analyzed at the saturation pressure of 20.86 MPa and then equilibrated at 8.72 MPa. The resulting equilibrium vapor and liquid phases were then analyzed. This was also done in order to provide some vapor-liquid equilibrium data for the fluid characterization process. The results of the saturation pressure measurements and the phase equilbrium measurements are given in Table 2 and 3. The experimental and calculated saturation pressure values at 350K are compared graphically in Fig. 4.

Table 2. Saturation Pressures for Solvent–Nasser Oil Mixtures at 350K

Solvent Conc.	Saturation Pressure, MPa Experimental	Calculated
0	8.13	8.32
15	10.58	10.91
30	13.78	13.82
45.6	17.53	17.30
62	20.86	21.66
86	34.82*	33.79

*Estimated.

The composition data taken on the 62 mole% mixture at 20.86 and 8.72 MPa were used to perform an overall molar balance at the flashed condition. A graphical representation of the overall and component balances is given in Fig. 5. Representations such as this are extremely sensitive to any inconsistencies in the data. The degree of consis-

Table 3. Comparison of Calculated and Experimental Data for the Vapor and Liquid Phase Compositions after flashing the 62% Mixture at 8.72 MPa and 350K

		Concentration, Mole%			
		Experimental		Calculated	
Component	Feed	Vapor	Liquid	Vapor	Liquid
N2	0.892	1.658	0.228	1.749	0.242
CO_2	1.867	2.692	1.284	2.644	1.278
H2S	0.654	0.584	0.617	0.649	0.658
C1	40.488	68.705	20.370	67.930	19.670
C2	10.932	12.223	9.923	12.510	9.731
C3	9.982	7.482	11.502	7.653	11.750
IC4	3.977	2.150	5.197	2.209	5.318
NC4	7.340	3.368	10.051	3.396	10.330
IC5	1.185	0.370	1.808	0.374	1.801
NC5	0.762	0.210	1.200	0.209	1.182
C6	1.798	0.257	3.028	0.283	2.948
C7–C9	5.539	0.257	9.544	0.339	9.484
C10–C14	6.376	0.044	10.979	0.049	11.180
C15–C19	3.414	—	5.899	0.003	6.002
C20–C29	2.929	—	5.135	—	5.151
C30+	1.866	—	3.234	—	3.282

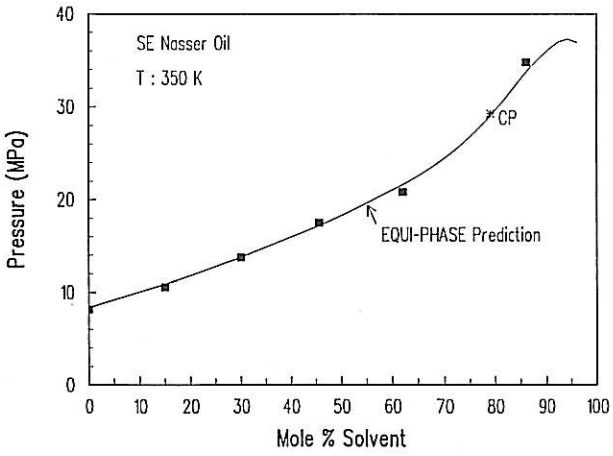


FIG. 4. The influence of solvent concentration on saturation pressure for SE Nasser oil-solvent mixtures.

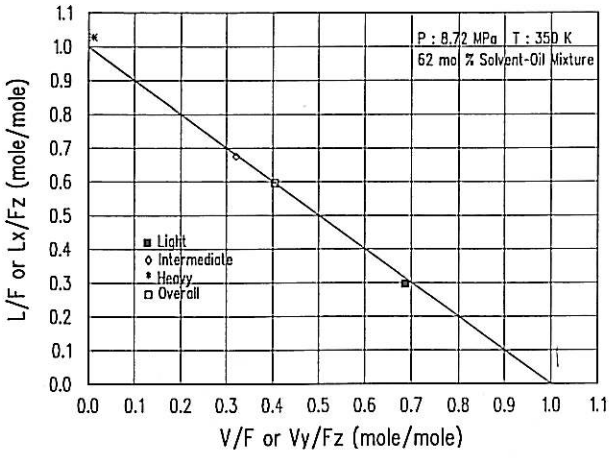


FIG. 5. Overall component molar balance.

tency shown in Fig. 5 indicates an excellent mass balance closure.

The observations made on the 86 mole% solvent mixture bear further discussion. This mixture appeared in the cell as a bright yellow upper phase and a second lower phase that appeared to be a thick black liquid. An increase in pressure on this system showed that the liquid volume decreased, thereby confirming that the system was in the retrograde region. However, further increases in pressure caused the black lower phase to become more sticky and thick but it never did disappear. Subsequent reductions in pressure caused the renewed formation of yellow liquid which washed the sticky material off the cell walls and re-created the black liquid referred to above.

It was concluded from these observations that the high solvent concentration in the oil had caused asphalthene precipitation at the conditions of the experiment. The upper retrograde dew point was estimated to be 34.82 MPa by graphically interpreting the data on liquid volume vs pressure after subtracting the volume of the asphaltic materials from the total condensed phase volume.

Slim Tube Displacements

During the course of the overall study on the Nasser reservoir fluid a series of slim tube displacements were carried out in order to determine the minimum natural gas liquid content of the solvent mixture required in order to achieve a miscible displacement. Some of the observations and calculations made using a solvent having the composition given in Table 1 (20 mole% NGL; 80 mole% dry gas) are reported here.

The slim tube apparatus consisted of a 6.4 mm O.D. by 12.15 m long stainless steel tube packed with 75 to 106 μm Ottawa Sand to an overall porosity of 35.1%. The total system volume inclusive of all lines and fittings up to the back pressure regulator was 68.88 cm^3. The absolute permeability was 3.4 Darcys. A high pressure capillary sight glass located downstream of the slim tube but ahead of the back pressure regulator provided an opportunity to make visual observations of the character of the effluent fluid stream. The flashed oil was collected in a calibrated glass receiver and the gas was measured in a precision gasometer. The entire displacement system exclusive of the collection devices was housed in a thermostated forced circulation air oven where the temperature was controlled at 350K. The run was carried out at a pressure of 15.94 MPa. The duration of the run was 14hr. by which time 1.42 pore volumes of solvent had been injected. After the run had been concluded, the residual oil in place was washed out using a toluene flood and then recovered by rotary evaporation.

In some ways, the sight glass observations made during this run suggested that it was a miscible displacement. However some subtle differences existed and these need to be discussed. Up to about 1.07 PV displacement, only parent oil production was indicated. At this time the first color change was observed. However, produced gas composition data indicated that a methane bank was present. The first indication of this bank occured at 0.79 PV, methane concentration peaked at about 0.96 PV and declined to a minimum which was below the solution gas and solvent composition by 1.10 PV.

Visual observations did not indicate a second phase during this period, suggesting that two phases must have been created somewhere in the transition zone earlier than the 1.07 PV displacement. The gas was undoubtedly rich in methane but of low total volume such that it redissolved in the oil as it moved ahead prior to reaching the sight glass. From this, one could conclude that the displacement is not first contact miscible but may be multiple contact miscible.

The first indications of two-phase production were observed at 1.111 PV when a few short bubbles followed by longer bubbles were produced. At 1.113 PV, two-phase flow with a clear liquid was observed. Shortly thereafter a single clear phase was evident. Thus, two-phase flow occured at the trailing edge of the transition zone close to the solvent interface. This phenomenon only lasted about one minute (0.002 PV). This suggests the possibility that an open phase envelope (pseudo ternary coordinates) exists towards the trailing edge of the transition zone and that the fluids in that period are probably dew point fluids. From the overall viewpoint, it appears as though the displacement started as a condensing drive mechanism but changed to a vaporizing drive mechanism towards the end of the displacement. These combination drives are classically immiscible but can be very efficient, often comparable to first contact or multiple contact miscible displacements.

On the basis of the fluid volumes collected in the separator, the oil volume was 103.0% of the original oil in place. However, when the residual recovery of oil in the tube based on the toluene flood is considered, the recovery reduced to 97.5% of original oil in place. The difference results from the expansion of the liquids caused by the extraction of hydrocarbons from the solvent by the oil. A graphical record of the slim tube recovery is presented in Fig. 6. The curve of cumulative fluid recovery represents the recovery based on oil volume collected in the separator. The calculated cumulative fluid recovery represents the separator volume less the solvent residual as shown at the bottom of the figure.

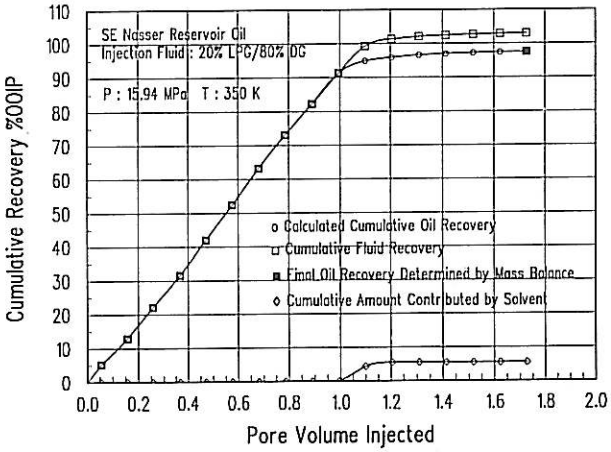


FIG. 6. Cumulative fluid recovery for slim tube run:4

It may be seen that this run, although evidently immiscible, was nevertheless highly efficient. Confirmation of the combined condensing/vaporizing drive mechanism occuring in this displacement will be seen in the pseudo ternary representation shown in Fig. 7. The EQUI-PHASE program with parameters developed from the swelling tests was used with an objective to predict the minimum multiple contact solvent concentration at the operating temperature and pressure of the SE Nasser reservoir.

The predictions suggested an unrealistically high natural gas liquid requirement. On plotting the calculated tie-line data of the contact sequence, it was found that the phase envelopes were open and divergent. Thus it was not possible to calculate the minimum multiple contact solvent concentration. These graphical representations indicate an immiscible drive form a fundamental standpoint. However, it is well known that these drives start as condensing

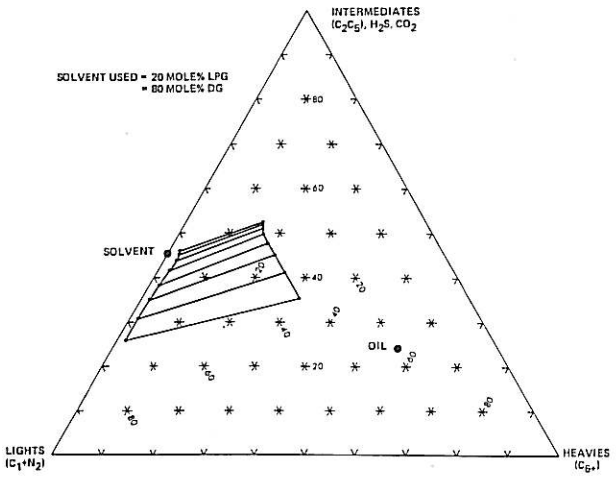


FIG. 7. Pseudo-Ternary plot of reverse contacts for the hydrocarbon solvent-SE Nasser oil system at 15.57 MPa and 350K.

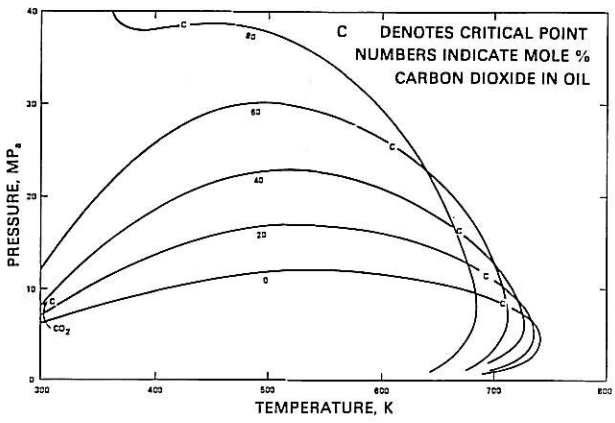


FIG. 8. The influence of carbon dioxide content on the phase behavior of SE Nasser reservoir fluid.

drives and convert to vaporizing drives providing a very efficient displacement, one that is often competitive with either first or multiple contact miscible displacements. Our experience with hydrocarbon solvent-oil displacements covering a wide range of reservoir fluids is that when the operating temperature is above about 335K, hydrocarbon solvent drives normally exhibit this behavior.

DISPLACEMENT WITH CARBON DIOXIDE

The second major portion of the overall enhanced oil recovery study of the SE Nasser reservoir involved the use of carbon dioxide as a displacing fluid. A systematic series of swelling tests were carried out for the purpose of characterizing carbon dioxide-reservoir oil mixtures for the EQUI-PHASE program. This was followed by a series of four slim tube runs in order to determine the minimum pressure required to achieve miscibility.

Thermodynamic Behavior

The thermodynamic behavior of carbon dioxide-reservoir fluid mixtures can be viewed in exactly the same way as the ethane-n-heptane and solvent-oil mixtures discussed earlier. In the case of the carbon dioxide mixtures, the solvent is a pure component and the oil is a multicomponent fluid having a composition similar to that given in Table 1.

Calculated phase envelopes for representative mixtures of carbon dioxide with the oil are shown graphically in Fig. 8. It will be noted that the phase envelope for the 80% mixture goes to very high pressures in a liquid-dense fluid region. Also, at this concentration a three-phase region consisting of a CO_2-rich liquid, a hydrocarbon-rich liquid and a gas exists in a pressure range from about 4 to 8 MPa at temperatures in the 250 to 325K range. This is not shown on Fig. 8 because of the congestion of lines on the graph.

Swelling Tests

Swelling tests using mixtures of carbon dioxide with SE Nasser reservoir fluid were carried out in a manner similar to those described earlier for the hydrocarbon solvent. Concentration of carbon dioxide of 15.0, 30.0, 45.0 and 60.0 mole% were used with the oil at a temperature of 350K. After the saturation pressure of the final mixture had been obtained at a pressure of 19.44 MPa, a sample of the single phase fluid was analyzed. The mixture was then equilibrated at a pressure of 8.13 MPa and both phases were analyzed. The data from these measurements were used to tune the parameters in the EQUI-PHASE program for use with mixtures of carbon dioxide with SE Nasser fluid. The results of the saturation and phase equilibrium measurements are given in Tables 4 and 5. The experimental and calculated saturation pressures are compared graphically in Fig. 9.

Table 4. Saturation Pressures for Carbon–Dioxide–Nasser Oil Mixtures at 350K

Solvent Conc.	Saturation Pressure, MPa Experimental	Calculated
0	8.13	8.14
15	10.16	10.00
30	12.51	12..22
45	15.20	15.13
60	19.44	20.15

Table 5. Comparison of Calculated and Experimental Data for the Vapor and Liquid Phase Compositions after Flashing the 60% Mixture at 8.13 MPa and 170°F

	Concentration, Mole%				
		Experimental		Calculated	
Component	Feed	Vapor	Liquid	Vapor	Liquid
N2	0.21	0.33	0.08	0.36	0.05
CO_2	59.37	79.31	36.85	79.33	37.30
H2S	0.49	0.46	0.50	0.49	0.48
C1	7.76	11.74	3.20	11.77	3.33
C2	3.70	4.13	3.20	4.13	3.22
C3	2.15	1.73	2.58	1.70	2.64
IC4	0.73	0.44	1.03	0.43	1.07
NC4	0.96	0.49	1.45	0.48	1.50
IC5	0.96	0.33	1.63	0.33	1.65
NC5	0.54	0.17	0.95	0.16	0.95
C6	1.96	0.33	3.78	0.34	3.74
C7–C9	5.97	0.44	12.21	0.41	12.12
C10–C14	6.73	0.09	14.30	0.06	14.11
C15–C19	3.61	0.01	7.71	0.01	7.61
C20–C29	3.16	—	6.62	—	6.66
C30+	1.70	—	3.91	—	3.57

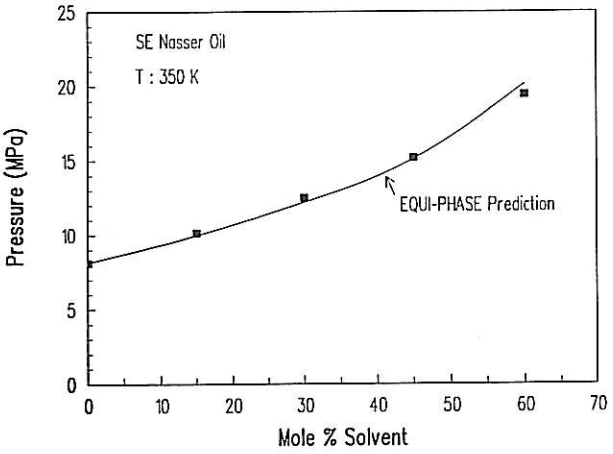


FIG. 9. The influence of CO_2 concentration on saturation pressure for SE Nasser-CO_2 mixtures.

A mass balance closure analysis of the equilibrium data taken on the 60.0 mole% mixture at 8.13 MPa was carried out as in the case of the hydrocarbon solvent. The results were similar to the hydrocarbon case.

Slim Tube Experiments

In order to determine the minimum miscibility pressure for carbon dioxide with the SE Nasser fluid, a series of slim tube displacements were carried out at 10.44, 13.89, 17.33 and 20.78 MPa.

Observations made during the 17.33 MPa run may be used as an example of the behavior of the fluids during the run. The black color of the original oil appeared in the sight glass for the first 0.99 PV of solvent injected. The color then changed to dark brown and at 1.02 PV, very small bubbles were observed near the top of the sight glass. The color had changed to yellow after 1.04 PV and a gas/liquid interface extended along the full length of the capillary. Immediately thereafter, the vapor phase disappeared, leaving only a very light yellow liquid being produced. No methane bank was detected from the off-gas analysis during the entire displacement. The overall recovery based on separator volumes was 102.7% of original oil in place while the recovery based on toluene residual determination was 97.2%. On the basis of the short transition zone, the absence of the methane bank and the level of recovery, the run was judged to be miscible.

A graphical representation of the recovery profile is shown in Fig. 10. As in the case of the hydrocarbon solvent displacement shown in Fig. 6, both the recovery based on separator volumes and on volumes corrected by the toluene extracted residuals are shown.

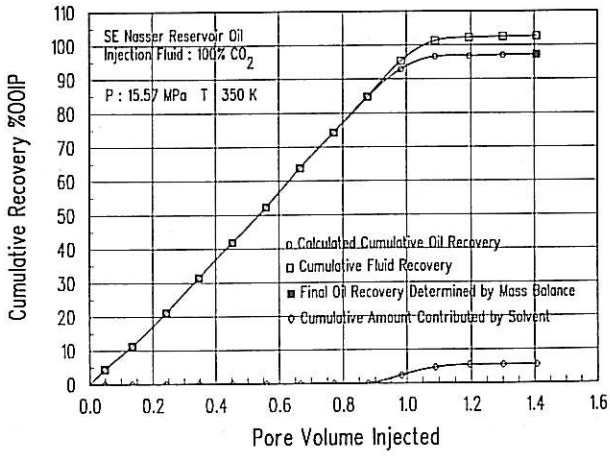


FIG. 10. Cumulative fluid recovery for slim tube run:3.

On the basis of the recoveries obtained at all four pressures, the minimum miscibility pressure for carbon dioxide with SE Nasser oil was found to be 15.57 MPa at 350K. This was obtained by interpolation of the recovery data for the four runs shown in Fig. 11. The runs at 17.33 and 20.78 MPa were judged to be miscible and those at 10.44 and 13.89 were judged to be immiscible.

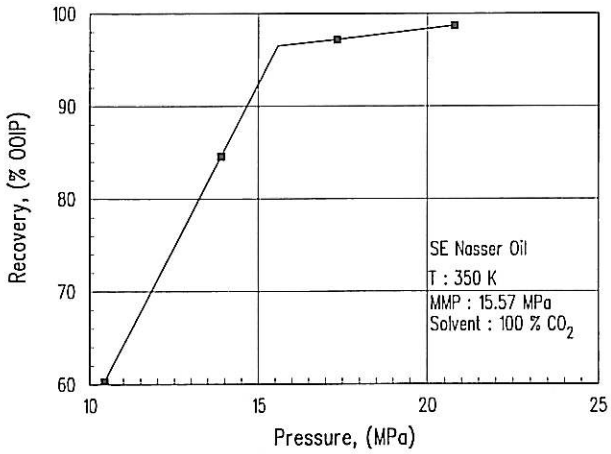


FIG. 11. Recovery vs pressure.

Predictions and Discussions

The parameters required for the EQUI-PHASE Enhanced Oil Recovery package were evaluated from the swelling test and vapor liquid equilibrium data. Since it has been widely assumed [1, 9, 13, 14, 15] that carbon dioxide displacements are vaporizing drives, this methodology was used for initiating the minimum miscibility pressure prediction. The predictions indicated an open divergent envelope at both 20.78 and 15.57 MPa on a pseudo ternary diagram. The results for the 15.57 MPa case are shown in Fig. 12. We are not aware that this kind of divergent behavior has ever been observed before for a carbon dioxide system.

The behavior of the oil in the presence of carbon dioxide bears further discussion. Normally, in carbon dioxide slim tube displacements the separator recovery is less than the toluene extracted recovery of the original oil in place. This happens because during a vaporizing drive, components which were originally part of the oil are taken away with the gas thereby causing a shrinkage of the oil. However, in the work reported here, three of the runs had separator recoveries which were higher than the toluene based recoveries. These were the runs at the three higher pressures.

It is well known that carbon dioxide can extract higher carbon numbered compounds from oils, particularly in the C7 to C20 range [9, 13, 15]. It is also known that when carbon dioxide dissolves in oil it causes significant swelling. This is particularly true

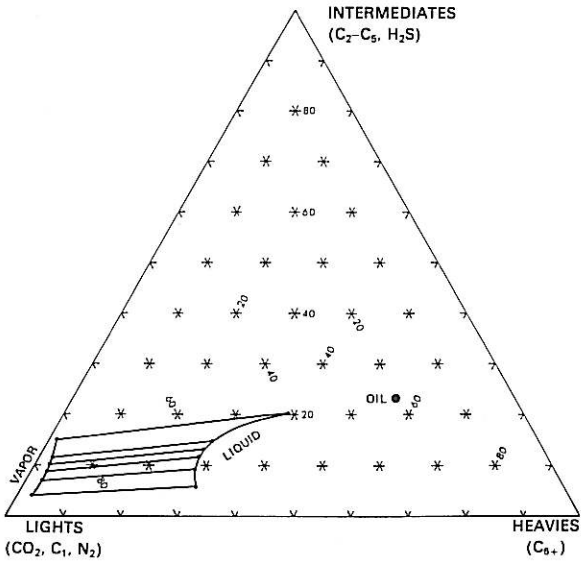


FIG. 12. Pseudo-Ternary plot of forward contacts for the CO_2-SE Nasser oil system at 15.94 MPa and 350K.

for heavier oils and bitumens which have a significant content in the C15–C30+ range. It is possible that a swelling and an extractive type mechanism are acting simultaneously and interactively in such a way that the relative magnitude of each will determine whether the separator based recovery will be greater or less than the toluene based recovery. The information gained from these and related experiments with carbon dioxide suggest that the C6+ distribution in the oil plays an important role in determining which effect will dominate.

In an attempt to explain this phenomenon, all of the displacement data available from our laboratory with pure carbon dioxide or high carbon dioxide solvents were analyzed. Studies on five different reservoir oils were available. The C6+ composition of each of these oils was grouped into five sub-fractions, namely C6–10, C11–15, C16–20, C21–25 and C26–30+. The resulting composition distributions are shown in Fig. 13. It will be seen that oils A, B and C have a high concentration of the lighter fractions (C6–C15) relative to the heavier fractions.

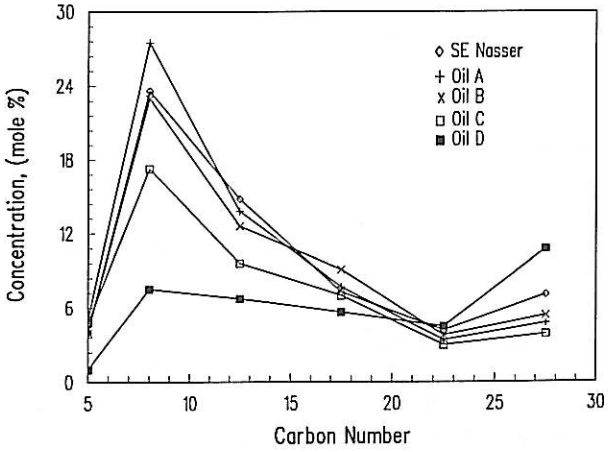


FIG. 13. C7+ component distribution of several oils.

With this information as background, a comparison was made between the separator based and toluene based recoveries at several pressures for each carbon dioxide displacement that had been run. The results of these comparisons are given in Fig. 14 which represents the difference between the two recoveries as a function of pressure. As a general observation, it will be seen that the difference becomes smaller and more negative as the pressure declines. These declining regions represent the immiscible displacements and in one sense this plot is analogous to the recovery-pressure plot shown in Fig. 11.

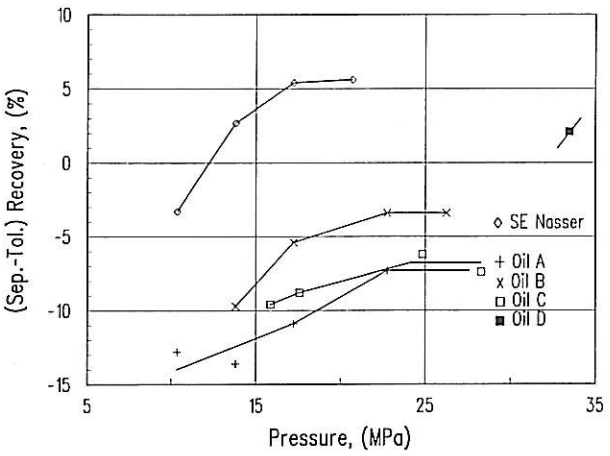


FIG. 14. The effect of oil character on the difference between seperator and toluene recoveries.

If one contemplates the recovery mechanism, it is realized that a lower separator recovery will be obtained when a significant fraction of the oil is extracted by carbon dioxide within the slim tube and goes with it in the off-gas after the back pressure regulator. The lighter extracted compounds in the C6–C15 range would yield very little liquid in the separator. Thus the difference between separator and toluene based recoveries tend to be negative.

On the other hand, positive differences are observed between the separator and toluene based recoveries for the oils (Oil D and SE Nasser) that have a substantially higher heavy fraction (C25–C30+). It appears that these oils swell significantly in the presence of dissolved carbon dioxide and that the evolution of carbon dioxide at the separator is relatively slow. In other words, the measured high separator recoveries observed may include some transient effects due to swelling, where the carbon dioxide does not come out of solution immediately.

At the grossly immiscible low pressure displacement for the SE Nasser oil as shown at 10.44 MPa on Fig. 14, the carbon dioxide evidently still acts as a good extractant and removes a significant fraction of the light and intermediate compounds from the oil. However, the swelling of the heavier components is reduced because of the lower carbon dioxide solubility at the low pressure.

The above observations indicate the influence oil composition can have on the behavior of the oil during carbon dioxide displacements.

CONCLUSIONS

The use of enriched gas hydrocarbon solvents as displacing fluids often leads to a combined condensing/vaporizing drive mechanism where miscibility may not be attained. Nevertheless, the displacement efficiency and thus the degree of recovery possible with these fluids is often comparable to that obtained with first contact or multiple contact miscible solvents.

The response of a reservoir oil to carbon dioxide depends, to a considerable extent, on the relative amounts of the C6–C15 fraction and the C25–C30+ fraction in the oil. The C6–C15 components tend to be extracted by the carbon dioxide, thereby decreasing the apparent liquid production. The C25–C30+ compounds on the other hand tend to swell in the presence of carbon dioxide and hence increase the apparent volume of liquid produced.

ACKNOWLEDGEMENT

The permission granted by the Sirte Oil Company to use some of the data obtained on a study of the enhanced oil potential for the SE Nasser reservoir is greatly appreciated.

REFERENCES

[1] Novosad Z. and Costain T.G., 1988, New Interpretation of Recovery Mechanism in Enriched Gas *Drives*, *J. Can. Pet. Tech.* 27, No. 2, 54–60.

[2] Novosad Z., 1989, EOR by Rich Gas Injection: The Role of Multiple Liquid Phases in Crude Oil-Solvent Miscibility Development, Proceedings of the Fifth International Conference on Fluid Properties and Phase Equilibria for Chemical Process Design, Banff, Alberta, Canada, April 30–May 5.

[3] Stalkup F.I., Jr., 1983, Miscible Displacement, Monograph Series 8, SPE of AIME, Dallas, Texas.

[4] Benham A.L., Dowden W.E. and Kunzman W.T., 1960, Miscible Fluid Displacemet – Prediction of Miscibility, Trans. AIME, 219, 229–237.

[5] Hutchinson C.A. and Braun P.H., 1961, Phase Relations of Miscible Displacement in Oil Recovery, AICHE J., 7(64–72).

[6] Metcalfe R.S., Fussel D.D. and Shelton J.L., 1973, A Mulicell Equilibrium Separation Model for the Study of Multiple Contact Miscibility in Rich-Gas Drives, SPE J., 3, 147–155.

[7] Fussel D.D., Shelton J.L. and Griffith J.D., 1976, Effect of Rich Gas Composition on Multiple-Contact Miscible Displacement-A Cell-to-Cell Flash Model Study, SPE J. 6, 310-316.

[8] Slobod R.L. and Kock H.A., Jr., 1953, High Pressure Gas Injection – Mechanism of Recovery Increase, Drill. and Prod. Prac., API, 82–96.

[9] Holm L.W. and Josendal V.A., 1974, Mechanisms of Oil Displacement by Carbon Dioxide, Journal of Petroleum Technology, 26, 1427–1436.

[10] Sibbald L.R., Novosad Z. and Costain T.G., 1990, Analysis of One-Dimensional Rich Gas Displacements With an Equation of State Simulator, J. CPT, 29, No. 1, 43–49.

[11] Zick A.A., 1966, A Combined Condensing/Vaporizing Mechanism in the Displacement of Oil by Rich Gases, SPE paper 15493, Presented at the 61st SPE Annual Meeting held in New Orleans, LA, Oct. 5–8.

[12] EQUI-PHASE™, 1990, Comprehensive Fluid Property and Phase Behavior Computer Software, DB Robinson & Associates Ltd., Edmonton, Alberta, Canada.

[13] Holm L.W. and Josendal V.A., 1982, Effect of Oil Composition on Miscible-Type Displacement by Carbon Dioxide, SPE J., 1, 87–98.

[14] Orr F.M. and Taber J.J., 1981, Displacement of Oil by Carbon Dioxide, Report DOE/ET/12082–9, Final Report for U.S. DOE, Contract No.-DE-AC 21–78ET12082(May).

[15] Orr F.M. Jr., Yu A.D. and Lein C.L., 1981, Phase Behavior of CO_2 and Crude Oil in Low Temperature Reservoirs, SPE J., 4, 480–492.

PRJ, Vol. 3 (January 1991); P. 13–20, 5 FIGS, 2 TABLES.

ADVANCED RESERVOIR MANAGEMENT ASPECTS OF ENHANCED OIL RECOVERY

G.L. Chierici*

آثار إدارة المكامن الحديثة على الإسترداد الإضافي

كياريتشي ج. ل.

في هذه الورقة عرض لفلسفة وتقنيات إدارة المكامن الحديثة. والغرض من إدارة المكامن الحديثة الآتي: (أ) الحصول على نموذج فريد ومفصل لمنشأ المكامن (تركيبها الداخلي) من معلومات المسح السطحي والجيولوجيا وسلوك الحقل. (ب) المتابعة الدقيقة لمدى تقدم وإزاحة الموائع في المكامن. (جـ) لإجراء عمليات المعالجة الهندسية وذلك للحصول على الحد الأقصى من إنتاج الزيت بطرق الإنتاج الأولية وبطرق عمليات حقن الموائع (مثل الماء والغاز وغيرها من الموائع المستعملة في الإسترداد الإضافي).

إستخدامات تقنيات إدارة المكامن الحديثة بداية بتطوير وإستغلال الحقول النفطية مروراً بتكوين فريق عمل موحد من الجيولوجيين والجيوفيزيائيين والمهندسين والخبراء في مجال الجيواحصاء تعتبر من أساسيات فلسفة إدارة المكامن الحديثة. تعتبر المعلومات المتحصل عليها من تطبيق تقنيات المكامن الحديثة بالغة الأهمية للمهندسين وكذلك للسيطرة على عمليات الإسترداد الإضافي.

ABSTRACT

The philosophy and techniques of Advanced Reservoir Management (ARM) are described. ARM is aimed (i) at obtaining a unique and detailed model of reservoir architecture (i.e. its internal structure) from seismic, geological and field performance data, (ii) at accurately tracking the progress of the fluid front(s), and (iii) at engineering remedial action in order to maximize oil recovery by primary depletion and fluid (water, gas or EOR fluids) injection. The use of ARM techniques right from the start of field development and exploitation, and the synergetic team work of geologists, geophysicists, engineers and experts in geostatistics are the essential points of ARM philosophy. Information provided by ARM techniques is of vital importance for engineering and controlling EOR processes.

INTRODUCTION

A good pragmatic definition [1] of reservoir management is "maximizing the economic value of a petroleum reservoir by optimizing production rate and hydrocarbons recovery, while minimizing capital investments and operating expenses".

This is evidently not an engineering definition: it is a definition which is based on yardsticks related to market economics. Descriptors such as present worth, rate of return, pay out time and investment efficiency are used to measure the success or failure of the reservoir management techniques practiced in developing and exploiting an oil or gas field. In certain economic environments, different descriptors are used; for instance, acceleration of production and maximization of oil recovery.

The task of the reservoir manager is to maximize (minimize, in the case of investments and operating expenses) the values of the above-mentioned descriptors.

The reservoir manager thus trades off expenditures (which drain present worth) against the chance of increasing present worth by adding reserves and/or increasing production rates. This process is a continuous balancing act, which begins the very moment a field is discovered.

In the world of market economics, enhanced oil recovery (EOR) is a tool (not the only one!) for optimizing reservoir exploitation. Currently, EOR processes are considered as the "last chance" to

*Faculty of Engineering, University of Bologna, Italy.

"scrape the barrel" when the conventional improved oil recovery processes (water injection, immiscible gas injection) are reaching the economic limit.

This is only partially corrrect: in fact, advanced reservoir management (ARM) techniques, if applied to an oilfield from the start of its exploitation, can sometimes maximize the economic value of the field without resorting to EOR processes.

In any case, ARM techniques applied to an oilfield throughout its life provide most of the information needed for the sound engineering of EOR processes used in the tertiary mode, thus increasing their probability of success.

In the following pages advanced techniques will be discussed which, if applied to an oil reservoir from the time of its discovery, will increase its economic value and maximize the probability of success of EOR processes, if needed.

RESIDUAL OIL: HOW MUCH IS THERE? AND WHERE IS IT?

As is well known, the average oil recovery factor from oilfields worldwide ranges between 30% and 34%. It should be stressed that this is an *average* value. Peaks as high as 80% have been reached in some cases (like the East Texas field [2], which was developed with extremely closely spaced wells), and throughs as low as a few percent have been experienced in some heavy-oil reservoirs in primary porosity rocks.

Let us remember that the oil recovery factor, E_R, is the product of two quantities, that is:

$$E_R = E_D \cdot E_V \tag{1}$$

where:

E_D = microscopic displacement efficiency (fraction of oil displaced from the pores in those parts of the reservoir rock which have come into contact with the displacing fluid), and

E_V = volumetric efficiency (fractional coverage of the reservoir rock volume by the displacing fluid).

As a consequence, at any time in the life of a field the volume of the residual oil in a reservoir whose original oil in place was Nm^3 at stock-tank conditions, can be split as follows:

$$N_{r,v} = N(1 - E_v) \tag{2}$$

m^3 of stock-tank oil remaining in the reservoir rock volume not yet contacted by the displacing fluid, and:

$$N_{r,D} = NE_v(1 - E_D) \tag{3}$$

m^3 of residual oil remaining in the reservoir rock volume which has come into contact with the displacing fluid.

Before considering any EOR project in a field, one of the main questions to be answered is: "how much oil still remains in the reservoir, and how much of it could be recovered?"

Usually, standard numerical model simulations "matched" on reservoir past history are used to answer these questions.

Only in the last few years, after many post-mortem analyses of pilot and fieldwide EOR projects which had technically failed, has another question been raised: "*where* is the residual oil? How is it split between oil remaining in the reservoir rock streaks not swept by the displacing fluid ($N_{r,v}$, Eq. 2), and residual oil in the pores of those parts of the reservoir rock which did come into contact with the displacing fluid ($N_{r,D}$, Eq. 3)?".

This is not an academic question: it is one of the most important questions to be answered before one may even consider an EOR process for a field.

In fact, if most of the residual oil is of the $N_{r,v}$ type (poor E_v), there is no point in considering a miscible process with a gas, or a micellar/polymer flooding. These fluids will preferentially flow along the same paths as the water or gas) which displaced the oil before, and only a small amount of the oil left in the pores will be displaced. In these conditions a miscible or surfactant flooding is bound to be a failure.

On the other end, if most of the residual oil is of the $N_{r,D}$ type (poor E_D), there is no point in considering a process designed for increasing the rock conformance factor, such as polymer flooding.

To obtain reliable information on the split of the residual oil between $N_{r,v}$ and $N_{r,D}$ and to gather the basic data needed before starting to engineer an EOR process, the following steps should be taken:

1. build a reliable *geological* model of the reservoir based on all "static" information gathered during the exploration and development of the field (3D seismic data, well logs, core studies, reservoir rock outcrops, if any);
2. validate (and, if necessary, modify) the geological model by embedding all "dynamic" information gathered during the exploitation of the field. Special tests, which will be discussed in a following chapter, must be run for this purpose;
3. periodically run numerical model simulations in a "feedback" mode (Fig. 1) and, at each step, validate the dynamic model against actual reservoir behavior. To this end, probabilistic numerical models are preferable;
4. before engineering the EOR process, check again the spatial distribution of the residual oil, and its split between $N_{r,v}$ and $N_{r,D}$ by running cased-hole logs [3] specially designed for this purpose.

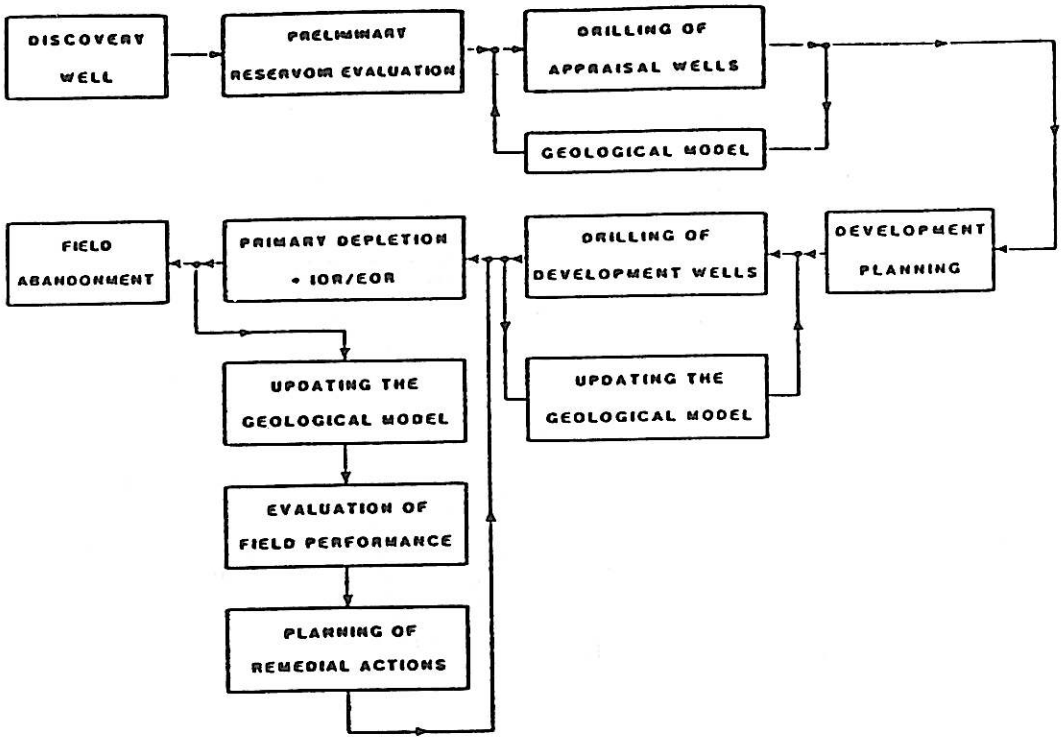


FIG. 1. Reservoir management: the iterative (or "feedback") system.

The above steps are typical of Advanced Reservoir Management (ARM) [4], where "advanced" does not only apply to the techniques used, but also to the attitude of top managements towards reservoir geology and engineering problems.

Time and money should be spent freely to provide the information needed, a complete team of specialists should be available in-house, access should be provided to last-generation probabilistic reservoir models.

All this costs money but, after all, it is certainly much cheaper than an EOR project failure.

THE "STATIC" GEOLOGICAL MODEL

The first step in every reservoir study consists in building a detailed and reliable geological model of the reservoir.

To this end the following information, collected in the exploration, field appraisal and development stages is used:

- 3D seismic surveys interpreted in stratigraphic mode [1, 5],
- sedimenthological, petrophysical and petrographical studies on cores;
- sedimenthological studies at basin scale,
- well logs interpreted in terms of lithology, porosity and water saturation,
- drill-stem and production test results.

The problem which always confronts the reservoir geologist is "how do we extrapolate to the inter-well areas, rock parameter values which are (and can only be) measured at the wells?".

For instance, let us consider permeability values measured on cores and confirmed, as an average value for the pay zone, by well tests.

At the well the picture looks like Fig. 2A. But what about the lateral extent of each streak with different permeability? Are they continuous layers (Fig. 2B), or is it a randomly heterogeneous (sometimes also called "homogeneously heterogeneous") sedimentary unit (Fig. 2C), or is it made up of intercommunicating lenses of different size (Fig. 2D) and, in this case, what is the average size of these lenses and the standard deviation from the average?

And what about the interbedded shale streaks (which are so common in sand/shale sequences deposited in high-energy environments) and their influence in reducing vertical permeability?

All the above factors affect the E_v value in a displacement process.

An insight into the situation can be provided by a sedimentological approach. The well known Weber diagram [6] (Fig. 3) shows how the statistical distribution of interbedded shale layers depends on the environment where they have been deposited: a similar approach can be considered for sand layers.

In a heterogeneous reservoir, the problem immediately arises of the continuity (or "connectivity") between injection and production wells.

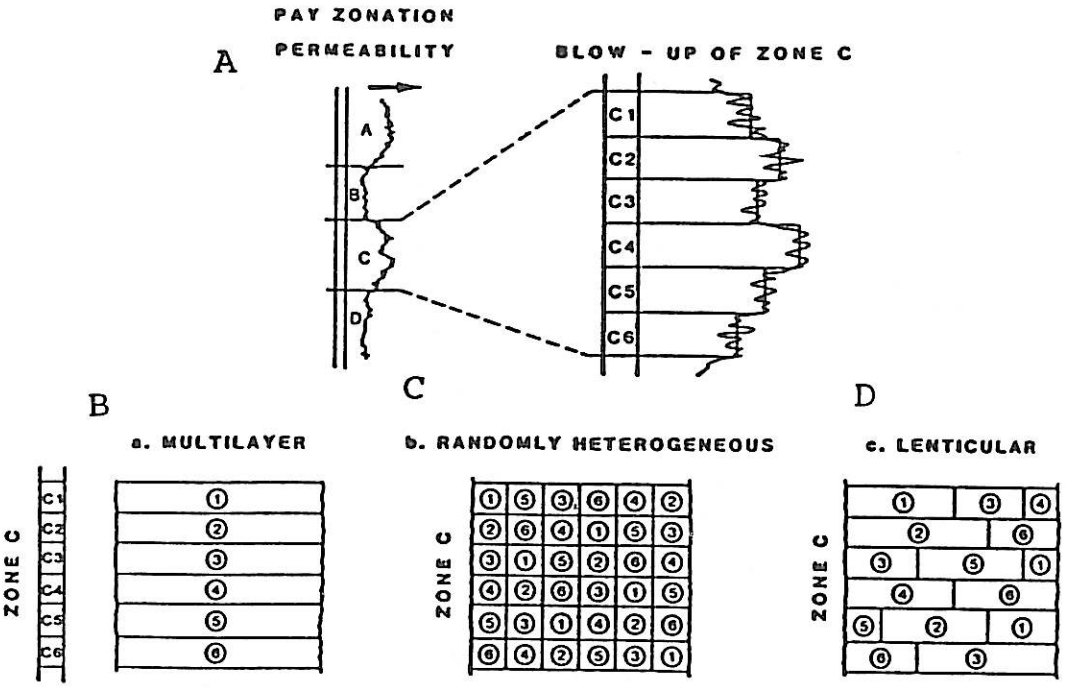


FIG. 2. Permeability variations within a reservoir zone, as shown by core analysis; (a)–(c) different geological models to explain and extrapolate them to the well drainage area.

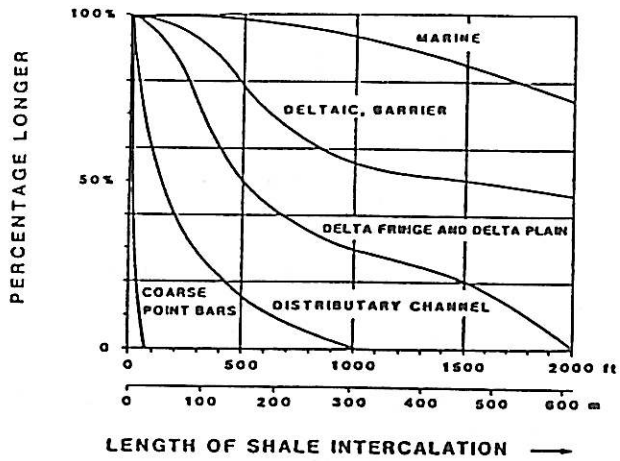


FIG. 3. Statistical distribution of the size of shale intercalations as a function of the depositional environment. (From Ref. 6).

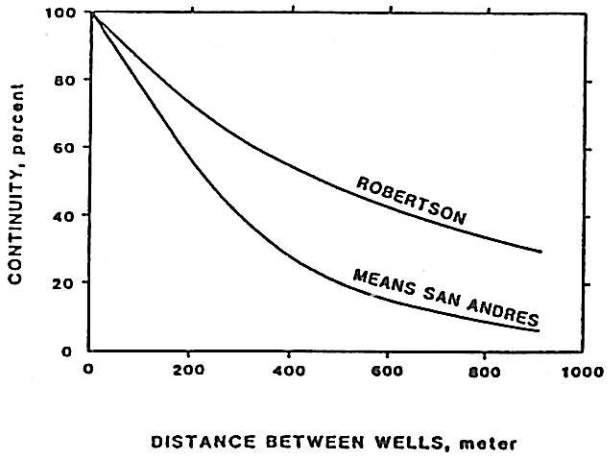


FIG. 4. Pay continuity between wells versus interwell distance, Means San Andres and Robertson Clkearfork units, TX. (From Ref. 4).

Obviously, in order to displace (and produce) the oil from a reservoir layer, at least one injection and one production well must be drilled in it.

For a given numbers of wells drilled in a field, the percentage of oil-bearing rock with which the injected fluid comes into contact (that is, E_v) is a function of the average areal extention of the permeable streaks, and of the standard deviation of the extention.

Viceversa, in a heterogeneous reservoir rock the connectivity between injection and production wells is a function of well spacing: the closer the spacing, the higher the connectivity (and, therefore, the higher the E_v and the oil recovery).

Figure 4 shows an example [4] of how interwell connectivity is influenced by well spacing in two oilfields in Texas. It must be noted that in the San Andreas reservoir the connectivity (and therefore, to stress this once again, E_v and oil recovery) increased by 50% when the spacing was reduced from 40 to 20 acres/well(!).

It should be noted that the influence of well spacing on oil recovery was recognised as early as in the 1920s, on an empirical basis (Cutler's rule [7]). This concept was then rejected when reservoir engineering "science" was forced to forget about heterogeneity, due to the difficulties it caused in the calculation of

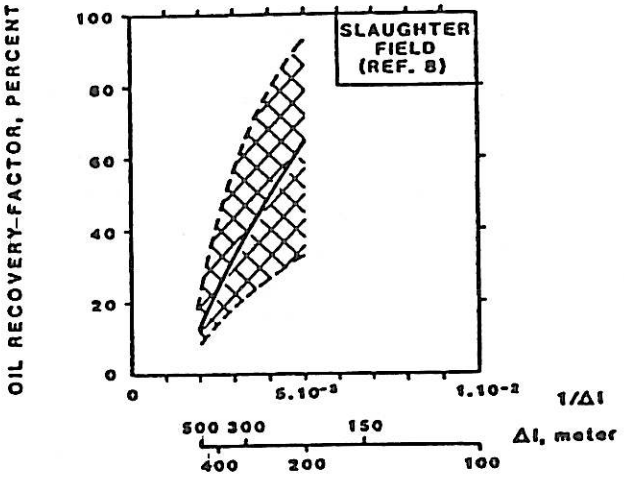


FIG. 5. Oil recovery versus interwell distance, Slaughter field, TX. (Data from Ref. 8).

reservoir behaviour. Figure 5, based on data presented in a classical paper [8], shows how Cutler's rule holds good for a real oilfield.

If outcrops of the producing formation are known to exist, they must be studied in very great detail, as they are the only source of direct (even if only qualitative) information on facies distribution, permeability trends, presence of impermeable barriers, etc. The statistical treatment of such data can result in information of the utmost importance in understanding the "architecture" of the reservoir.

It must be noted that the study of outcrops as an aid to evaluate reservoir architecture was carried out for the first time some 27 years ago [9], but it is only recently that this technique has become common practice both in the U.S.A. and Europe [10].

Crosswell seismics [11], and its interpretation in tomographic mode, is still in its infancy. This technique shows excellent potential for describing interwell characteristics of the reservoir rock: it is hoped that it will soon grow to the stage when it becomes a routine tool for reservoir description.

It should be borne in mind that only the data from cores and outcrops are *direct* measurements of reservoir rock properties. All the other information and data mentioned above are *indirect* evaluations of these properties. In order to merge all direct and indirect data to build the most reliable geological model(s) of the reservoir, and in particular in order to extrapolate the information to interwell areas, statistical techniques must be used (cluster analysis [12], fractal distribution [13], etc.). A very efficient technique for describing the statistical distribution of shale lenses within the reservoir rock has been proposed by Haldorsen [14].

The interpretation and evaluation of reservoir architecture calls for the *joint* effort of specialists from many disciplines: sedimentology, petrography, petrophysics, regional geology, log analysis, geochemistry, seismics, reservoir engineering, and geostatistics.

Only team work can provide the synergy needed to build the more realistic and probable geological model of the reservoir. And sometimes a number of geological models show the same probability of representing the actual architecture of the reservoir, being equally consistent with the basic data and information available.

"DYNAMIC" DATA FROM RESERVOIR PERFORMANCE

When the field starts producing a lot of information on its dynamic behaviour can (and *must*) be gathered.

Data on well performance (oil, gas and water production rates, shut-in and flowing bottom-hole pressures, standard pressure drawdown, buildup and production logging tools, PLT surveys) as routinely measured and collected in the data-base are very valuable, but they provide only a partial picture of reservoir behaviour.

The other very important part is provided by the following non-routine tests and data:

- inter-well connectivities and transmissibilities,
- vertical communication between zones in layered reservoirs, with the measurement (or evaluation) of vertical permeability,
- advance in time of the displacing fluid front(s).

In standard petroleum engineering practice these measurements are seldom taken.

In ARM they must be taken at regular intervals *from the start of production.*

Only by so doing a detailed picture of how oil moves in the reservoir, and where "pockets" of rock not flooded by the displacing fluid(s) are located, can be obtained.

Long-duration interference tests [15], pulse tests between groups of wells [16], and between layers in the same well [17], "coloured" tracer tests between injection and production wells [18], if properly interpreted by means of *ad hoc* numerical models, can provide valuable information on interwell connectivity and transmissibility, as well as on vertical communication between layers and vertical permeability.

The progress of the displacing fluid front(s), and the spatial distribution of rock "pockets" which have been by-passed by the displacing fluid(s) can be located by means of cased-hole logs.

Pulsed neutron capture (PNC), pulsed neutron spectral (PNS) or induced gamma-ray spectral

(IGRS) logs [3], as well as nuclear magnetism logs [19] (NML) are the most suitable tools for this purpose. For locating gas fronts the routine neutron + density logs (CNL + FDC) combination can give good results.

When the wells are completed in open-hole, standard focused resistivity logs can be used to locate the displacing water (or water-bearing fluid) front.

When ARM techniques are used, the most suitable combination of the above-mentioned tests and logs must be engineered for each reservoir and displacing fluid considered.

This combination of tools must be run at regular intervals during the life of the field. In addition, special campaigns must be arranged when something "unexpected" happens (an early breakthrough of water or gas in a well, an abnormal pressure drop in an area of the reservoir, etc.).

NUMERICAL MODELS AS AN ADVANCED RESERVOIR MANAGEMENT TOOL

In the early stage of field development, numerical models based on the initial geological model are used for locating wells and defining drilling schedules. A stochastic approach [20] should be used in order to provide a scenario of the various possible reservoir architectures which show an equal probability of representing the actual reservoir structure.

This calls for a lot of Central Processing Unit (CPU) time. The use of parallel computers, when it becomes standard practice, will drastically reduce this time.

As soon as dynamic data from reservoir performance are available, they should be embedded into the geological model(s), so as to validate them against the actual reaction of the field to the production history. In this way the number of models which match reservoir performance is progressively reduced, until such time as only a few models show the same probability of describing the actual reservoir architecture.

It is of the utmost importance that each modification to the model be based only on data gathered from well and field tests [21]. The current "garbage in, garbage out" approach of modifying reservoir parameters (mainly vertical permeabilities and relperms) with the only aim of matching well behaviour, without being consistent with the geological model, must be avoided.

The trial-and-error approach of matching model results to actual reservoir performance should be repeated at sufficient intervals during reservoir life.

Every time, the information gathered from the model on the position of the displacing fluid front(s), and the presence and location of reservoir rock "pockets" which have not been swept, should be used to engineer remedial action aimed at improving the conformance factor, E_v, of the reservoir.

Well workovers and recompletions, drilling of infill wells [22], changing the production/injection well pattern should be planned according to the results of model simulations. And field reaction to the planned remedial action should be evaluated on the model before being carried out in the field.

Infill wells aimed at improving interwell connectivity may be very efficient in enhancing oil recovery. A recent study [23] shows (Table 1) how some 73% of oil reserve additions in Texas from 1973 to 1982 was provided by infill drilling, against a mere 21% resulting from new field and new pool discoveries.

Table 1. Composition of Oil Reserve Additions in Texas from 1973 to 1982 (from Ref. 23)

	Volume (10^6 m^3)	% of Total
– New-field wildcat discovery, with appreciation	103.4	11
– New-pool discovery	95.4	10
– Infill and extension drilling	696.4	73
– Tertiary projects	38.8	4
– Delayed abandonment	22.3	2
	956.3	100

The same study [23] estimates at 12.7 billion m^3 the amount of *movable* oil in place in U.S. oilfields which is not swept by the current well patterns, and could be recovered by infill wells (Table 2).

Table 2. U.S. Oil Distribution (from Ref. 23)

	Volume (10^9 m^3)	% of Total
– *Recoverable oil by primary depletion and waterflooding*		
• produced	21.6	27.8
• remaining	4.5	5.8
– *Recoverable oil after waterflooding*	26.1	33.6
• recoverable by currently implemented EOR processes, with an oil price up to 30 $/bbl	2.6	3.3
• mobile oil in unswept zones (target for infill drilling)	12.7	16.3
	15.3	19.6
– *Immobile Oil*	36.4	46.8
TOTAL	77.8	100.0

Accordingly, conventional water-flooding with infill drilling could raise to 50% the average oil recovery from U.S. fields, against the currently estimated value of 33.6%.

ARM techniques as described in this paper are already in use in some oilfields. The case of the Stratfjord field in the Norwegian sector of the North Sea has recently been described in technical literature [24], and it is known that the same technique is being applied to the Oseberg oilfield, in the same area. An earlier case where an ARM approach was used [25] is the Bu Attifel field, GSPLAJ.

The use of numerical models for ARM calls for a number of improvements in simulation techniques. For instance, it is known that standard numerical models almost always indicate little or no sensitivity of the ultimate oil recovery to production rates [26]. This is one of the areas which deserves further investigation.

EOR OR NO EOR FOR THIS FIELD?

As already discussed, when the decision is made to explore the feasibility of a suitable EOR process in a field, the first questions needing an answer are:

- is a reliable and detailed description of reservoir architecture available?
- how much residual oil remains in the reservoir at this stage of the game?
- how is the residual oil split between:
  - residual oil in the pores of the rock volume swept by the displacing fluid(s)
  - oil in the reservoir rock "pockets" which have not come into contact with the displacing fluid(s)?

If ARM techniques have been used in developing and exploiting the field, the information which has been collected provides reliable answers to the above questions.

Moreover, a good connectivity between injection and production wells should already exist, and a good volumetric efficiency, E_v, should have been attained.

And, it ought to be stressed here, a good connectivity is *the* prerequisite for the success of any EOR process, as it assures a good coverage of the reservoir by any kind of injected fluid.

This is a very valuable by-product of ARM techniques used in the primary and waterflooding (or gas injection) phases of reservoir exploitation.

It may be that, due to the high E_v, the oil recovery factor attained thus far is very high, so the amount of oil left in, the reservoir does not warrant any EOR process.

This is good news, as EOR processes are usually very expensive, require front-end investments and, so far, do not guarantee a success.

If ARM techniques have not been used, a lot of work remains to be done along the lines sketched in the previous pages. But the information that could have been provided by monitoring reservoir peformance is lost for ever.

Based on the foregoing considerations it appears that the use of ARM techniques right from the beginning of the life of an oilfield represents the most efficient (and cost-effective) way of optimizing, throughout its life, the exploitation of an oilfield, including the "scraping" phase of EOR.

Obviously, the same ARM techniques must then be used in order to monitor and control field performance in the EOR production phase.

CONCLUSIONS

The Advanced Reservoir Management (ARM) techniques described in this paper provide the vital information needed to:

- determine the internal structure (or "architecture") of the reservoir, so as to build a realistic and unique geological model,
- track the advance of the displacing fluid front(s) and define the volume and location of reservoir rock "pockets" not swept by the displacing fluid(s),
- properly engineer remedial action (well recompletions and workovers, changes in the injection/production pattern, drilling of infill wells, etc.) in order to maximize reservoir coverage by the displacing fluid(s),
- provide basic data for the selection of the most cost-efficient EOR process
- monitor and control progress of the EOR process.

ARM techniques should be used from the start of the development and exploitation of the oilfield.

If properly and continuously used, ARM techniques may result in oil recovery by primary depletion plus waterflooding (or immiscible gas injection) which make recourse to EOR processes no longer necessary.

A complete and efficient team of specialists (geologists, geophysicists, engineers and experts in geostatistics), and their synergetic team work is needed to apply ARM techniques to a field.

Moreover, a lot of well and interwell tests, as described in this paper, must be run throughout the life of the field to provide basic data on its internal structure and dynamic performance.

Obviously, the ARM approach calls for additional costs. Top managements of the oil companies should be made aware that the extra time and money spent

to run special tests in the field, and to process them by teams of specialists, is not a waste of time and money.

Afterall, a mere 1% increase in oil recovery from a field with 1 billion barrels (159 million m^3) of *oil in place* means, in present worth, some 100 million dollars of additional income for the oil company.

NOMENCLATURE

E_D = microscopic displacement efficiency, fraction
E_R = oil recovery factor, fraction
E_v = volumetric efficiency, or conformance factor, fraction
N = initial oil in place, m^3 STO
$N_{r,D}$ = oil remaining in the reservoir rock volume which has come into contact with the displacing fluid, m^3 STO
$N_{r,v}$ = oil remaining in the reservoir rock volume which has not yet come into contact with the displacing fluid, m^3 STO

REFERENCES

[1] Robertson J.D., 1989, Reservoir Management Using 3D Seismic Data, *J. Pet. Tech.*, 663–667.
[2] Van Everdingen A.F., 1978, Dialogue, *J. Pet. Tech.*, 209–210.
[3] Felder R.D., 1988, Cased-Hole Logging for Evaluation Bypassed Reserves, *J. Pet. Tech.*, 969–973.
[4] Chierici G.L., 1989, ARM (Advanced Reservoir Management) vs. EOR, Proc., 5th European Symposium on EOR (Budapest), 32–42.
[5] de Buyl M., Guldish T., and Bell F., 1988, Reservoir Description From Seismic Lithologic Parameter Estimation, *J. Pet. Tech.*, 475–482.
[6] Weber K.J., 1982, Influence of Common sedimentary Structures on Fluid Flow in Reservoir Models, *J. Pet. Tech.*, 665–672; Trans., AIME 273.
[7] Cutler J.W., Jr., 1924, Estimation of Underground Oil Reserves by Oil-Well Production Curves, *Bull. USBM*, 228.
[8] Van Everdingen A.F., and Kriss H.S., 1980, A Proposal to Improve Recovery Efficiency, *J. Pet. Tech.*, 1164–1168; Trans., AIME 269.
[9] Montadert L., 1963, La sedimentologie et l'etude detailee des heterogeneites d'un reservoir. Application au gisement d'Hassi messaud, *Rev. Inst. Franc. du Petrole*, 18, 258–283.
[10] Lake L.W., Kokurek and Miller M.A., A Systematic Procedure for Reservoir Characterization, DOE/BC 10849–5 (December 1987), and DOE/BC 10849–10 (November 1988), The University of Texas at Austin, and U.S. Department of Energy, Bartlesville Project Office.
[11] Iverson W.P., 1988, Crosswell Logging for Acoustic Impedance, *J. Pet. Tech.* 75–82.
[12] Descalzi C., Rognoni A., and Cigni M., 1988, Synergetic Log and Core Data Treatment Through Cluster Analysis. A Methodology To Improve Reservoir Description, Paper SPE 17637 presented at the International Meeting on Petroleum Engineering (Tianjin, China).
[13] Hewett T.A., 1986, Fractal Distributions of Reservoir Heterogeneity and Their Influence on Fluid Transport, Paper 15386 presented at the 1986 SPE Annual Technical Conference and Exhibition (New Orleans, LA).
[14] Haldorsen H.H., 1983, Reservoir Characterization Procedure for Numerical Simulation, PhD Thesis, University of Texas at Austin.
[15] Kamal M.M. and Hegeman P.S., 1988, New Developments in Multiple-Well Testing, SPE Formation Evaluation, 159–168.
[16] Chopra A.K., 1988, Reservoir Descriptions via Pulse Testing: A Technology Evaluation, Paper SPE 176658 presented at the SPE International Meeting on Petroleum Engineering (Tianjin, China).
[17] Hirasaki G.J., 1974, Pulse Test and Other Early Transient Pressure Analyses for in-Situ Estimation of Vertical Permeability, *Soc. Pet. Eng. J.*, 75–90; Trans., AIME 257.
[18] Smith L.J., and Brown C.E., 1984, Tne Interpretation of Tracer Test Response from Heterogeneous Reservoirs, Paper SPE 13262 presented at the 1984 SPE Annual Technical Conference and Exhibition (Houston, TX).
[19] Freedman R. and Rouault G.F., 1989, Remaining Oil Determination Using Nuclear Magnetism Logging, SPE Formation Evaluation, 121–130.
[20] Emanuel A.S., Alameda G.K., Behrens R.A., and Hewett T.A., 1989, Reservoir Performance Prediction Methods Based on Fractal Geostatics, *SPE Reservoir Engineering*, 311–317.
[21] Chopra A.K., Stein M.H., and Ader J.C., 1989, Development of Reservoir Descriptions To Aid in Design of EOR Projects, *SPE Reservoir Engineering*, 143–150.
[22] Gould T.L., 1989, Infill Drilling for Incremental Recovery, *J. Pet. Tech.*, 229–237.
[23] Fisher W.L., 1987, U.S. Oil Outlock, The University of Texas at Austin, Chair of Mineral Resources.
[24] Haugen S.A., Lund O. and Hoyland L.A., 1988, Statfjord Field: Development Strategy and Reservoir Management, *J. Pet. Tech.*, 863–873.
[25] Erba M., Rovere A., Turriani C. and Safsaf S., 1984, Bu Attifel Field – A Synergetic Geological and Engineering Approach to Reservoir Management, Proc., 11th World Petroleum Congress, 3, 89–99.
[26] Thomas G.W., 1988, An Assessment of rate Sensitivity by Reservoir Simulation, Paper SPE 17601 presented at the International Meeting on Petroleum Engineering (Tjanjin, China).

PRJ, Vol. 3 (January 1991); P. 21–26, 4 FIGS, 6 TABLES.

RHEOLOGICAL PROPERTIES OF SARIR CRUDE OIL

M. Elgarni,* H.H. Beck,* S.M. Debbah* and N.A. Faruqi*

خواص الدفق لخام نفط السرير

محمد القرني ، هيثم حسن بك ، سالم الدباح ، نور الدين الفاروقي

تم استخدام مقياس اللزوجة ذو الإسطوانتين متحدتي المحور لتعيين خواص الدفق لخام السرير وكذلك استخدام نموذج قانون القوة «المعروف» لتفسير سلوك الإنسياب للخام المذكور. كما تم استخدام علاقة والتر ومعادلة أخرى متعددة الحدود لصياغة تأثير درجة الحرارة على متغيرات قانون القوة السالف الذكر.

أوضحت هذه الدراسة أن إجهاد الخضوع «متغير يستعمل لحساب ضغط إعادة تشغيل خط الأنابيب» شديد الحساسية لمنظومة القياس وظروف التشغيل.

ABSTRACT

The rheological properties of Sarir crude oil have been determined using coaxial cylinder viscometer. Power law model was used to relate the flow behavior. The temperature dependency of the power low parameters were modelled by using Walthers and polynomial type correlations.

The yield stress was shown to be very sensitive to the measurement system and conditions.

INTRODUCTION

Pipelines are the cheapest and the most efficient means for the transportation of crude oils and their distillate and residual products. An important design criterion of the crude oil pipelines is the volume of oil handled at any time during their service life. Considerable uncertainty is often involved in predicting the flow rate on day to day basis due to various operational reasons. Therefore a pipeline system is always designed to handle a wide range of flow rates. Waxy oils may create considerable handling problems in their transport over wide flow rates. For example at low flow rates and during cold season the oil may cool down to temperatures very close to the pour point or even lower as a result of increase in the residence time. At a relatively lower temperature the pipeline may have to handle highly viscous oil at a high pressure drop and there would be large wax deposition requiring more frequent pigging [1]. There is nothing wrong in handling oil at temperatures below the ASTM pour point as long as the pipeline remains continuously operational. In the event of a shutdown with the oil shutin, the oil may form hard three dimensional gel [2]. In order to restart the pumping, the gel structure need to be broken down. Sometimes the restarting pressure may exceed the bursting pressure of the pipeline causing severe problems. A careful evaluation of the rheological and the deposition characteristics of waxy crude oils are required in order to prevent difficulties during the operation. This is not an easy task either. In contrast to the lighter and low waxy oils, the waxy oils do not possess definite and easily predictable rheological properties. The viscosity, for example may change at a given temperature by several hundred percent depending upon the previous thermal and shear history of the oil. The seperation of wax in the form of various sizes and shapes and the intercrystalline forces are responsible for the anamolous behavior of the waxy oils. This paper describes the experimental

*Petroleum Research Centre, P.O. Box 6431, Tripoli, G.S.P.L.A.J.

techniques and modelling work carried out to characterize the flow behavior of a waxy crude oil through a pipeline system.

THEORY

Most crude oils contain high molecular weight components [3] typically C_{20+}, which at low temperatures may precipitate out as wax. Wax generally crystallize in orthorhombic structure [3]. The crystals usually form plate like crystals on slow cooling and needle shape crystals upon the conditions of fast cooling or in the presence of additives [5]. The plate type crystals form cages and are responsible for early gelling of oils. The needle shape crystals have higher solubility in oil [5] and gel at relatively lower temperatures. The flow behavior at lower temperatures depend upon several factors, including the type of crystals, size, quantity and intercrystalline forces. The variation of many of the above factors would produce a different rheology. Therefore it is of utmost importance that conditions identical to those occuring in a pipeline be reproduced while measuring the flow characteristics.

Paraffins which have higher freezing points as shown in Table 1, constitute bulk of the wax. Aromatics are also present in traces to very small quantity [3] and influence the crystallization behavior by distorting the crystal lattice.

Wax crystals are mainly responsible in introducing thixotropic (time dependent non-Newtonian behavior) and pseudoplastic behavior into the flow properties of waxy oils. Three important flow related properties required in the design and simulation of pipelines are:

- Relationship between shear stress, shear strain and temperature
- Yield strength
- Deposition rate

The flow behavior of waxy crude oils may be taken as Newtonian over 10 to 20°C above the ASTM pour point. The properties turn towards pseudoplastic at lower temperatures. The change in the behavior may be related to the appearance of wax. Fig. 1 qualitatively sketches different flow behaviors (time independent). The basic behavior in the above case was thixotropic as shown in Fig. 2. The apparent viscosity approaches asymptotic value after the elapse of a definite time. Fortunately it is the asymptotic value which is required in design and simulation work. The apparent viscosity is given as:

$$\mu = \tau/S \tag{1}$$

The yield stress indicated in Fig. 1 is an important

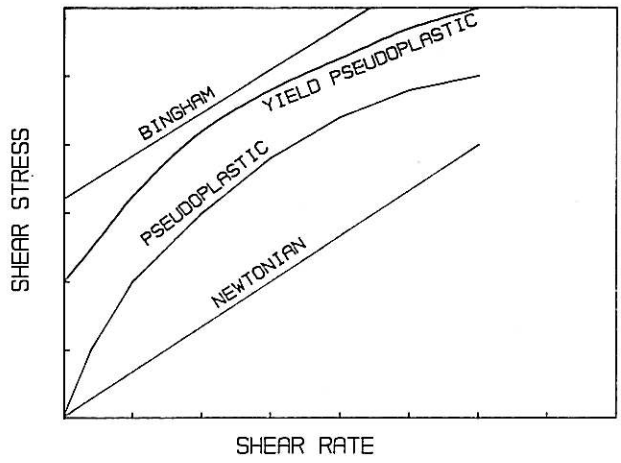


FIG. 1. Flow behavior of different types of fluids.

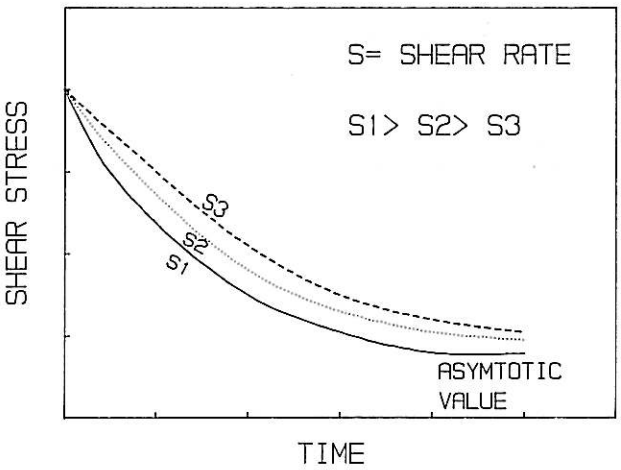


FIG. 2. Thixotropic fluid behavior.

Table 1. Melting and Boiling Points of Some High Boiling Compounds [4]

CN	(In Deg C) Lin. Paraffins		Alky. CYC5			Alky. CYC6			Alky. Ben.		
	B.P.	M.P.	Name	B.P.	M.P.	Name	B.P.	M.P.	Name	B.P.	M.P.
18	317	28	TRDE	326	5	DODE	328	13	DODE	328	3
22	369	44	HEDE	377	27	HEDE	380	34	HEDE	378	27
26	412	56	HCOS	420	42	EICO	422	49	EICO	420	—
30	450	66	PCOS	456	54	TECO	458	60	TECO	454	57

parameter for the yield-pseudoplastic (Bingham plus pseudoplastic) fluids. It is also required in the computation of the restarting pressure as given in the Eq. (2).

$$(\Delta p)_{R.S.} = \int_{x=0}^{x=L} \frac{4\tau_0}{D} dx \qquad (2)$$

The yield stress used in the Eq. (2) depends upon a number of parameters, the most important of them are:

- Final temperature
- Thermal history
- Shear history
- Duration of shutdown time

The yield stress was found by several workers [7, 8] to be very sensitive to the presence of dissolved gases and lighter hydrocarbons as well as to the high molecular weight polymeric additives and natural polymeric materials such as asphalthenes. A careful inclusion of all the factors, no doubt, would lead to more precise measurements.

In order to simulate the actual conditions some companies have used commercial long pipelines [1, 6–8] to measure the yield stress and viscosity. A quick but approximate estimation of the Yield strength [5] can be made by using Rotary viscometer, a method adopted in the present studies.

Wax deposition rate is yet another consideration. It decreases flow area and influences pipe roughness. It can even cause pig blockage. At temperatures above the wax appearance temperature (WAP) the deposition is of lesser significance. The deposition gains importance at lower temperatures. Frequent pigging [8] may keep the surface clean. The quantification of deposition rate in the operating lines is always uncertain. The operators monitor the pump discharge pressure and adjust pigging frequency accordingly. A more detailed treatise of the subject may be found elsewhere in the literature [9–10].

MODELS

A large number of models have been suggested in the literature [1] to relate the flow behavior of time-independent non-Newtonian fluids. The asymptotic behavior of time dependent thixotropic fluids may also be described by the same models. All the models are empirical curve fitting techniques. Selected forms of models are given in Table 2. Isothermal conditions are applicable in each of the relationships given in Table 2.

The model parameters are themselves temperature dependent, therefore other correlations must be used to obtain temperature dependency. The simplest and

Table 2. Rheological Models for the Time Independent Non-Newtonian Fluids

Name	Model		Fluid Type*
Power law	$\tau = k(S)^n$	(3)	
	$n<1$		P/D
	$n>1$		
Eyring	$\tau = A\ \text{ARC Sinh}(-1./B\,S)$	(4)	P/D
Ellis	$S = [A + B(\tau)^{m-1}]$	(5)	P/D
Reiner-Philippoff	$S = \tau\left[A + \frac{(B-A)}{1+(\tau/C)^2}\right]^{-1}$	(6)	P/D
Bingham	$\tau = \tau_0 + K(S)^n$	(7)	
	$n=1$		Bingham
	$n<1$		P
	$n>1$		D

*P = Pseudoplastic D = Dilatant

the most widely used model is the Power low model modified to include the yield strength. It is given by Eq. 7.

$$\tau = \tau_0 + K(S)^n \qquad (7)$$

The flow behavior index (n) approaches unity as the flow behavior turns Newtonian. The consistency index (k) could be correlated to the absolute temperature (K) by using Walthers type equation given by Eq. 8:

$$\ln\ln(k + A_1) = B_1 + \ln(T + C_1) \qquad (8)$$

A polynomial type fitting was used for the flow behavior index (n):

$$n = a_0 + a_1 T + a_2 T^2 + a_3 T^3 \qquad (9)$$

EXPERIMENTAL WORK

A modified Fann model 35SA co-axial cylinder rotary viscometer was used to determine the rheological behavior of Sarir crude oil. The viscometer was earlier modified to control the temperature at any predetermined value or vary according to some program. A 6 mm diameter copper tube was tightly wound around the cup and thereafter insulated. A programmable thermostatic circulating bath was used. It was possible to control the temperature to within 0.2°C. The Sarir crude oil used in the present investigations was the pipeline crude, collected from 34 inch Sarir–Tobruk main line. Initial properties and rheological tests indicated that small amount of light components originally present in the crude oil had flashed out during the sampling. The losses were made up prior to

the rheological testing. The properties of Sarir main line oil as reported by the Sarir field laboratory were used as reference for the reconstitution. In order to simulate the pipeline conditions as far as possible, the oil sample was taken in viscometer cup at 54.5°C. The oil was then cooled at a rate of 1.0°C/hr until the measuring temperature was reached. Since waxy oils are structurally sensitive, different experiments were planned for different shear rates. The shearing was continued until the asymptotic conditions were reached. The qualitative description of the conditions prior to reaching the asymptotic conditions are given in Fig. 2. Whereas Fig. 3 provides the asymptotic data (actual) in the form of flow curve.

The yield strength or the gel strength was determined by:

- first cooling the sample under dynamic conditions and
- subsequently cooling at static (without shearing) to the final measurement conditions

The gel strength was determined at the lowest possible speed of rotation corresponding to a shearing rate of $5.11\,s^{-1}$. The maximum deflection was taken as the Initial Gel Strength (IGS) and the deflection after one minute and ten minutes were taken to calculate one minute and ten minutes Gel strengths. The difference between different strengths is an indication of the thixotropic nature of the oil.

RESULTS AND DISCUSSION

Equation 10 provides the temperature dependency of the consistency index.

$$\ln \ln(k+5) = 154.829 - 26.981 \ln T \qquad (10)$$

The regression constants of the Eq. 9 are given in Table 3.

Table 3. Flow Behavior Index Coefficients (Eq. 9)

a_0	$-0.92313583 \times 10^{3}$
a_1	0.88226129×10
a_2	$-0.28116445 \times 10^{-1}$
a_3	$0.29908855 \times 10^{-4}$

The viscosity of oil in the Newtonian range (above

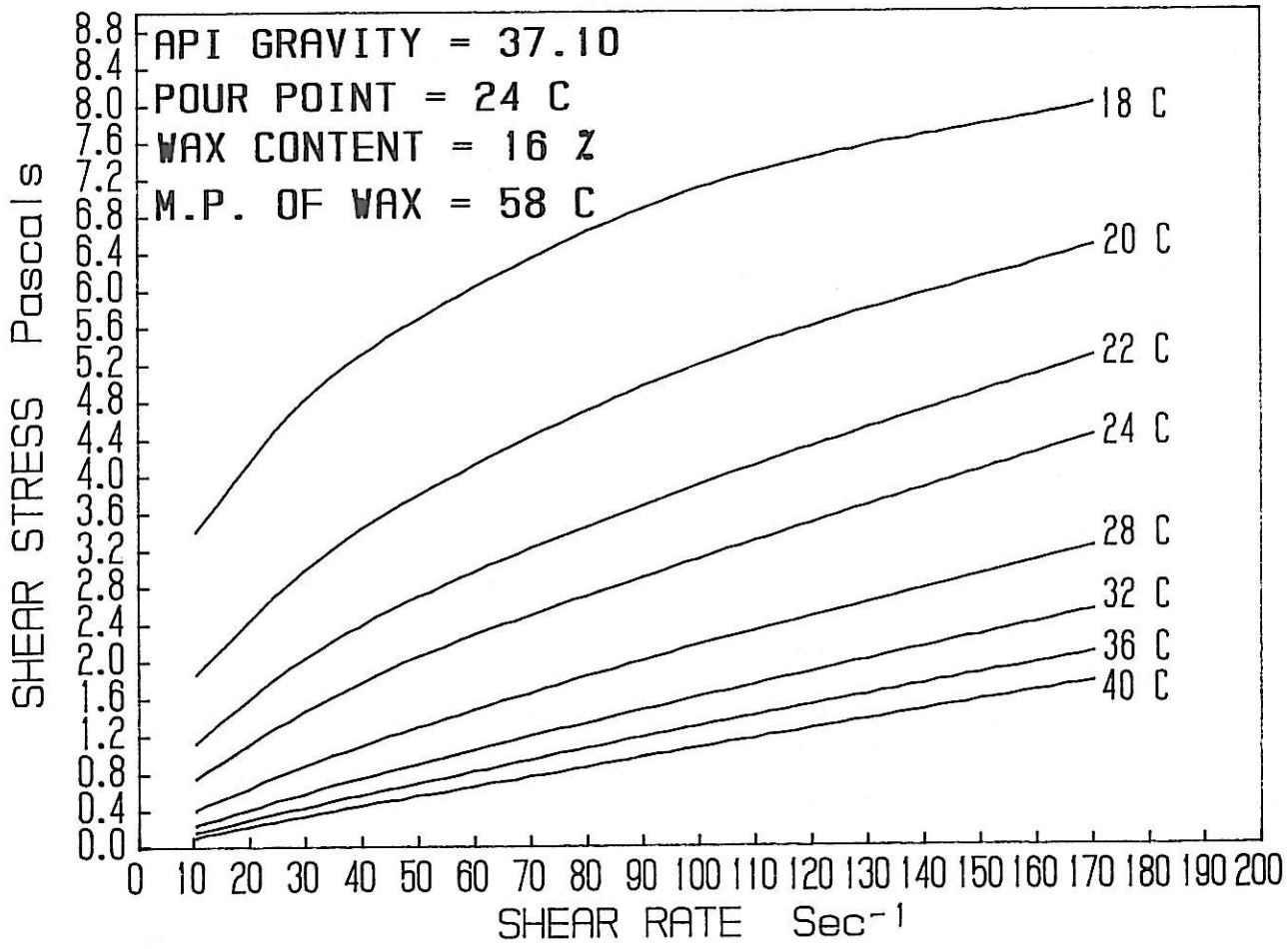


FIG. 3. Flow curves for the waxy oil.

40°C) was correlated by using Eq. 11:

$$\ln \ln \mu = 3.58479 - 0.731745 \ln(T°C) \quad (11)$$

It is obvious from Fig. 4 that the asymptotic value of the apparent viscosity rises steeply as the pour point (24°C) approaches. This reflects the influence of the formation of the oil cages or traps. The rate of cooling was very slow and therefore only plate shape crystals could grow under these conditions. Figure 3 indicates that the oil is very sensitive to the shear strain at temperatures below above 3 to 4°C of the pour point. For example at 20°C the apparent viscosity decreases by half by increasing the shear rate three times. Similar effect is also seen on the Flow behavior index (n). The value of n (Table 4) departs

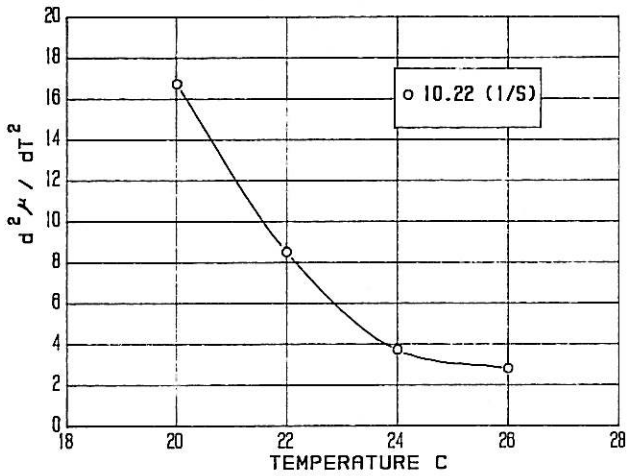


FIG. 4. Viscosity–Temperature relationship.

significantly from unity as the temperature is lower below 24°C, the pour point of the crude.

Similar behavior was also noticed by Fariss [6] and Smith [13].

Table 4. Power Low Parameters for the Waxy Oil

Temperature Deg C	K Pa. S	n
20	0.66098	0.44584
24	0.17591	0.62599
28	0.07622	0.72655
32	0.035732	0.82800
36	0.021605	0.88910
40	0.014362	0.93670

Table 5 gives the yield stress data for a measurement (final) temperature of 29°C. Ford *et al.* [9] used Sarir crude oil in their investigations to determine the yield strength. A model pipeline apparatus initially pioneered by Shell Co. [7] was used by them. Table 6 presents the data collected by Ford *et al.* [9]. A comparison of the data from two different apparatus is provided in this paper. The yield strength was found to be 141.0 Dynes/sq. cm. at 29°C (Table 5). Ford *et al.* [1] reported the yield strength at 29°C to be zero. A different type of apparatus was used by

Table 5. Gel Strength of the Sarir Waxy Oil at 29°C
(Initial temp. = 54.5°C, Static cooling from 30°C)

	Dynes/Sq. Cm.
Initial	141.6
1 Minute	88.5
10 Minute	63.2
(Total cooling time	5.6 Days)

Table 6. Gel Strength of the Sarir Crude Oil from the Reference Ford *et al.* [8]

Initial oil temp.	Final oil temp.	IGS
26.7	23.9	0.0
26.7	22.2	18.0
26.7	21.1	35.0
26.7	18.9	100.0
23.9	22.2	18.0
23.9	18.9	100.0
23.9	21.1	7.0

them. This indicate the importance of the measuring method on the yield value. Similar trend in the yield strength was also noticed by other workers [14]. Different techniques employed to measure the yield strength were:

- Rotary viscometer
- Short capillary tube (Few centimeters)
- Long capillary tube (Few meters)
- Model pipeline apparatus (15 meters)
- Commercial lines

The short capillary tube gave the highest yield strength and the model pipeline gave almost the right value (as compared to actual data). The viscometer also gave higher values and one of the reasons advanced [13] was the loss of light components and gases during the measurement. Perhaps the loss of light components from the oil sample partially explained the high value of yield strength obtained in the present work. Further work would be required to study the influence of the light components on the yield strength.

CONCLUSIONS

- Waxy crude oils behave as thixotropic fluids below 10 to 15°C above the pour point.

- The asymptotic behavior of oil was found to be pseudoplastic with yield pseudoplastic behavior below 5 to 10°C above the pour point.
- Power low model could be used to correlate the flow properties.
- The consistency index was correlated to temperature by using Walthers type equations and the flow behavior index using polynomial fitting.
- The yield stress measurements were found to be very sensitive to the measuring system and the conditions. The coaxial cylinder viscometer gave high yield values.

RECOMMENDATIONS

- The apparent viscosities, measured in the present work need to be compared with the effective viscosity values in the commercial lines.
- The yield strength should be determined using model pipeline apparatus.
- The influence of pipeline deposition on pressure drop, pipeline roughness and finally on the effective viscosities requires further investigations. It is recommended that field scale or pilot scale pipeline set-up should be constructed to study the rheological and deposition properties of the crude oil.

ACKNOWLEDGEMENT

The authors are indebted to the Manager and Staff of Sarir Field Laboratory of Arabian Gulf Oil Company (AGOCO) for supplying the crude oil sample used in our work and some other information related to Sarir–Tobruk pipeline.

NOMENCLATURE

$a_0, \ldots a_3$	Constants
A, B, C	Constants
K	Consistency index
m	Constant in Eq. 5
n	Flow behavior index, (dimensionless)
p	Pressure, (pa)
S	Shear rate, (Sec^{-1})
T	Temperature, (Deg K)
X	Distance, (m)

Greek

μ	Viscosity, (Pa S)
τ	Shear stress, (Pa)
τ_0	Yield stress, (Pa)

REFERENCES

[1] Ford P.E., Ells J.W. and Russel R.J., 1965, Handling High Pour Point crudes in pipelines, American Petroleum Institute Pipeline Conference.

[2] Sifferman T.R., 1978, The flow properties of difficult to handle waxy crudes, SPE paper No. 7409 Sept. 1978.

[3] Hansen J.H., Fredenslung Aa., Pedersen K.S. and Ronningsen H.P., 1988, A Thermodynamic Model for Predicting Wax Formation in Crude Oils, AICHEJ, vol. 34, 1937.

[4] American Petroleum Institute, 1976, Technical Data Book Petroleum Refining.

[5] Mazee W.M., 1975, Petroleum Waxes in Modern *Pet. Tech.* by G.D. Hobson, 4th ed. (1975) Applied Science Publications.

[6] Fariss T.F. and Desouky S.E.M., 1990, Calculations Allow Program to Design Pipelines for Waxy Crudes, Oil and Gas J. 88, No. 1, 69.

[7] Shell Chemicals, 1976, Wax Problems with Sarir Crude Oil, Rept. No. Cr/K/1/77.

[8] Iran C. and Zajak J., 1982, Handling of High Pour Point West African Crude Oil, J. of *Pet. Tech.*, vol. 34, No. 2, 289.

[9] Ford P.E., Ells J.W. and Russel R.J., 1965, Frequent Pigging help move waxy crude below its pour point, Oil and Gas J., vol. 63, 183–89.

[10] Burger E.D., Perkins T.K. and Striegler J.H., 1981, Studies of wax deposition in the trans Alaska pipeline, J. of *Pet. Tech.*, vol. 33, 1075.

[11] Weingarten J.S. and Eucher J.A., 1988, Methods of predicting wax precipitation and deposition, SPE *prod. eng.* Feb. 121.

[12] Holland F.A., 1973, Fluid Mechanics for chemical engineers, p. 9–10 Edward Arnold, London.

[13] Smith B., 1979, Pumping heavy crudes, Oil and Gas Jl., vol. 77, No. 21.

[14] Private communication.

PRJ, Vol. 3 (January 1991); P. 27–34, 13 FIGS.

ACOUSTIC PROPERTIES AS FUNCTION OF DEPTH IN THE GULF OF SUEZ, EGYPT

Adel A.A. Othman* and G.H. Hamada**

خصائص انتقال الموجات الصوتية كدالة للعمق في خليج السويس بمصر

د. عادل علي علي عثمان ، د. حمادة غريب

يتعلق إضمحلال الموجات السيزمية وسرعاتها بالصفات والخصائص الطبيعية للصخور. تتغير العوامل المتحكمة في هذه الصفات معتمدة على الحالة الفيزيائية المؤثرة في الصخور.

في الدراسة الحالية ، تم إجراء مضاهاة تفصيلية بين إضمحلال وسرعة وتردد الموجات السيزمية. كذلك تم إختبار الصفات الصوتية للتغيرات الصخرية ، أما تأثير العمق على درجة الحساسية لهذه المعاملات فقد درست بالتفصيل.

ABSTRACT

Seismic wave attenuation and seismic wave velocity are related to the physical properties of rocks. The controlling factors of these properties are varying, depending upon the physical conditions of the rocks.

In the present study, a detailed correlation between the seismic wave attenuation, seismic wave velocity, and propagating frequency has been reported. The sensitivity of the acoustical parameters to the change of lithology is well tested. The effect of depth on the degree of sensitivity of these parameters is also studied.

INTRODUCTION

The relative sensitivity of velocity and attenuation as a function of lithology has been a contro-versial matter. Extensive processing and analysis of the recorded seismic data and integrating the results with geological information from other sources like well logs, can often make accurate estimates of the subsurface geology, together with lithology, depositional environment and, in some cases, the fluid content.

*Geology Dept., Al-Azhar University, Nasr City, Cairo, Egypt.
**Min. Pet. and Metal. Dept., Cairo University, Giza, Egypt.

Many attempts have been made by the seismologists throughout the history of seismic exploration, to reduce the amount of uncertainty and the number of unresolvable problems. The exact nature of the travelling seismic signal or its waveform, and its distortion and attenuation by the medium are not quite clear and are still questionable.

Vertical seismic profile (VSP) data can provide information that decrease some types of uncertainties and can help to resolve many of them. McDonal *et al.* (1958), and Tullos *et al.* (1969) have measured in-situ attenuation of seismic frequencies. Attwell *et al.* (1966) and Hamilton (1967) have conducted experiments on attenuation and they found a linear relationship between attenuation and frequency. An important contribution using VSP was made by Hauge (1981).

The objective of the present study is to measure the cumulative attenuation termed by Hauge (1981) on one VSP, the average velocity and the average frequency. These parameters were plotted against depth and were shown side by side with the composite log to emphasize the response of each parameter to variations in lithology.

GEOLOGIC SYNOPSIS

The topmost 1200 feet of the geologic section encountered in the studied well is predominantly

sandstones with a limestone bed occupying the depth interval from 1525 to 1800 feet and minor shale, limestone and anhydrite intercalations through the rest of the interval. At the base of this interval, another type of anhydrites and shales of cyclic nature starts which was deposited alternatively, with one salt intercalation. This interval goes down to a depth of 4825 feet. The depth interval from 4825 down to 7100 feet is occupied by rock salt with five minor intercalations of anhydrites and shales. Below 7100 feet and to a depth of 10 450 feet, the section is dominated by shaly sandstones with frequent thin beds of limestone sandstones with frequent thin beds of limestone through the entire depth interval. The interval includes also a 300 feet thick anhydrite-shale bed at the upper part, and another one 30 feet thick at 10 000 feet depth.

THEORETICAL CONCEPTS

The displacements associated with propagated seismic waves in a medium can be written as:

$$U_{x_2}(f)=G_x(x)U_{x_1}(f)\,e^{-\alpha x x}\,e^{i\omega(t-(x_2-x_1)/v)};\quad x_2>x_1 \qquad (1)$$

where α_x is the spatial attenuation between distance x_1 and x_2. $U_{x_1}(f)$ is the reference spectral amplitude. x is the distance difference from the reference event. v is the velocity of the propagated wave in the medium. ω is angular frequency. $G_x(x)$ is a geometrical factor which includes spherical divergence, reflections, transmissions, between distances x_1 and x_2. Knopoff (1964) and McDonal *et al.* (1958) assumed that the spatial attenuation is a linear function of frequency. In the present study, we will assume that α_x varies linearly with frequency and is expressed in decibel as:

$$\alpha_x(f)=\beta_x f/8.686 \qquad (2)$$

with:

$$\beta_x=\int_{x_1}^{x_2}\beta_0\,dx \qquad (3)$$

Where the factor β_x is a function of the separation distance (x_2-x_1), and cannot be considered as intrinsic rock property. By considering the constant Q-model in this work, this leads to express β_x as frequency independent factor.

This factor β_x will be refered as cumulative attenuation (Schoenberger *et al.*, 1978; Hauge 1981). β_0 is the interval attenuation over the separation interval $[x_1, x_2]$. It is equal to

$$\beta_0=\pi Q_i^{-1}/v_i \qquad (4)$$

where v_i is the interval velocity over the separation interval $[x_1, x_2]$ and Q_i^{-1} is the specific dissipation factor also over the same separation interval.

An important concept is the validity of the assumption that the geometric factor has the same frequency independence allower the separation interval $[x_1, x_2]$. The spatial attenuation may be expressed as function of delay time between the sample event and the reference one (Tullos *et al.*, 1969; Hauge, 1981).

By using the decibel units (dB) for calculating the interval attenuation β_0, equation (4) will take the following form:

$$\beta_0=27.2878\,Q_i^{-1}/v_i \qquad (5)$$

Combining equations (1), (2) and (3) leads to:

$$U_{x_2}(f)=G_x(x)U_{x_1}(f)\,e^{-x\beta_x f/8.686} \qquad (6)$$

The spectral ratio method is merely a rearrangement of equation (6) as:

$$\ln U_{x_2}-\ln U_{x_1}=-x\beta_x f/8.686+\ln G_x \qquad (7)$$

where U_x is now taken as the reference pulse, the pulse to which all other pulses are referenced. Equation (7) may be written as follows:

$$\ln\left(\frac{U_{x_2}}{U_{x_1}}\right)=-x\beta_x f/8.686+\ln G_x \qquad (8)$$

The ratio on the left side of equation (8) is linear with respect to frequency and has negative slope $x\beta_x$ which can be determined via least-squares technique. After values of β_x are determined for all depths, they are plotted versus depth to produce cumulative attenuation curve.

MEASUREMENT OF ACOUSTIC PROPERTIES

The lateral subsurface stratigraphic changes, related to water or petroleum presence, might be observed on surface or VSP seismic profile. In the present study a trial to measure acoustic properties at different depths in a well drilled in Gulf of Suez offshore area, to determine if significant lateral changes in stratigraphic horizons correspond to acoustic changes in these horizons.

(1) Measurement of Attenuation

Attenuation is the observed decrease in the amplitude of a transmitted seismic wave that cannot be calculated by geometric effects. Attenuation is usually a small quantity that is difficult to measure, especially

in-situ. This attenuation includes losses in amplitude due to anelastic effects and to scattering.

VSP can be used to correlate the relationship between attenuation and significant rock parameters such as sand percentage or sand–shale ratio. Therefore, attenuation can be a useful diagnostic property in seismic stratigraphy and reservoir investigations.

The relation between attenuation and lithology was made by Hauge (1981). The accuracy of the slope of cumulative attenuation curve depends on the density of observations (Spencer *et al.*, 1981).

By using Eq. (8), the estimated β_x values for all depths are plotted in Fig. 9. The cumulative attenuation, increased by increasing depths (Fig. 9). The values range from 0.025 to 0.08 dB/Hz.

(2) Predominant Frequency Calculation

Average frequency is the parameter that normally describes the predominant frequency, which is the frequency with maximum amplitude spectrum. Since higher frequencies decay faster than lower ones, this parameter is expected to decrease with travel path.

The average frequency changes with depth may be used as a measure for the wavelet shape changes also with depth. Sheriff (1983), has defined an expression for calculating the average frequency of a downhole event as follows:

$$f_{ave} = \left\{ \sum_{i=0}^{n} f_i U_x^2(f_i) \right\} \Big/ \left\{ \sum_{i=0}^{n} U_x^2(f_i) \right\} \tag{9}$$

In Eq. (9), f_{ave} is the average or predominant frequency of the wavelet at depth or distance equal to x from source. f_i is the *i*-th frequency value of the amplitude spectrum. $U_x(f_i)$ is the amplitude spectrum at distance x. The low and the upper boundaries of the summations run over all the discrete frequencies f_i up to the Nyquist frequency. The calculated average frequency are plotted against depth and shown in Fig. 10.

(3) Estimation of Average Velocity

Velocity analysis for real seismic surveys is necessary. The main sources of velocity information are the velocity log and a check-shot survey that should have been run in the borehole, and the travel time of the VSP direct wave. Kohler and Koenig (1986) found errors by comparing the calculated traveltimes of the direct wave with the traveltimes picked in the VSP records. These errors are quite clear for large offsets, while for zero offset the traveltime were correct. They explained these differences as due to a laminated structure velocity anisotropy. Salo and Schuster (1989) demonstrated that the velocity structure can be reconstructed using both reflected and direct-wave traveltimes from VSP data. The velocity errors estimated by using only direct-arrival traveltimes are 6.08% but are 4.72 percent in case of using direct- and primary-arrival traveltimes in VSP velocity inversion (when the layers are horizontal). Kennett *et al.* (1971) discussed the velocity measured from well velocity surveys and the use of calibrated acoustic logs.

In the present study, the first arrivals were detected at different levels in a well drilled in the Gulf of Suez. The average velocity along the source-receiver offset is given by the general form (Al-Chalabi, 1974):

$$v_{ave} = (1/T) \int_0^T v_{inst}(t)\, dt \tag{10}$$

where v_{inst} is the instantaneous velocity, defined as the velocity in an infinitesimally small interval, and T is the total travel time.

The next expression will be used for the average velocity along the normal incidence trajectory for the VSP data:

$$v_{ave} = (1/T_0) \sum_{n=1}^{N} v_n (t_n - t_{n-1}) \tag{11}$$

where T_0 is the total zero offset time. v_n is the *n*-th interval velocity over the interval time $[t_{n-1}, t_n]$. N is number of sample intervals. T_0 can be written as:

$$T_0 = \sum_{n=1}^{N} t_n - t_{n-1} \tag{12}$$

Figure (11) shows the average velocity measured in feet per second plotted against the depth in feet.

DATA HANDLING AND DISCUSSION

The analysed VSP, acquired off-shore in the Gulf of Suez, was digitized only for the direct, downgoing events at an equal sampling rate equal to 0.0025 second. The spectral band-width equals to 200 Hz. This sampling interval turned out to be most suitable; because spectral amplitudes at frequencies higher than 120 Hz are negligibly small. Deconvoluting the source pulse was conducted on the assumption that since the firing pressure was constant, at 120 bars, throughout the recording, the spectral ratios should eliminate its effect.

The reference pulse and the frequency range in this technique over which the cumulative attenua-

tion is calculated are chosen by trial and error. The best results were obtained, with the reference pulse at 1200 feet and a least-squares fit of the spectral amplitude ratio taken between 10 and 100 Hz. To smooth out the spectra for the effect of finite pulse duration, a time domain filter is considered. The Hanning window was used, which is given by:

$$u(t)=0.5-0.5\cos(2\pi t/T_c); \qquad 0\leqslant t\leqslant T_c \tag{13}$$

where the T_c is the truncation interval. Different time windows were tried out; e.g. the Hanning, trapezoidal, and the rectangular window. The Hanning proved to be most appropriate and did not alter the original spectral texture, at least not below 140 Hz.

The amplitude spectra were calculated using the discrete Fourier transform which is given by (Brigham, 1974)

$$U(n/Nt)=\sum_{K=0}^{N-1} u(kt)\, e^{-i2\pi nk/N} \tag{14}$$

$$n=0, 1, 2, \ldots, N-1$$

where N is the number of digits, t is the sampling interval, u(kt) is the sample amplitude, U(n/Nt) is the Fourier transform which was normalized for varying truncation intervals.

Figures 1–7 show plots of frequency spectra of the downward-travelling first arrival at different depths of 1200, 1800, 2600, 4400, 5600, 7600, and 10400 feet, respectively. The plots show the spectral amplitude in decibel which is normalized to the maximum amplitude. In general, the amplitudes have been normalized, trace by trace, so the amplitude loss due to the increase of depth cannot be seen in these figures. This can be easily seen in the composite plot in Fig. 8.

Having accepted the assumption that the attenuation is roughly proportional to frequency, the cumulative attenuation at different depths has been calculated. The overall picture of the cumulative attenuation curve increases with increasing depth. Generally, lithologic zonation can be established. Rate of cumulative attenuation increases over the intervals dominated by sandstones. On the other hand, it is relatively constant, with the rate of interval attenuation being approximately zero over the intervals occupied by anhydrites and rock salt.

Another important point is the lateral changes of the recorded event from a target stratigraphic horizon. This might indicate significant change in rock lithology like porosity build up or sand pinch out. These changes may be expressed also in frequency domain; i.e. the propagating predominant frequencies. According to Fig. 10, it is noticed that higher frequencies events are shown in shallow depths. Hence, the higher frequency events suffer small attenuation. (Figs 9 and 10).

The average velocity as a function of depth, shown in Fig. 11, could be differentiated on the basis of the curve gradient into five distinct zones, which roughly correspond to the topmost sandstone zone (from 1000 to 3200 feet), the anhydrite-shale zone (from 3200 to 4800 feet), the salt-zone (from 4800 to 7100 feet), the shaly sandstone-limestone zone (from 7100 to 9600 feet); and the bottom of sandstone zone (from 10400 to 10700 feet). No further information on the variations in lithology through each zone could be drawn from the plot.

A closer look into the fine texture of the cumulative attenuation curve, Fig. 13, reveals two outstanding phenomena that correlate well with two lithologic identities, consequently meriting some detailed discussion. First the physical unrealisable phenomenon of negative attenuation, which is confirmed by increasing average frequency. This is particularly prominent over the depth intervals 5600 to 6000 feet and 7200 to 7600 feet. On the composite log, the only common thing at these two intervals is the presence of anhydrites. This anhydrites caused some sort of compensation and attenuation to the propagated waveforms. Secondly, the leaps of cumulative attenuation values at depths equal to 1400 and 8800 feet, correspond to limestone beds. The average frequency curve, Fig. 13, shows the leap at 8800 feet which is of

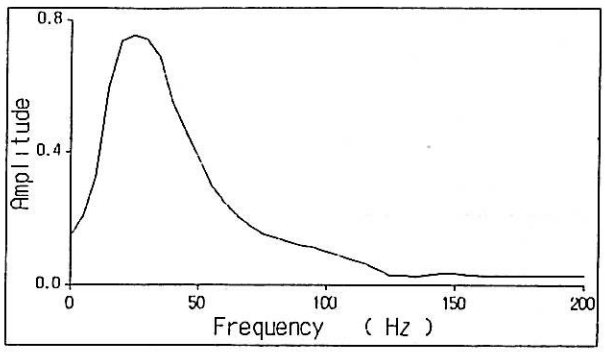


FIG. 1. Amplitude spectrum of seismic pulse at depth equal to 1200 feet.

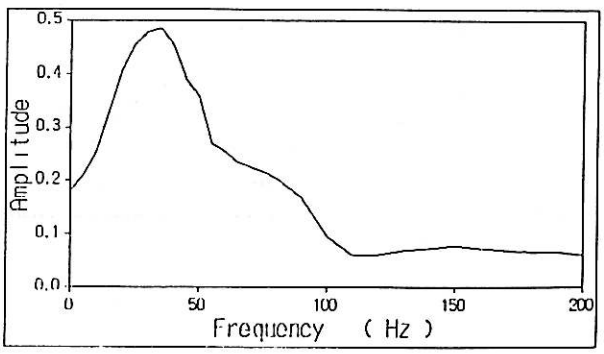


FIG. 2. Amplitude spectrum of seismic pulse at depth equal to 1800 feet.

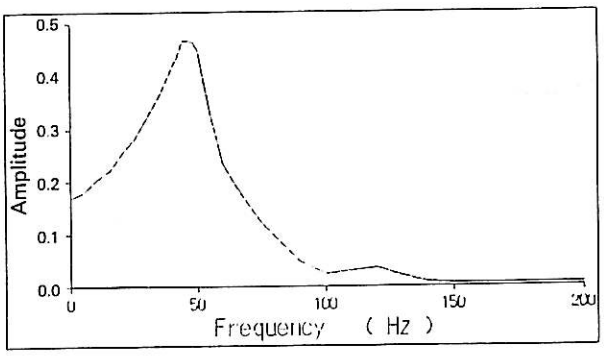


FIG. 3. Amplitude spectrum of seismic pulse at depth equal to 2600 feet.

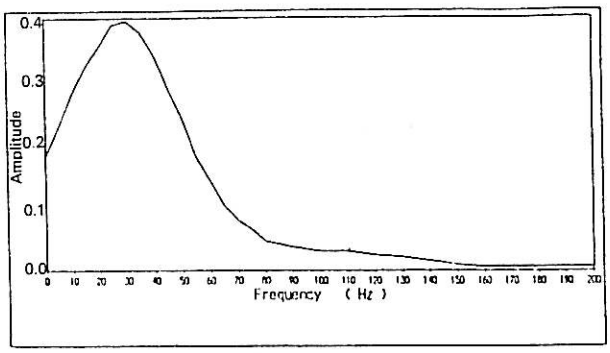


FIG. 4. Amplitude spectrum of seismic pulse at depth equal to 4400 feet.

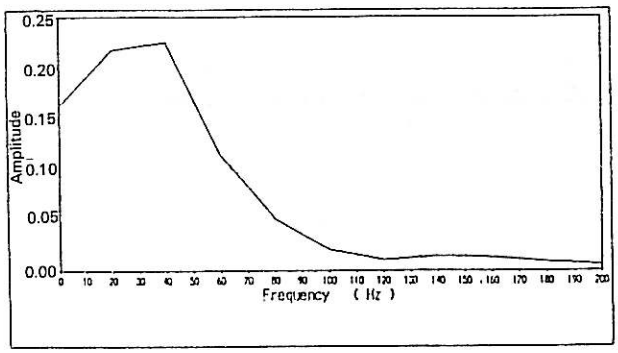


FIG. 5. Amplitude spectrum of seismic pulse at depth equal to 5600 feet.

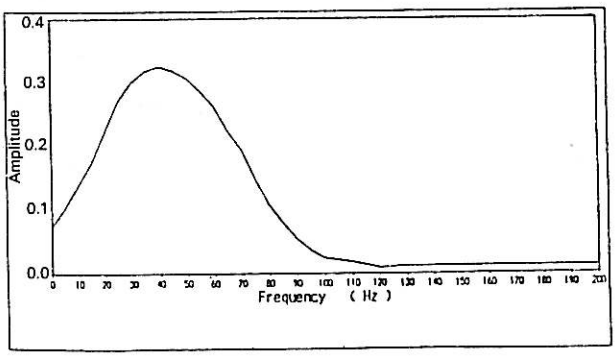


FIG. 6. Amplitude spectrum of seismic pulse at depth equal to 7600 feet.

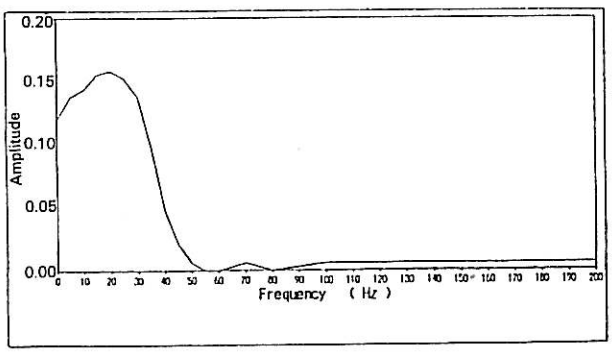


FIG. 7. Amplitude spectrum of seismic pulse at depth equal to 10400 feet.

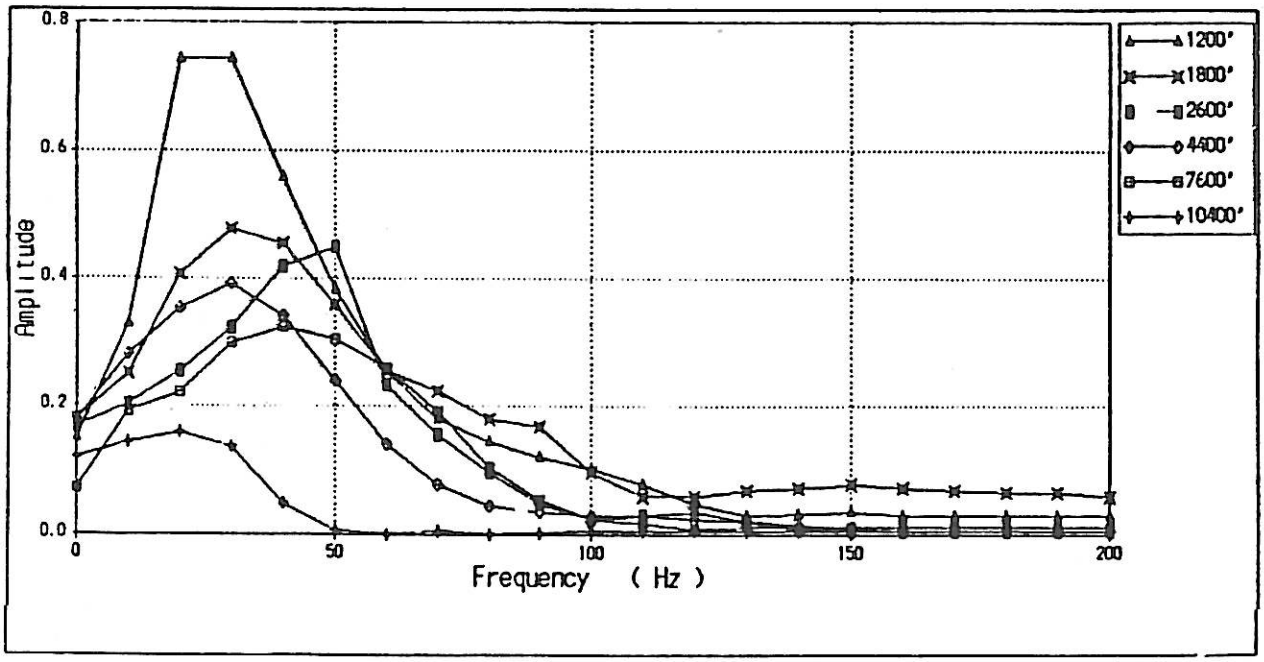


FIG. 8. Amplitude spectra of seismic pulses at some selected depths equal to 1200, 1800, 2600, 4400, 7600, and 10400 feet.

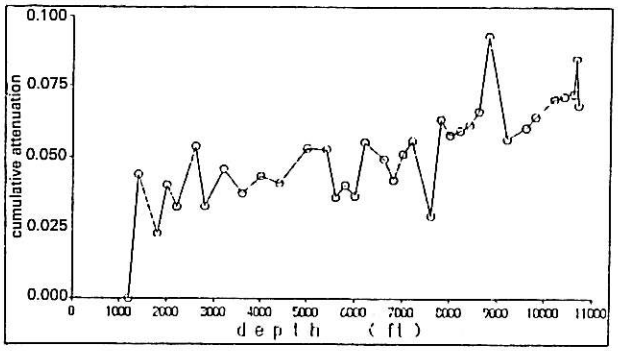


FIG. 9. Cumulative attenuation at different depths calculated over the frequency interval 10–100 Hz.

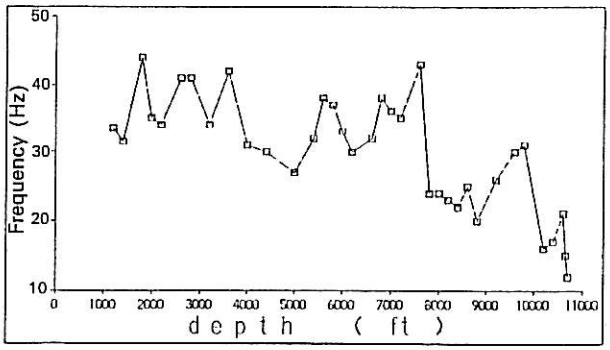


FIG. 10. Predominant frequency calculated over the frequency interval 10–100 Hz.

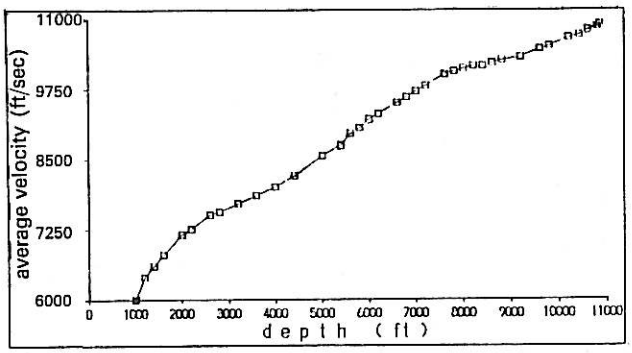


FIG. 11. Average velocity calculated as function of depth in a Well drilled in Gulf of Suez.

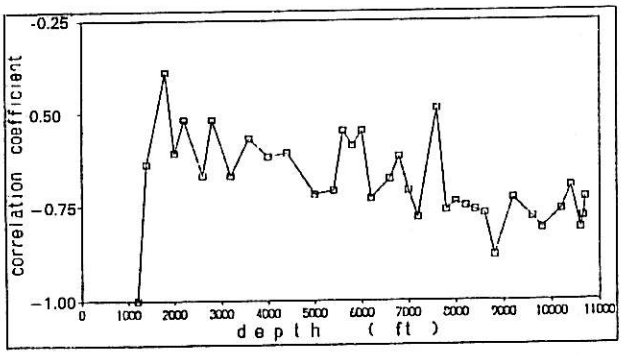


FIG. 12. Correlation coefficients calculated over the frequency interval 10–100 Hz, at selected depths.

a magnitude less than that at 1400 feet, as normally expected for attenuation which tends to decrease with depth due to increasing confining pressure.

The correlation coefficient of the determined attenuation is plotted faced to the geologic composite log (Fig. 12). Their values range between 0.5 up to 0.75, and have increased as cumulative attenuation and depth increased.

CONCLUSION

Attenuation represented by the cumulative attenuation is a far mere sensitive parameter to variation in lithology than velocity and frequency. Two lithologic identities were associated with two prominent phenomena on the cumulative curve. Anhydrites were associated with the phenomenon of negative attenuation and were interpreted as responsible for partial compensation of attenuated downhole pulses.

Limestones were engaged to sudden jumps in values of cumulative attenuation with lower average frequencies, and were interpreted as sources of high attenuative effects. An evident point scatter is shown on the average frequency.

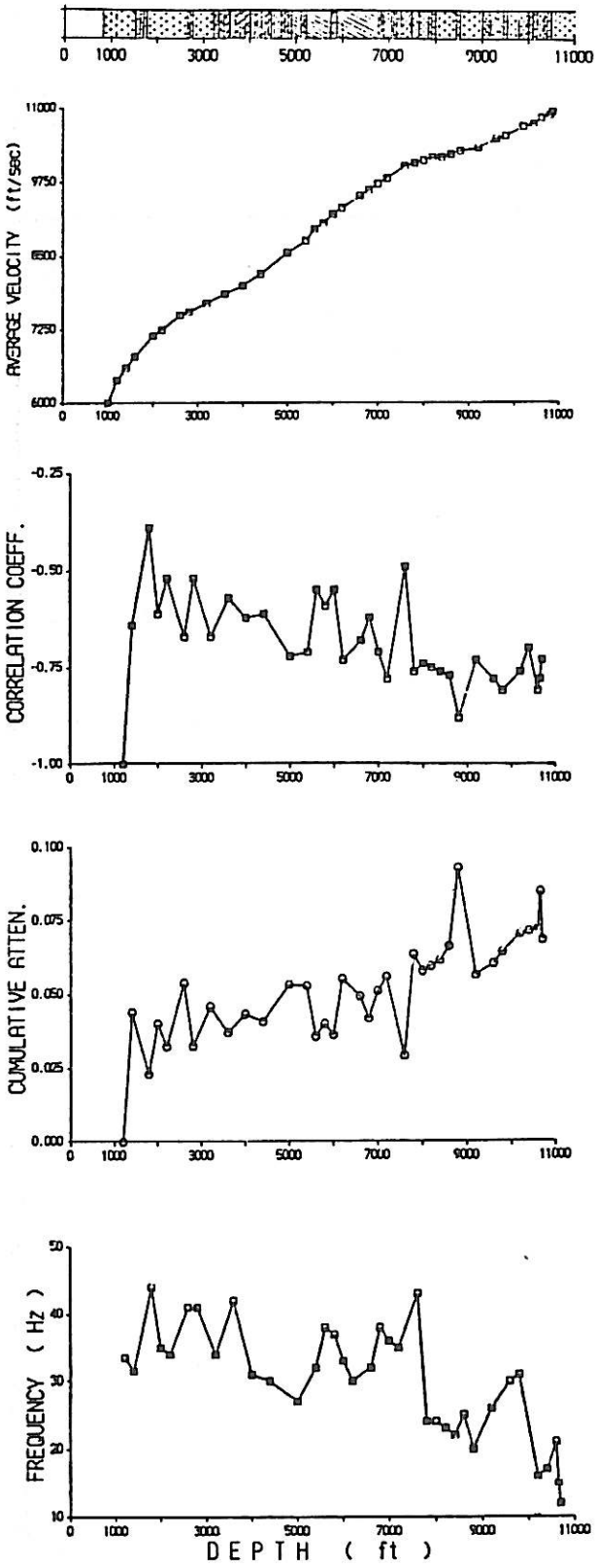


FIG. 13. The average frequency, cumulative attenuation, average velocity, and correlation coefficients as function of depth, correlated with the geologic log.

REFERENCES

Al-Chalabi M., 1974, An analysis of stacking, rms, average, and interval velocities over a horizontal layered ground. *Geoph. Prosp.*, v. 22, p. 458–475.

Attwell P.B. and Ramana Y.V., 1966, Wave attenuation and interval friction as function of frequency in rocks. Geophysics, v. 31, p. 1049–1056.

Brigham E.O., 1974, The fast Fourier transform, Prentice-Hall, Inc., 252 page.

Hamilton E.L., 1976, Sound attenuation as a function of depth in the sea floor. *Acoust. Soc. Am. J.*, v. 59, p. 528–535.

Hauge P.S., 1981, Measurements of attenuation from vertical seismic profiles. *Geophysics*, v. 46, p. 1548–1558.

Kennett P. and Ireson R.L., 1971, Recent developments in well velocity surveys and the use of calibrated acoustic logs. *Geophys. Prosp.*, v. 19, p. 395–411.

Knopoff L., 1964, *Q. Rev. Geophys. Res.*, 2, p. 625–660.

Kohler K. and Koenig K., 1986, Reconstruction of reflecting structures from vertical seismic profiles with a moving source. *Geophysics*, v. 51, p. 1923–1938.

McDonal F.J., Angona F.A., Mills R.L., Sengbush R.L., van Nostrand R.G. and White J.E., 1958, Attenuation of shear and compressional waves in Pierre shale. *Geophysics*, v. 23, p. 412–439.

Salo E.L. and Schuster G.T., 1989, Traveltime inversion of both direct and reflected arrivals in vertical seismic profile data. *Geophysics*, v. 54, p. 49–56.

Sheriff R.E., 1983, Encyclopedic dictionary of exploration geophysics. 2nd edition, SEG, Tulsa.

Spencer T.C., Sonnad J.R. and Butler T.M., 1982, Seismic Q-Stratigraphy or dissipation. *Geophysics*, v. 47, p. 16–24.

Tullos F.N. and Reld A.C., 1969, Seismic attenuation of Gulf Coast sediments. *Geophysics*, v. 34, p. 516–528.

PRJ, Vol. 3 (January 1991); P. 35–43, 10 FIGS.

PETROGRAPHY AND DIAGENESIS OF THE LIDAM FORMATION (CARBONATE UNITS)—FROM SELECTED WELLS IN SIRT BASIN, LIBYA

M.T. EL Bakai*

دراسة مجهرية لصخور تكوين الليدام — حوض سرت ليبيا

محمود البكاي

قسم تكوين الليدام إلى وحدتين رئيسيتين هما : وحدة صخور الحجر الجيري ، ووحدة صخور الدولوميت . هاتين الوحدتين تمثلان بوضوح صخور مترسبة في بيئة سطح مدى ، أي ما بين المد والجزر ، وتتكون من ثلاث مناطق بيئية هي : منطقة السبخة ، منطقة مغمورة بالماء ، ومنطقة ما بينها .

من الظواهر الدالة على البيئة السبخية هي الطبقات الطولية المنظمة والغير منظمة ، طبقات الطحالب ، الجبس ، الدلته ، وغياب الحفريات البحرية . أما الظواهر الدالة على وجود البيئة ما بين السبخة والمنطقة المغمورة فهي طبقات رقيقة من الطحالب ، الجبس ، الحجر الرملي ، الدلته ، بعض الحفريات الشوكية وغيرها . أما بالنسبة للظواهر التي تشير إلى البيئة المغمورة كلياً بالماء هي وجود حفريات دقيقة بحرية مثل الشوكيات ، فورامينيفيرا ، اوستراكودا وغيرها .

المسامية والنفاذية في المناطق البيئية الثلاثة لهذا التكوين غالباً ما تكون ثانوية تكونت من جراء ذوبان المواد القابلة لذلك والغير مدلته ، أما بالنسبة للمسامية والنفاذية الأولية فقد أنسدت نتيجة للدلته ، وترسب المواد اللاحمة بين الحبيبات .

ABSTRACT

The Lidam Formation is divided into two units: limestone unit and dolomite unit. These units exhibit clearly tidal flat setting of supratidal, intertidal and subtidal.

The most indicative features of supratidal environment is the regular and irregular laminae (aggregates of pellets) algal mat, anhydrite, replacive dolomite and absence of marine fauna. This particular supratidal environment is present in Masrab high, As-Zahra–Hofra Platform, Beda Platform and Kotla Graben wells P16–59, Z1-59, 3V1-59, F8-59 and F10-59.

The intertidal environment is dominated by algal laminae, anhydrite, quartz and dolomite with echinoderm fragments, ooids and pellets. This environment is present in Ajdaby Trough and Gatter Ridge in wells 5N1a-59, E1-57 and 001–11. The subtidal environment is characterized by mudstone and wackestone facies with abundant marine fauna e.g. echinoderm fragments, ostracods and foraminifera.

Locally at D1-32 L1-32, 01-32, C1-NC57, D1-NC57 wells, (Azahra–Hofra Platform), and DD2a-59 (Ajdabya Trough) oolitic grainstone with peloids and bioclasts are abundant with indication possibly of shallow shoals reflecting high energy conditions. From the lateral distribution of the Lidam Formation one can conclude that the supratidal and intertidal environments were formed mainly on highs, during the Cenomanian transgression (Vail et al., 1977).

Porosity of intertidal and supratidal environments of the Lidam Formation is mostly secondary, generated by dissolution of materials survived from dolomitization. However, primary porosity either in subtidal or intertidal-supratidal environments had been totally occluded during cementation stage of diagenesis.

Dolomitization of matrix, marine cementation and dissolution are the most diagenetic stages which took place in the different environments of the Lidam Formation in the Sirt Basin.

*Petroleum Research Centre, Tripoli, G.S.P.L.A.J.

INTRODUCTION

The Cenomanian period began with marine transgression advancing from the north and NW towards the south (Klitzsch, 1981). The Cenomanian strata in the Sirt Basin are principally carbonates and shales. These carbonates (Lidam Formation) are widely spread and extending over much of the Sirt Basin. Its thickness varies in structurally high and low areas. Barr and Weegar (1972) concluded that the maximum thickness of the Lidam Formation is more than 600 feet in the middle of the Zella Trough, but the actual maximum thickness is more than 1000 feet in the south Zella Trough (D1-85 well). This formation was deposited in a shollow marine environment (Barr & Weegar 1972).

The Lidam Formation unconformably overlaps various units including the Nubian Formation, the Bahi Formation, and Igneous-metamorphic basement. It is usually overlain by the Upper Cretaceous Etel Formation or its equivalent Argub Formation with apparent conformity. The Lidam formation is considered as Cenomanian in age by Barr & Weegar (1972), who recognised that the rare microfossils of this formation consist mainly of ostracods, miliolids and large benthonic foraminifera, *Ovalveolina Ovum (d'Orbigny)*. This later species is diagnostic of Cenomanian age.

The conclusion in this paper is based on the data collected from selected wells scattered in a wide range all over the Sirt basin.

LITHOLOGICAL TYPE

North West Sirt Basin-North Zella Trough and Azahra–Hofra Platform

The lower part of this Formation is medium to coarse, laminated dolomite with quartz grains scattered through dolomite indicating a local mixing with the underlying sands of the Bahi Formation, and abundance of glauconite pellets. The middle part of the Lidam Formation, in this region, is mainly well cemented oolitic limestone interlaminated with very fine irregular laminae of shale. The dominant bioclasts being echinoderms, brachiopods and molluscs. The upper part is fine, laminated dolomite with anhydrite nodules and glauconite.

South Central Sirt Basin–Beda Platform and Kotla Graben

The lower part of the Lidam Formation, in this area (wells F8-59 and F10-59), is mainly dolomitized limestone, with sand grains indicating a local mixing with the underlying sands. The upper part of the formation consists of a well cemented pellet calcarenite. The pellets exhibit indistinct rings suggestive of an algae origin. Subordinate constituents of this facies include ooids, algae, and miliolids and rare quartz grains.

South East Sirt Basin-Masrab High and Agedabia Trough

The lower part of the Lidam Formation, in this region, is argillaceous dolomitized mudstone with anhydrite (nodular and chicken-wire texture). Pyrite nodules are also observed within this lithology. The dominant bioclasts being echinoderms. This dolomitized mudstone is highly porous in some intervals. The upper part of the Lidam Formation is mudstone partially dolomitized with nodules of anhydrite and interlaminated shale. Pressure solution is quite common. This lithology is overlain by chicken-wire anhydrite which, probably, grades upward to the Etel Formation of Turonian age.

THIN SECTION MICROSCOPY

General Statement

The lithology of the cored interval in the different areas were assessed from the microscopic examination of 131 thin-sections taken from core samples and cuttings at different depths. These samples were collected from specific horizons in order to provide information concerning the lithological variation and reservoir potential of carbonates, evaporites and clastics present in the sequence.

Skeletal Allochems

Echinoderms: Whole crinoids and fragments have been either totally and/or partially replaced by dolomite or still in original condition, i.e. calcite composition (Fig. 1). Some of these crinoids form nucleous of ooids (Fig. 2), while others have a calcite overgrowth cement showing an optical continuity with the grains.

Mollusca: Long shells display prismitic or foliated structure at depth 6934–6935 feet in well D1-32, some of these shells have overgrowth cement. There are also long shells displaying crossed lamellar structure. At depths 10080 feet 5 inches in well P17-59 and in well Z1-59 at depth 10980 feet, the shell fragments of Mollusca have completely been dissolved out and replaced by anhydrite and dolomite (Figs. 3 and 4). At depths 10690 and 10709 feet in well 5N1a-59 there are long bivalve shells preserving original mineralogy and structure.



FIG. 1. Photomicrograph showing echinoderm plates.



FIG. 2. Photomicrograph showing echinoderm being as nucleus of ooids.



FIG. 3. Photomicrograph showing gastropod shell, replaced by dolomite and anhydrite.

Gastropods: Transversal sections through a single gastropods occur. All traces of the original wall structure have been obliterated during inversion either to dolomite or calcite, but the recognizable outlines are preserved (Fig. 2).

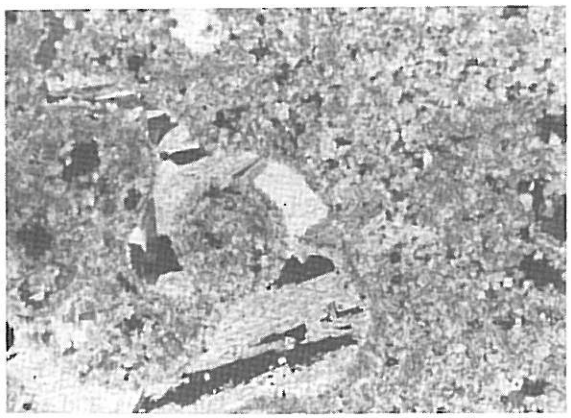


FIG. 4. Some as Fig. 3, but under X.N.

There are also transverse sections of gastropod that have been dissolved out and totally replaced by anhydrite, but their recognizable outlines are preserved. At depth 10690 and 10695 feet in well 5N1a-59, gastropods are partially replaced by dolomite and/or ferroan calcite.

Ostracods: Pairs of valves showing common overlap of one valve over the other exist. Between the valves single crystals of ferroan and non-ferroan calcite or dolomite as a cement phase (Fig. 5) are present. Other ostracods valves were observed in well D1-32 at depth 7122–7137 feet and in well 5N1a-59 at depths 10690, 10695 and 10709 feet, these valves have been totally replaced either by calcite or dolomite, but the recognizable outlines are still visible.

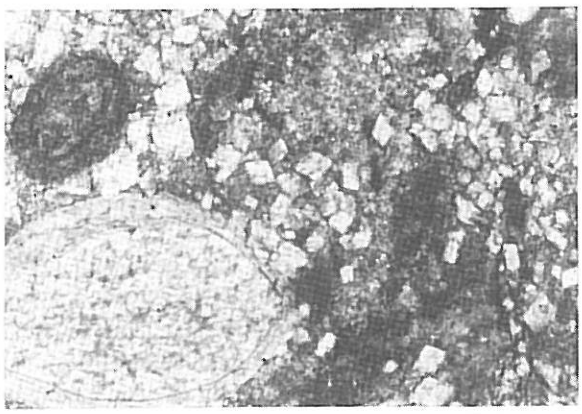


FIG. 5. Photomicrograph showing two halves of ostrocods, and single crystal of calcite and/or dolomite between them.

Foraminifera: In well F10-59 at depth 7606 feet the chambers of globigerinid Foraminifera are filled with calcite, while the chambers of miliolid Foraminifera are filled with neomorphic spar. At

depth 10009–10009–10010 feet in well P9-598, benthonic uniserial Foraminifera have either been dissolved out leaving moldic porosity or partially occluded by dolomite. The dominant skeletal grains in well 5N1a-59 at depth 10690, 10695 and 10709 feet are miliolid and benthonic uniserial Foraminifera. These chambers are generally filled with ferroan calcite. In well N1-32 at depths 5360–5370, 5400–5410, 5440–5450 and 5470–5480 feet, Foraminifera are small and replaced by dolomite. At depth 6975–6976 feet in well D1-32 the miloilid Foraminifera are present as nucleous of ooids within interclasts, their walls have largely been micritized (micrite envelope), and some pores are also filled with sparite. Globigerinids are common in the lower part of the Lidam Formation in well D1-32.

Algae: Not very well developed and laminated blue-green algal mat have been observed in wells P6-59 and P11-59 at depths 10166, 10167 and 10131 feet respectively. These blue green algae are characterized by pelletal texture, irregular lamination (Fig. 6). Well preserved coralline algae are common in the middle and upper part of the Lidam Formaton in D1-32 well.

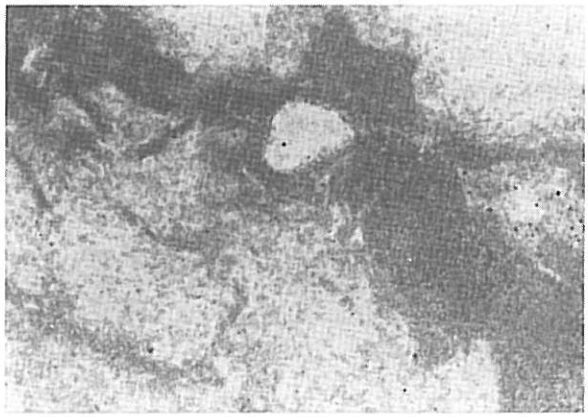


FIG. 6. Photomicrograph showing algal laminae.

Microfossils: At depth 7226-7228 feet in well D1-32 the spherical microfossils (Calcispheres) are well defined, which are difficult to distinguish from uniserial Foraminifera or spherical algal balls. The chambers of these grains are filled either with ferroan calcite or ferroan dolomite.

Non-Skeletal Allochems

Pellets: These grains are observed throughout the dolomite facies; these grains are oval and well rounded. Some elongate micritic grains, have partially been replaced by dolomite. They are probably of Foraminifera or fecal origin.

Stromatolites: Pellets are aggregated together into laminae making stromatolites structure or algal mat associated with anhydrite (Fig. 6).

Peloids: Present in the whole dolomite facies, they are large, rounded and micritized grains, probably of foraminifera or algae origin. Some of these grains are unaffected by dolomite and the micrite of others are slightly aggrading to neomorphic spar.

Incompletely Micritized Particles: At depth 10695 feet in well 5N1a-59, the incompletely micritized particles have low magnesium calcite in the centre and micrite at the outer.

Ooids: In well D1-32 at depth 6975, 6993–7007 and 7029–7058 feet the oolids are well rounded and/or oval, showing concentric and radial structure. Some of these ooids enclose Foraminifera, echinoderm plates and/or a single crystal of calcite or dolomite as a nucleous (Fig. 2).

Interclasts: In well D1-32 at depths 6934, 6975 and 6933–7007 feet and in well 5N1a-59 at depths 10690 and 10695 feet, the interclasts are not very common. They are large, rounded and subrounded micritic grains. They enclose some clastic grains and skeletal fragments, e.g. echinoderm fragments, Foraminifera, ooids, small micritic grains and glauconite grains. Some of these grains are cemented by calcite.

Non-Carbonate Grains

Quartz: Most of the Lidam carbonates contain fine to coarse sand grade, rounded to angular unicrystalline and polycrystalline as well as strained and unstrained detrital grains scattered throughout the dolomite. Well formed authigenic quartz are observed in well 5N1a-59 at depths 10690 and 10695 feet. The quartz percentage increases with depth where the underlying formation is mainly sandstone.

Feldspar: At depth 6974 and 6978 feet in well D1-32, some of the feldspar grains are partially altered to clay, whereas, the rest are largely unaffected. Some strained grains (only one set of twin lamellae) are observed in wells P9-59 and Z1-59 at depths 10051 and 10989 feet respectively.

Glauconite pellets: The glauconite pellets are common in the north-west (D1-32 well). They are moderately to well sorted and are usually larger than the dolomite crystals and quartz grains. The glauconite pellets are mainly well rounded to elliptical with rare irregular and narrow cracks. They occur in three different colours; grass-green pellets, light green pellets and brownish-yellow pellets.

PETROGRAPHY AND ENVIRONMENT OF DEPOSITION

The Lidam Formation in the Sirt Basin can be divided into two major units (Fig. 7).

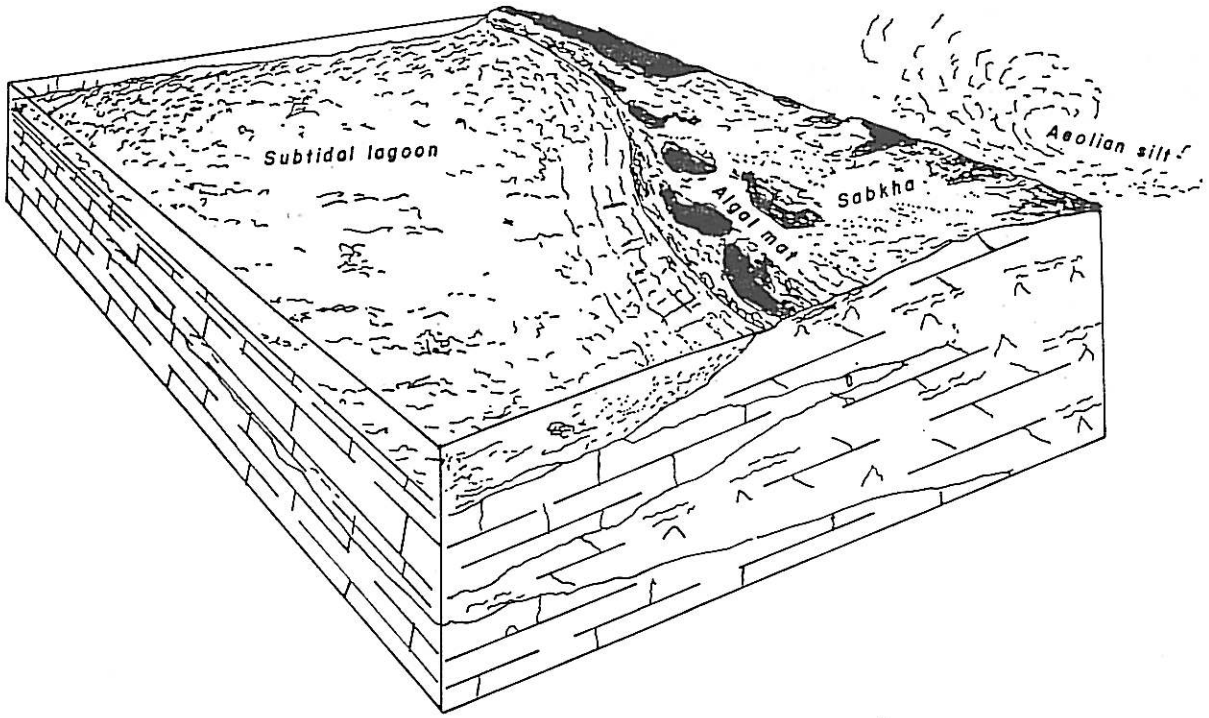


FIG. 7 Idealized Environmental Reconstruction for sedimentation of the Lidam Formation.

The Upper Lidam Limestone Unit

The upper limestone unit has been recognized in the Masrab High and Agedabia Trough, South East Sirt basin (wells 3V1-59 and 5N1a-59), and in the Zella Trough and Azahra-Hofra platform (D1-32 Well).

Petrography: For the unit as a whole, particle assemblages are dominated by diverse fauna comprising molluscs, gastropods, echinoids, ostracods and Foraminifera. Non skeletal allochems are represented by ooids, peloids and pellets, but intraclasts also occur locally. Trace amounts of quartz sand grains and variable clays are the only non-carbonate components. Presence of primary porosity at some intervals; generally the porosity in this facies is scarce.

Primary fabrics: The dominant depositional fabric is wackestone, grading into mudstone with a decrease in alochems. Poorly defined packstone intercalations are present in 3V1-59 and 5N1a-59 Wells. In Well D1-32 the facies show horizons of grainstone. The limestone are generally massive and unbedded, bioturbation is apparent in Well 5N1a-59. Fine scale lamination is preserved in the upper part of limestone facies in this well; suggesting very low energy deposition.

Environment of Deposition: The limestone unit broadly represents carbonate sedimentation in a normal marine shallow subtidal environment (Fig. 8), the biota is diverse and indicates hospitable substrates. The environment was predominantly one of low energy, but the local packstone and grainstone intercalations indicate periods of moderate turbulence and winnowing of lime-mud. More lithological variation is apparent in wells 3V1-59, 5N1a-59 and D1-32. The vertical successions in these wells display broad similarities, especially towards the top of the facies, where evidence of incipient regression is apparent (Wilson, 1975). The sequence takes an upward-shallowing aspect. In these wells there are an upward gradation from packstones with interclasts into wackestones, suggesting decrease in the contemporary energy of the environment towards the top of the facies. Laminated calcareous and unfossilliferous shales form intercalations with the limestone, and the biota in the latter reveals a drastic decrease in diversity. The origin of the shales is uncertain, but they are probably very localized deposits of topographically controlled, restricted lagoons.

The Lower Lidam Dolomite Unit

The contact between the Lower Dolomite Unit, in the wells selected for this study, and the overlying upper limestone unit is everywhere fairly abrupt. The

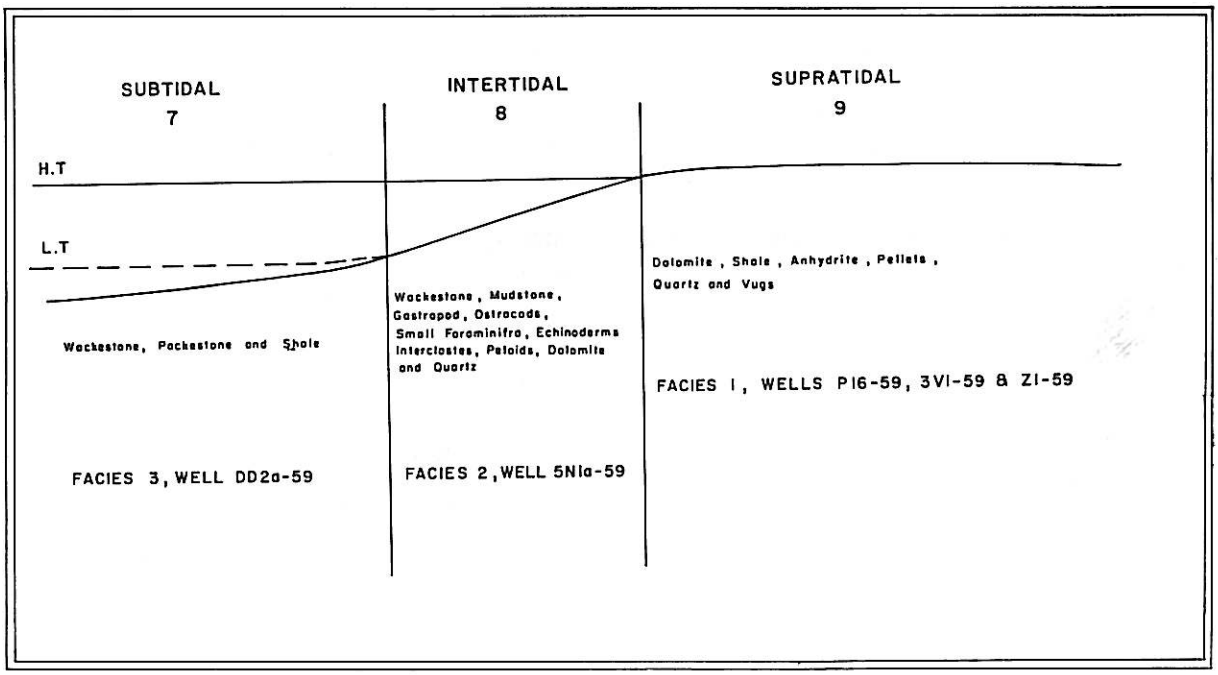


FIG. 8. Generalized Depositional Model for the Lidam Formation.

facies display thin development towards the centre of the troughs and thickest towards the platform.

Petrography: Uniform, microcrystalline "aphantic" to finely crystalline dolomites are the dominant lithologies. Particle assemblages (whether preserved or as relicts) are sparse. Skeletal allochems are representative of low density biota of ostracods, echinoids and algae, while non-skeletal allochems are dominated by abundant fecal pellet materials. Peloids are not widespread. Non carbonate constituents comprising fine sand to silt grade, detrital quartz and clasts of siliciclasts clay, are abundant in 5N1a-59, F8-59 and D1-32 wells rare phosphatic nodules and very common glauconite pellets are also present.

Primary Fabrics: The dominant depositional fabric before dolomitization was probably massive mudstone (argonite lime-mud). Discrete burrows are present. These, often, have fillings of pellets and bioclasts producing pockets of wackestone/packstone (wackestone whole-rock fabric are rare). Algal boundstones representing algal mat developments are abundant in some wells, e.g. F10-59 or P16-59. These are characterized by wavy, buckled laminae or microdolomite. The primary trapped sediments are generally strong pelletal lime-mud, or pelmicrite packstone with small admixture of clay. Associated with these boundstone horizons are nodules of "primary" felted lath anhydrite. The anhydrite, regularly, forms thick cloudy bedded developments displaying well formed chicken-wire structure.

Environment of Deposition: The change form limestones into diagenetic dolomites is indicative of the onset of regression and fairly rapid establishment of supratidal sabkha. Slight variation is provided by 5N1a-59 where an apparent absence of algal boundstone and evaporites suggests that the immediate area did not actually become emergent. But the fabrics present (intense bioturbation, abundant fecal pellets) suggest a nearshore subtidal "lagoon", sufficiently close to the shore line, for diagenetic dolomitization to have been effective. Relatively thick supratidal sequence were build up in A1-17, N1-32, 3V1-59 and F8-59 wells. In 5N1a-59 and D1-32 wells "subtidal", the transgression introduced bioturbation, large interclasts, well cemented ooids and sparse fauna and pushed the shoreline back such that diagenetic dolomitization became less intense. In D1-32 and 3V1-59 wells, the anhydrite algal boundstone fade and gave way to massive dolomites with thin intercalations dolomitic shale; these may represent topographically restricted lagoons generated by the first floodings of the supratidal which stands up as massive/laminated non-evaporitic dolomites with bioturbation fabrics and abundant quartz silt, this lithology is interpreted as a low intertidal flat.

DIAGENESIS

The initial sediments micrite and clay, consisted of skeletal allochems (composed mainly of argonite and calcite), and non-skeletal allochems (ooids,

pellets and peloids). Ditrital grains such as quartz, feldspar, pyrite and glauconite are also present. Most aspects of limestone diagenesis (post depositional changes), can be related to this plan of hydrological zones (Fig. 9). As limestones pass, from their place of origin through them, under the influence of changes in sea level or progradation of the land, then each environment of change places upon the rock fabric.

ment in response to rainfall. Though cementation is not the only process that takes place here, dolomitization is thought to be significant. This variety of dolomite is generally coarsely clean and ferroan crystalline, and the process is very effective leaving little calcite unaltered. As a result, this sort of dolomite is a cement phase. Formation of stylolites (pressure solution) also takes place in this zone.

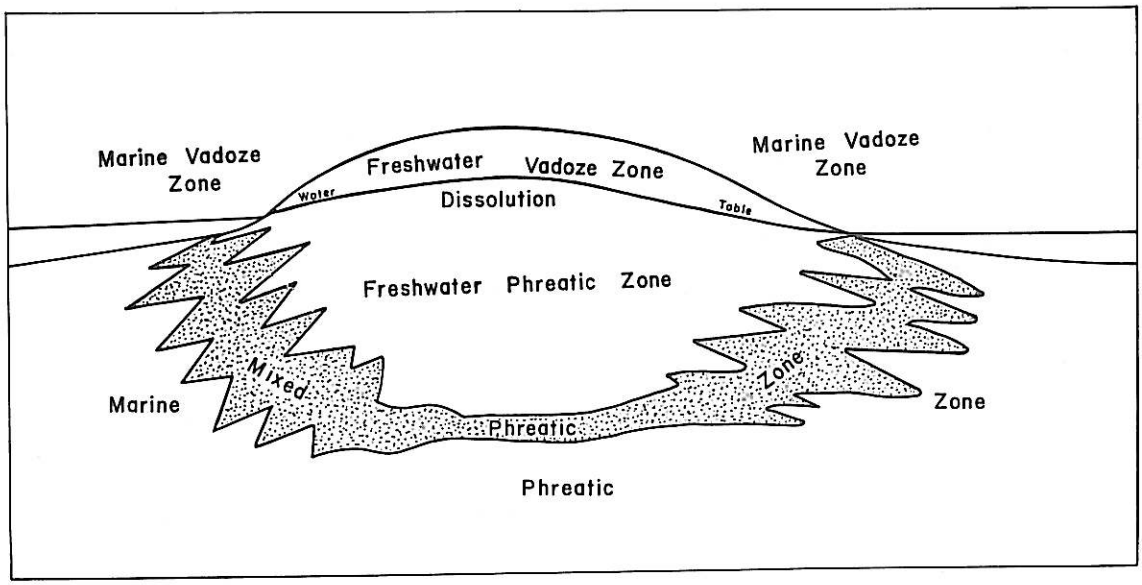


FIG. 9. Major hydrological zones important in carbonate diagenesis.

Terminology

(a) Where all the rock pore-space is filled with water, then the rock is said to inhabit a PHREATIC ZONE (Longman, 1980, 1981). If the water is fresh, this is the Freshwater Phreatic Zone. If the water is brakish, this is the Mixed Phreatic Zone. Phreatic zone extends from beneath the sea to a depth of rock beneath the land, which lies under the Water Table. The transition from marine to fresh occurs over the mixing or mixed phreatic zone.

(b) Where all the pore space is not completely filled with water all the time, but is occasionally filled with air, the rock inhabits the VADOZE ZONE (Longman, 1981).

Marine Phreatic Zone: The active marine phreatic zone is nearest to the seabed, here the water is pumped through the sediments and cementation by aragonite and high-Mg calcite takes place.

Mixed Phreatic Zone: This zone is narrow, but moves backward and forward through the sedi-

Freshwater Phreatic Zone: This is the most important diagenetic zone where rapid cementation and dissolution takes place.

Dissolution: Local dissolution of skeletal grains, non-skeletal grains and relict micrite took place and created different types of porosity.

Cementation: In the saturated active zone, rapid cementation by fringe low-Mg calcite, phreatic ferroan calcite, equant calcite spar and also by anhydrite took place. The water contacts the water table from the vadoze zone having passed down through limestones; it may therefore, be at a variable degree of $CaCO_3$ saturation, depending on the time spent in migration. Solution is therefore, common in the uppermost regions of the phreatic zone.

Dissolution is intense and creates large vugs similar to the freshwater vadoze zone.

Freshwater Vadoze Zone: This zone passes upwards into the soil zones. Calcrets and other deposits may form distinctive units. Evaporation also is important, so the precipitation of calcite took place at the grain contacts (meniscis cement).

Marine Vadoze Zone: In this limited zone environment, beachrock develops. Here, aragonitic microcrystalline cements may blind the deposits. Aragonite and some high-Mg calcite are the major cement types. Evaporation (anhydrite of felted lath, chicken-wire and nodules structure) and early dolomitization (diagenetic dolomite) of xenomorphic to hypidimorphic crystal shape and xenotoic to hypidiotopic texture. This dolomite (pervasive and saddle), which replaced the original sediments, is the most dominant control in this zone.

POROSITY

Types

Porosity is diminished or lost through diagenetic changes e.g. cementation, compaction, dolomitization and pressure solution. Porosity in the Lidam Formation can be divided into two main types according to Choquette and Pray (1970).

Fabric Selective

(a) *Intercrystalline porosity:* This type occurs between dolomite crystals; it is better developed where dolomite is coarsely crystalline (Fig. 10). This type of porosity is created by dissolution of survived micrite and calcite in fresh water phreatic zone.

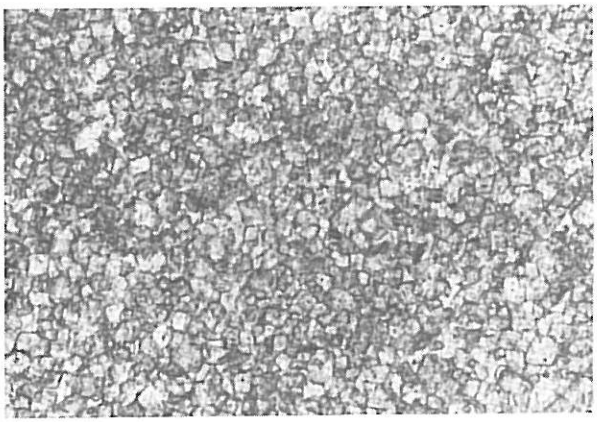


FIG. 10. Photomicrograph showing intercrystalline porosity within dolomatized mudstone.

(b) *Moldic porosity:* It is formed by selective, but extensive, removal of predominantly aragonitic pellet materials. As a result, only relicts of the pellets remain, because micrite commonly fills the interstices between the pelletal grains. The molding porosity, which is more in the intertidal environment, is considered to be comparatively unimportant and ineffective porosity.

(c) *Intraparticle or interskeletal porosity:* This type of porosity is primary. It is present within individual skeletal particles, in miliolid Foraminifera in particular, where the individual chambers remain unfilled in a high energy subtidal environment, e.g. in well F10-59 at depth 7606 feet.

Non-Fabric Selective

(a) *Vuggy porosity:* This type of porosity is generated by leaching out of micrite, calcite, cement and/or bioclasts leaving vugs or by the enlargement of intercrystalline porosity.

(b) *Channel porosity:* This type of porosity is likely solution enlarged fractures. It occurs in wells A1-17 and F8-59 at depths 5776 and 6596–6958 feet respectively.

Distribution

The development of porosity in the Lidam Formation is largely controlled by dolomitization, compaction and freshwater phreatic leaching or dissolution. Generally, good secondary porosity is present in wells located on the highs or platform, but poor or absent in wells located within throughs. However, poor porosity at the supratidal and intertidal environment and moderate to very good porosity at subtidal environments. The most common types of porosity in the Lidam Dolomite is intercrystalline occuring between the dolomite crystals. It is the result of pervasive dolomitization, in some intervals calcite cement has reduced the porosity. Vuggy porosity is the second most common type in the Lidam dolomite. This type of porosity has resulted from dissolution of calcite and anhydrite and/or by solution enlarged intercrystalline porosity. Moldic and intraparticle porosities are developed in subtidal environment (shallow shoals) where the currents are strong enough to winnow away the intertidal micrite particles. The chambers of some skeletal allochems, e.g. Foraminifera remain unfilled.

RESERVOIR QUALITY

Porosity in the Lidam Formation (mainly secondary) has been generated by dissolution of the original lime-mud, which survived from dolomitization or by the dissolution of calcite and anhydrite crystals. The diagenetic changes has also destroyed the primary porosity such as in Well D1-32, where the cement has totally occluded interparticle porosity in the shallow shoal sediments.

Good secondary porosity in Well A1-17 at depths 5644–5655 feet and 5668–5713 feet, but the remaining clay has reduced permeability, so poor reservoir qual-

ity is inferred. In Well F8-59 at depth 10829 feet the secondary porosity is quite good and connected by throats, therefore, good permeability and good reservoir quality is inferred. Generally there is absence of porosity in the limestone unit because of diagenetic changes, so the reservoir quality is poor. Secondary porosity is well developed and connected in some intervals of the dolomite unit, and good reservoir quality is inferred.

SUMMARY

The core material of Cenomanian age collected from the different wells scattered throughout the Sirt basin is divided into two units; summarized as:

1. *Limestone Unit:*

This unit, as a whole, is dominated by oolitic limestone, cemented by ferroan calcite and dolomite (oosparite grainstone and biomicrite wackestone/mudstone) with common galuconite pellets. It is deposited in moderate to high energy environment.

2. *Dolomite Unit:*

This unit is characterized by diagenetic laminated and pervasive dolomite, with good porosity at some intervals. Nodules and chicken-wire structure of anhydrite also occur within the dolomite unit. This unit represents sedimentation in a restricted marine environment.

The petrographic description of samples collected from the different depths, show that the dominant primary depositional fabric before dolomitization is that of massive mudstone, subsequently subjected to arid sabkha type shoreline diagenesis. The dominant type of porosity in the dolomite facies is secondary (intercrystalline and vuggy), created by dissolution of the survived matrix in freshwater phreatic zone. These porosities are partially occluded by cement and remanent matrix.

ACKNOWLEDGEMENT

I gratefully acknowledge the support of the management of the Petroleum Research Centre (P.R.C.), Libya. I am indebted to my colleagues in P.R.C.

Special appreciation is extended to Dr. A.M. Sbeta, Geology Department, Faculty of Science-University of Al-Fateh, for his encouragement and supervision during all stages of this Project.

Special thanks are extended to Mr. K.G. Nair of P.R.C. for his assistance in typing the manuscript.

REFERENCES

Barr F.T., and Weegar A.A. 1972, Stratigraphic Nomenclature of the Sire Basin, Libya. *Publication of Petr. Expl. Soc. Libya*: 179p.

Choquette W.P., and Prey L.C., 1970. Geologic Nomenclature and classification of Porosity in Sedimentary carbonates. *A.A.P.G. Bull., 54*: 207–250.

Hamayoni E.H., 1981, Subsurface study of the Upper Cretaceous ANF Formation Central Sirte Basin Libya. *Unpublished M.Sc. Thesis*, South Dakota School of Mines and Technology Rapid City, South Dakota: P.

Klitzsch E., 1981, Lower Paleozoic Rocks of Libya, Egypt and Sudan In: *L. Paleozoic of the Middle East, Eastern and Southern Africa and Antarctica*, C. H. Holand (Ed) 132–163.

Longman M.W., 1980, Carbonate Diagenetic Textures from Near surface Diagenetic Environments. *Bull. A.A.P.G. 64(4)*: 461–487.

Longman M.W., 1981, Carbonate Diagenesis as a Conrol on Stratigraphic Traps (with Examples from Wilkson Basim). *A.A.P.G. Education Series No. 21*: 159p.

Vail P.R. Mitchum R.M., and Thompson S., 111, 1977. Seismic Stratigraphy and Global Changes on sea level, Part 4: Global Cycles of relative changes of sea level. Mem. *A.A.P.G., 26*: 83–97.

Wilson J.L., 1975, Carbonate Facies in Geologic History. *Berlin-Heideberg-New York: Springer.* 471p.

PRJ, Vol. 3 (January 1991); P. 44–52, 13 FIGS.

DIAGENETIC HISTORY OF EARLY-MIDDLE EOCENE JDEIR FORMATION, FARWAH GROUP, NORTHWESTERN LIBYAN OFFSHORE

Ibrahim Y. Mriheel*

تغيرات المنشأ في تكوين أجدير — الرف القاري شمال غرب ليبيا

إبراهيم يوسف مريحيل

يمثل تكوين أجدير رسوبيات جيرية ضحلة تكونت أثناء عصر الايوسين المبكر — الأوسط بالمنطقة المغمورة بمياه البحر والواقعة شمال غرب ليبيا.

أظهرت الدراسة البتروغرافية أن تغيرات المنشأ التي طرأت على تكوين أجدير، كانت معقدة وقد حدثت هذه التغيرات في ثلاث بيئات أو مراحل أساسية :

المرحلة البحرية :

لقد نجم عن هذه البيئة تكون مادة لاحمة مبكرة وظاهرة التحول إلى الطفل الجيري.

المرحلة القارية :

نشأ أثناء هذه المرحلة مادة لاحمة ذات أحجام وأشكال متباينة مثل مادة لاحمة متساوية الأبعاد، ومادة متزايدة الأحجام ناحية مركز الفراغات.

كما يرجع تكوين المسامية العالية بتكوين أجدير للإذابة الشديدة التي تعرض لها أثناء بروز هذا التكوين للظروف القارية، وذلك أثناء تراجع مياه البحر.

مرحلة الدفن :

تميزت هذه البيئة عن غيرها بتكوين مادة لاحمة كبيرة الأحجام، وتشققات وظواهر الضغط، والتحول إلى السليكا.. كما صاحب نضوج المادة النفطية زيادة في مسامية تكوين أجدير.

نتائج تاريخ تغيرات المنشأ المختلفة يعكس التباين في كمية ونوعية المسامية بتكوين أجدير، كما أن المسامية في الخزان معقدة وتشمل أنواع أولية وثانوية.

ABSTRACT

The Jdeir Formation, a shallow carbonate platform deposit, was developed during Lower-Middle Eocene in the northwestern Libyan offshore. The diagenesis of the Jdeir Formation mainly involves marine phreatic, meteoric phreatic and burial stages. The phenomena vary from crystalline degradation (micritisation, dissolution) to crystalline aggradation (cementation, neomorphism). Stylolitisation and fracturing is common, the former mostly filled by bitumen and the later with calcite. The result of different diagenetic histories reflects the variation in the amount and kind of porosity within the formation. Porosity in the reservoir is complex and contains primary and secondary types.

Concentration of calcite spar, fracturing, compaction and pressure solution caused destruction of porosity.

INTRODUCTION

The Jdeir Formation, a shallow carbonate platform deposit, was developed during Lower-Middle Eocene in the Gabes–Tripoli–Misratah basin over extreme northern parts of the passive continental margin of the African Plate. This shallow platform was bounded by restricted platform deposits of Taljah Formation toward the then land and a deep platform-basinal facies of the Hallab Formation toward the sea side. The formation comprises the upper unit of the Farwah Group and is the main target for hydrocarbon exploration in the offshore area.

*Petroleum Research Centre, Tripoli, G.S.P.L.A.J.

Lithologically, the Jdeir Formation is subdivided into three main facies. These are, from landward to seaward, Orbitolites-Alveolina facies, Nummulitic facies, Fragmental-Discocyclina-Assilina facies. A fourth facies, the dolomitised limestone, is also observed but it has a very limited distribution. It is present in the extreme southwestern part of the area (Fig. 2).

Geologic studies commenced mainly during the last decade after a number of wells had been drilled. Available published work on the Jdeir Formation (Farwah Group) of the northwestern offshore Libya is very scarce although being petroliferous, it is fairly well studied by the operating companies e.g., Aquitaine, Sirt, and Agip.

Bernasconi *et al.* (1984) studied the petrography and diagenesis of the Farwah Group at the Bouri oil field and divided it into three main lithofacies i.e. nummulitic, dolomitic and micritic and proposed a nummulitic bank model.

Sbeta (1984) conducted a comprehensive sedimentological study of the Eocene sequence in the northwestern offshore Libya and related the lithofacies to depositional environments according to the standard facies model of Wilson (1975). The depositional environments of Jdeir Formation and the relationship between its lithofacies and structural framework of northwestern Libyan offshore have been described in greater detail by Etourbi, 1989.

This paper presents the diagenetic history of the Jdeir Formation as interpreted from petrographic analyses.

Data from fifty wells (Fig. 1) drilled in Agip NC41, Sirt NC35A and Aquitaine 137 concessions were utilised and cores from wells (B2, E1-NC41, E1, and I1-NC35A) were studied. The present study employs the stratigraphic terminology proposed by Hammuda *et al.* (1985) but with an emphasis on author's lithologic subdivisions of the Farwah Group (Etourbi, 1989).

STRATIGRAPHY OF THE JDEIR FORMATION

The Jdeir Formation ranges in age from Late Ypresian to Early Lutetian and represents the upper unit of the Farwah Group. It is the main target for hydrocarbon exploration in the region. The formation consists of three major facies distributed from south (landward) to north (seaward) as given below:

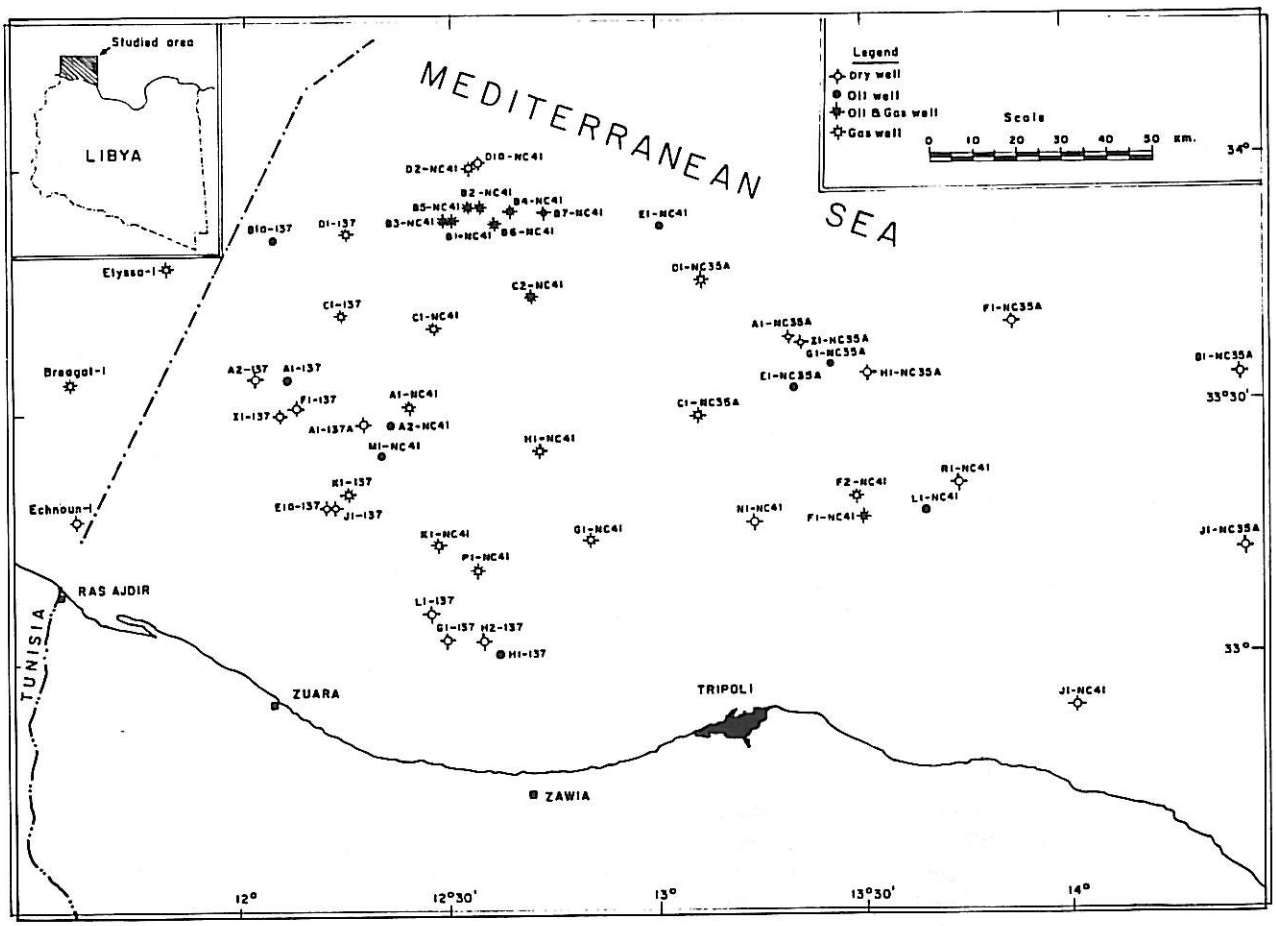


FIG. 1. Location map of the studied area.

(1) *Orbitolites-Alveolina back bank facies* (southernmost)

It comprises whitish-light brown and light grey, medium hard to hard compact wackestone-packstone occasionally grading to wackestone-mudstone. The facies is interpreted to have been deposited in a lagoon and/or a bay environment over an open shallow platform where a moderate water circulation of a few tens of meters depth and normal marine water salinity predominated the environment. This facies is structurally controlled by the main trough of Jifarah (Etourbi, 1989) and is absent over the Jifarah platform as well as the "saltic" high (Fig. 2).

Its position was structurally controlled by paleohighs (Etourbi, 1989), namely "saltic" uplift and Jifarah platform (Fig. 2).

(3) *Fragmental-Discocyclina-Assilina fore bank facies* (northernmost)

It is comprised of a thick sequence of light grey and tan to bluff, medium to coarse grained, medium hard wackestone-packstone with intercalated levels of grainstone. The facies is associated with abundant Nummulites and echinoderm fragments and is characterized by the presence of *Discocyclina spp. Assilina spp.*, and Operculina. The fore bank facies was deposited on the northern flanks of the outer platform (Etourbi, 1989) probably at the shelf slope margin (Fig. 2).

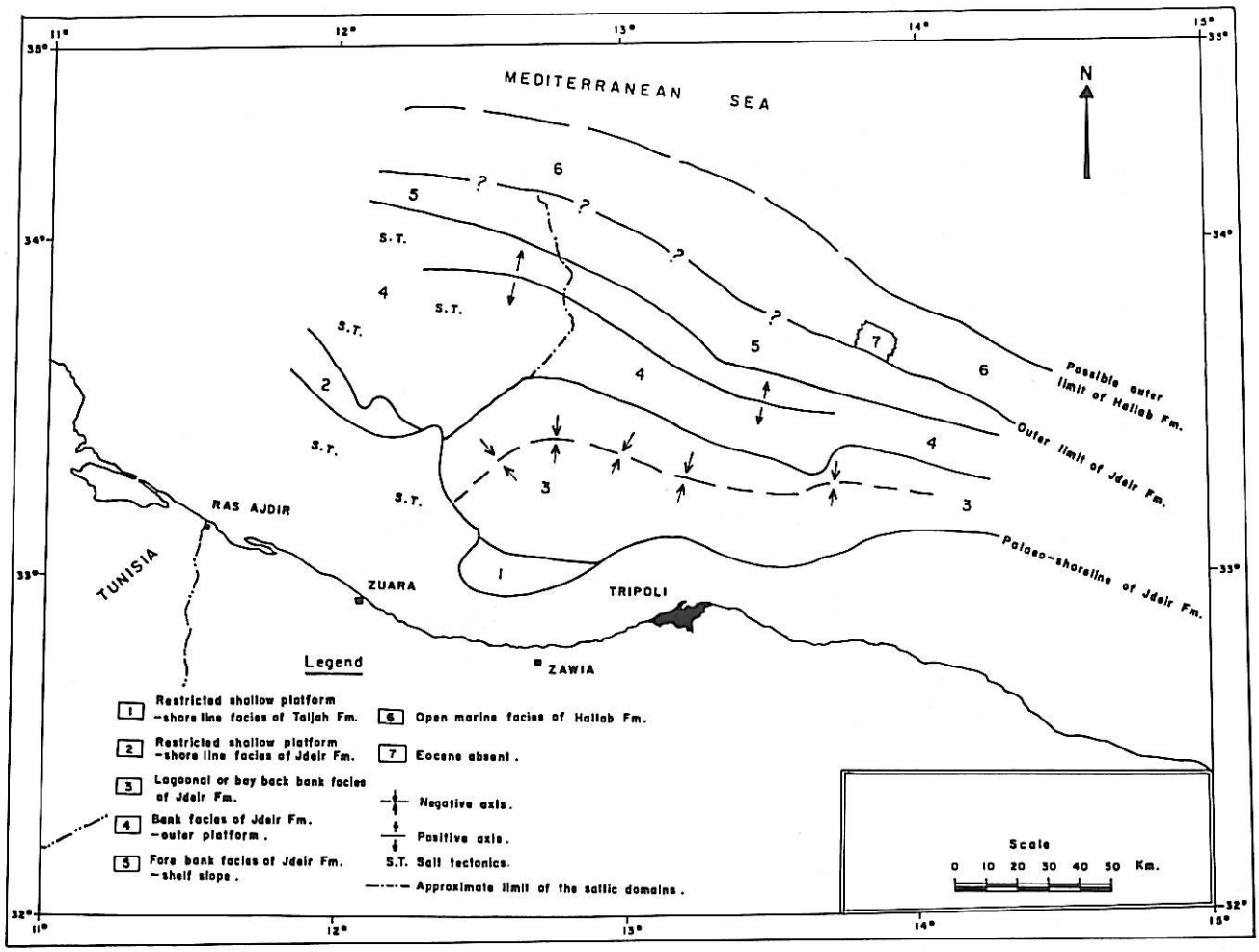


FIG. 2. Facies, structural setting and depositional environment of Jdeir Fm. and its equivalents (Taljah Fm. and Hallab Fm.).

(2) *Nummulitic bank facies* (central)

This facies consists predominantly of light brown-grey, medium hard, nummulitic packstone-grainstone and wackstone-packstone. Levels of wackestone-mudstone are present occasionally. The nummulitic bank facies was deposited at the outer platform in a water depth ranging from wave base to low tide level.

The Jdeir Formation is generally unconformably overlain by the Harshah Formation in the southern part and overlain by the Ghalil Formation toward the northern parts (Bouri oil field) of the area. It overlies the Bilal Formation in the north and in the south. In N1 and K1-NC41 wells it overlies unconformably the Late Cretaceous deposits.

DIAGENESIS

This section presents a brief outline of the main diagenetic process and their products which were recognized in the course of the petrographic study of the Jdeir Formation. Detailed petrography and relationship between the depositional environment and diagenesis is to be the aim of the later research.

The different diagenetic events and their response to both time and diagenetic setting in the studied sections of the Jdeir Formation are shown in Fig. 3.

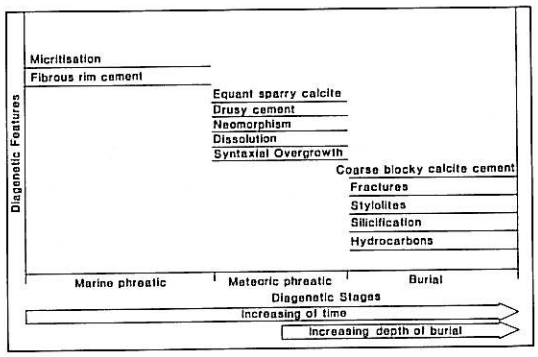


FIG. 3. Diagenetic events observed in the Jdeir Formation in relation to time and diagenetic environments.

The term diagenesis in this study refers to all natural processes acting on sediments since their initial deposition to the time of erosion. These include, dissolution, replacement, neomorphism, cementation, micritisation, and compaction. Other processes such as metamorphism and weathering are excluded from the definition.

To avoid confusion and/or further repetitive work, the reader is referred to (Longman, 1982 p. 92–105) for the classification of the diagenetic environment. For the main characteristic products of each environment, the reader is referred to Longman (1980 p. 461–487); Wilson (1975 p. 69–71); Flugal (1982 p. 62–95), Bathurst (1975) and Scoffin (1987 p. 89–130). The porosity classification of Choquette and Pray (1970) is used in this study.

The Jdeir Formation underwent severe diagenetic processes which have altered the original components and texture since the time of their initial deposition until the present time. The diagenetic history of Jdeir Formation commenced in the early marine phreatic environment as most of the carbonate rocks started their diagenetic history there, then passed via a fresh water phreatic environment to the last stage, the burial phase. The previously mentioned diagenetic environments have been distinguished one from another by their own characteristic processes and the resultant features such as processes enhancing porosity initiation (dissolution) and processes obliterating the porosity (cementation).

In this section the processes are described and subsequently their effects on the Jdeir Formation explained.

MARINE PHREATIC

Micritisation

This is one of the first stages of diagenesis seen in these sediments and it occurred during deposition. Micritisation of grains by boring algae and fungi result in the formation of a micrite envelope similar to those described by Bathurst (1966, 1975) and Kendall and Skipwith (1969). This has been observed throughout the studied sections except in the well E1-NC35A, where it has been observed mainly in the upper portion (Fig. 4). The process goes on centripetally within the grain and may completely convert it to micrite. These encrusting algae and boring organisms micritize the outer portions and occasionally the inner portions of the bioclastics as has been observed in Recent sediment of Abu Dabi by Kendall and Skipwith (1969).

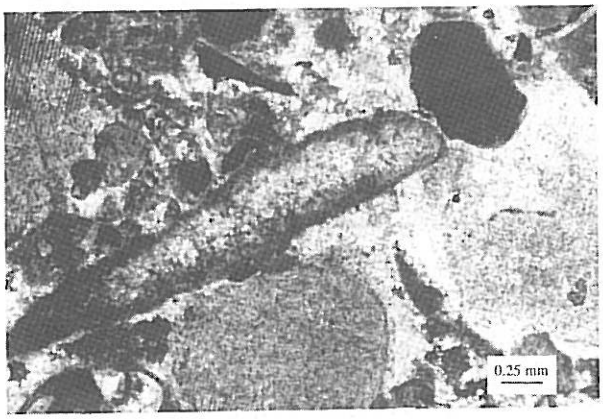


FIG. 4. Micritized molluscan envelope formed by fungi or algae boring, adjacent to echinoderm fragments rimed by syntaxial overgrowth.

Bathurst (1966, 1975) and Kobulk and Risk (1977) believe that this processes takes place in a marine phreatic zone, while May and Perkins (1979) consider it happens from near the sediment-water interface to a meter beneath the interface.

Absence of broken envelopes indicates that the dissolution and void-filling were completed before compaction, or both have occurred after the early (pressure-solution) phase of compaction similar to that described by Bathurst (1964).

Fibrous Calcite Crust

Isopachous crusts of fibrous calcite are observed in the upper parts of well E1-NC35A and are believed to be a very early post-depositional submarine cement (Becher and Moore, 1979) of the phreatic environment. Folk (1974) believes that the high Mg/Ca ratios found in normal marine water is responsible for these fibrous habits of marine calcite cement. A thin rim of calcite crystals (normal to grain surface) surrounding grains as observed in some thin sections is followed by blocky calcite which represents different stages of cementation, as discussed below.

Intraclasts which preserve a generation of radial-fibrous (Fig. 5) or -prismatic cement not observed in the host sediment have been observed only in one sample. This is interpreted not as a Jdeir Formation cement, but one formed in a laterally equivalent environment, which was the provenance of the intraclasts. This interpretation is similar to that of Schofield (1982).

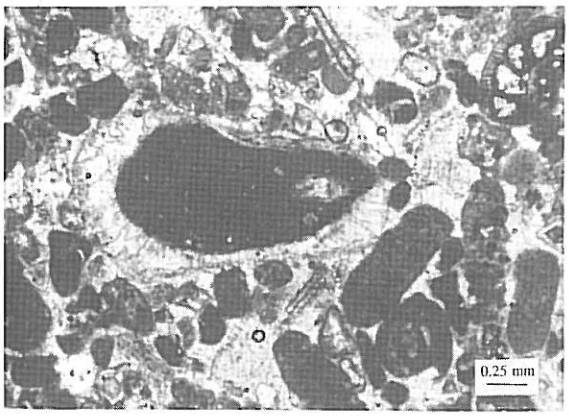


FIG. 5. Early radial fibrous cement around lithoclasts in grainstone. Well E1-NC35A, PPL.

METEORIC PHREATIC

Neomorphism

The dissolution and reprecipitation of the aragonite of shells (mainly molluscs) as a mosaic of sparry calcite is very rare in the upper parts of Jdeir Formation at well El-NC35A. In some intervals, Jdeir Limestone is observed associated with recrystallisation of some portions such as micritic matrix into microcrystalline calcite (Fig. 11). Relics of the original grains can be faintly seen.

Neomorphism is defined by Folk (1965) as transformation between one mineral and itself or a polymorph which results in the growth of new crystals that are larger or different in shape from the previous crystals. Carbonate minerals are very suceptible to such recrystallisation. Neomorphism in the limestones described in this paper was proceed by micrite enlargement, a process by which crystals that measure only a few microns in diameter enlarge to a size measuring tens of microns in diameter. This micrite enlargement creates neomorphic products similar to cement in crystal size. The new crystals are known as pseudospar (Folk, 1965) or neospar (Nichols, 1967 and Flugal, 1982). Depending on water chemistry and rates of water flow, micrite may recrystallize and neomorphose to coarser grains in a fresh water phreatic environment or in a fresh water vadose environment (Longman, 1980; Flugal, 1982).

This type of diagenesis has been observed in some of the studied sections of Jdeir Formation. The size distribution of the individual crystals is usually random and devoid of any regular pattern. This neosparite exists as isolated patches and thus appears to be floating in the rock. The parts of limestone which have undergone extensive micrite enlargement display relic patches of non replaced micrite. These patches reveal that the limestone originally was a micrite rather than a sparite.

Dissolution

Evidence of extensive dissolution is found in most of the studied sections of Jdeir Formation. It has a broad range of intensity and generally increases the pore system. Dissolution forms solution vugs and moldic voids (Fig. 6) which are locally interconnected by the enlargement of the basic intergranular porosity.

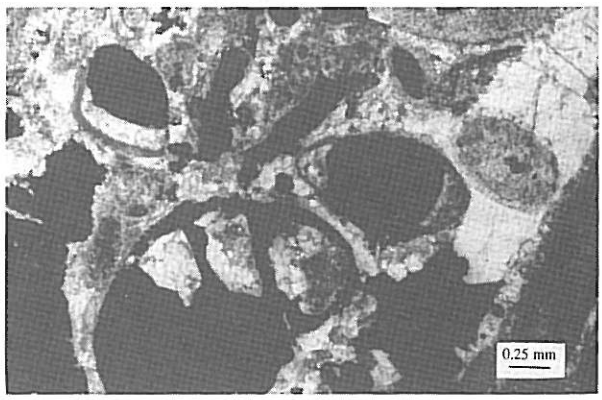


FIG. 6. Packstone showing good moldic and vugy porosity. Note syntaxial overgrowths around echinoderm. Well El-NC35A, XN.

As a matter of fact, the dissolution process has created a vast amount of vugy and moldic secondary porosity. In some intervals of Jdeir Formation, it

reaches more than 20% of mesopore size which in turn has enhanced its reservoir potential and the entrapment of hydrocarbon in the northwestern Libyan offshore. Similar hydrocarbon entrapment was discovered toward the Tunisian offshore in the nummulitic facies of El-Garia Formation within the same secondary porosity type (see Bishop, 1975).

Cementation

Syntaxial overgrowths on echinoderm fragments and/or crinoid fragments (Fig. 7) have been described in many sections of Jdeir Formation. Syntaxial calcite growing in optical continuity with echinoderm

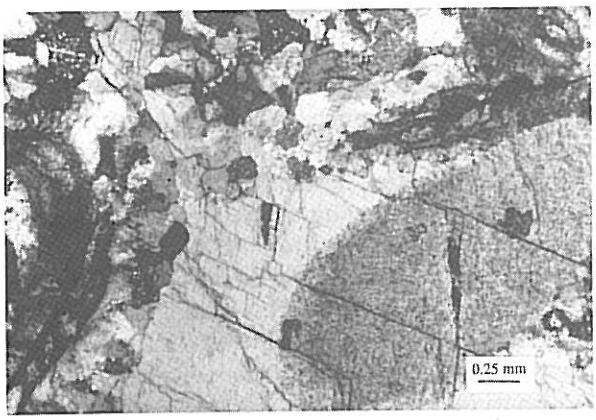


FIG. 7. Syntaxial overgrowth around echinoderm fragments adjacent to equant mosaic cement of non-ferroan calcite. Well El-NC35A, XN.

fragments generally surrounds the grains and is elongated along the C-axis similar to that described by Evamy and Shearman (1965, 1969). Because of the large crystal nucleus and absence of competitive crystal growth, they grew much faster than cements around adjacent non-echinoderm grains and locally lead to a polkilotopic texture as described in Bathurst (1975). Lucia (1962) and Evamy and Shearman (1975) have found that the volume of rim cement on echinodermal grains normally exceeds the volume of cement mosaic on the associated multicrystalline grains. These syntaxial overgrowths are developed in a meteoric phreatic environment, and Longman (1980) suggests that, although syntaxial overgrowths form most commonly in fresh water phreatic environment, they may also form, but rarely, in vadose and deeper subsurface diagenetic environments.

Drusy cement mosaics (Fig. 8), increasing in crystal size regularly to the centre of the former void-space, are not common. The pore-filling calcite is commonly an equant mosaic of non ferroan calcite (Fig. 9). The morphology of these crystals is similar to those described by Longman (1982), i.e. crystals of void-filling cement which are optically continuous over large

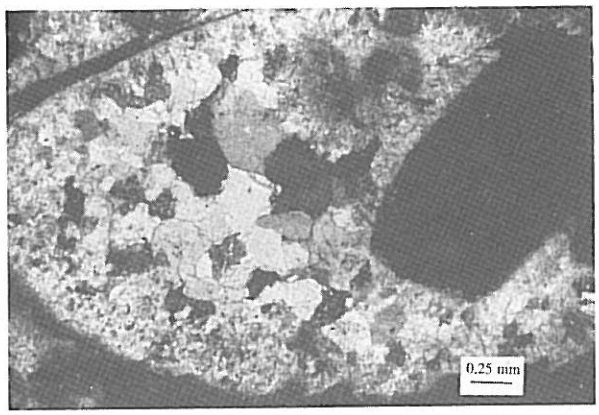


FIG. 8. Geopetal infilled by drusy mosaic of non-ferroan calcite cement. Well El-NC35A, XN.

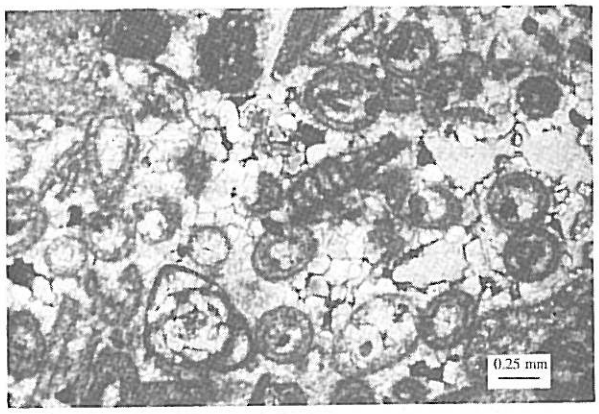


FIG. 9. Grainstone composed largely of dasycladacean algae and cemented by equant mosaic of non-ferroan calcite. Well I1-NC35A, PPL.

areas and showing almost irregular boundaries. They were probably deposited in the fresh water phreatic environment during exposing of Jdeir Formation to subaerial conditions.

BURIAL PHASE

Coarse Crystalline Calcite

Coarse crystalline calcite (Fig. 10) found in the Jdeir Formation probably formed during deep burial of sediment at a relatively late stage in their diagenetic history. These calcite crystals are commonly euhedral and partly fill the voids which remained. This cement is Fe-poor which indicates it formed in an oxidizing setting, which could include the deeper subsurface as described by Sultan (1985). Land (1971) observed the more rapid pore filling of coarse calcite in the phreatic environment than in the adjacent vadose environment.

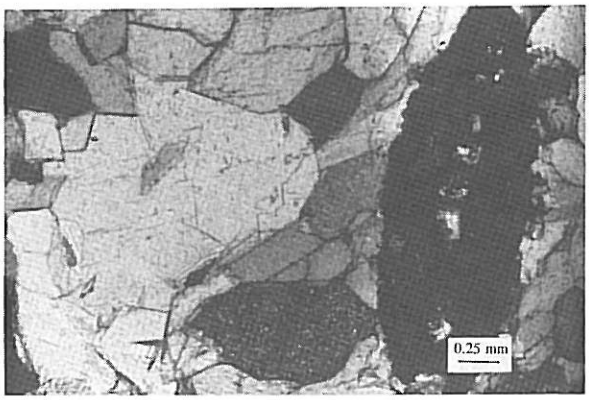


FIG. 10. Coarse crystalline non-ferroan calcite filling the voids adjacent to Nummulites. Well El-NC35A, XN.

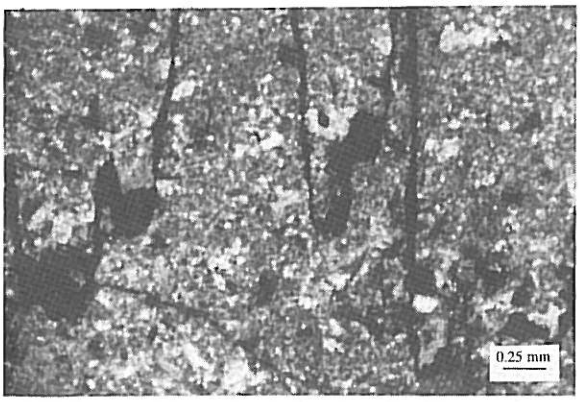


FIG. 11. Stylolites stained with oil in nemorphosed micritic substrate. Well I1-NC35A, XN.

Stylolites and Fractures

Several generations of stylolites affect the Jdeir Formation. The observed pressure-solution phenomena throughout most of the studied sections are represented by horizontal stylolites of simple or primitive wave-like type and sharp-peak type. The seams of the stylolites usually consist of residues of dark organic matter or bituminous substance occasionally with small-sized quartz grains. The maximum amplitude observed is 1 cm although the length of the stylolites peaks is variable and ranges down to 1 mm.

Dunnington (1967) suggested that undersaturated pore fluids play a role in the formation of stylolites and are necessary for solution-compaction processes. This requires increased overburden pressure or undersaturated water from an outside source (Becher and Moore, 1979). Solution resulted in the formation of stylolitic boundaries between clasts in response to the overburden pressure. Compaction and tight packing of clasts could be the result of this pressure solution (Longman, 1980).

Stylolitisation significantly affects carbonate reservoirs by providing pathways for hydrocarbon migration as is clearly indicated by the residue of bitumens (Fig. 11) found along most stylolites in the present area. Stylolites were formed after burial probably from dissolution associated with decarboxylation (the release of CO_2 during thermal maturation of organic matter and hydrocarbon generation) (see Longman, 1982).

At the Bouri oil field stylolites are frequently associated with open microfractures. The observed microfractures within Jdeir Formation at well E1-NC35A are predominantly associated with the lime wackestone intervals and resemble calcite veining (Fig. 12). The most characteristic features of most of them are their sharp edges and the type of infill which is usually pink-stained non-ferroan calcite, although, in a few instances, secondary silica is substituted for small amounts of the calcite mineral in the vein. The fractures are generally small ranging up to several centimetres in length and ranging from 0.3 mm to 0.7 mm in width. Some of the fractures run parallel to each other and a few show cross-cutting relationships. In a few samples, however, they tend to cut bioclasts with recognizable "microdisplacement". At the Bouri oil field, stylolites are frequently associated with the open microfractures (Bernasconi *et al.* 1984). The microfractures within are interpreted as mechanical fractures that developed after lithification, probably during localized uplift or compression. It is, however, difficult to assess the potential contribution of these microfractures to production. It is likely that the very small scale fractures which are often measured in centimetres would not en-

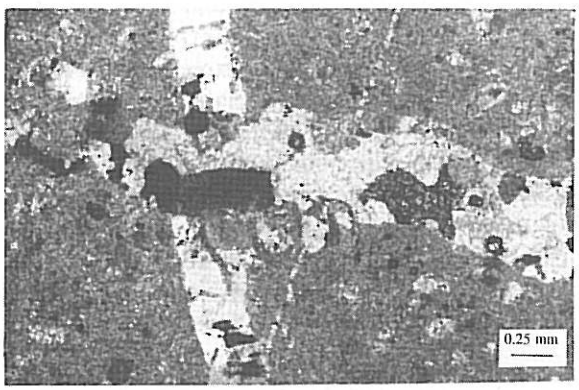


FIG. 12. Mudstone showing cross-cutting fractures represented by calcite veins. Note that some parts of the calcite vein are replaced by authigenic silica. Well E1-NC35A,XN.

hance the permeability of the reservoir significantly. The contribution of the large fractures to permeability can be expected to be significant provided these are open under reservoir conditions.

Silicification

Evidence of replacement by authigenic silica is rarely found in a few thin sections in the form of anhedral replacement of bioclasts (Fig. 13), void-infilling and in few cases secondary silica substitution of small intervals of calcite minerals in veins.

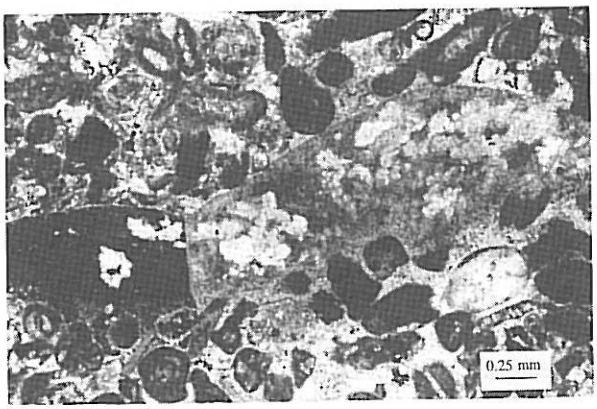


FIG. 13. Bioclasts replaced partially by authigenic silica in grainstone. Well E1-NC35A, XN.

Silicification took place after submergence following sub-aerial exposure, however, the source of silica which replaced parts of the component allochems in the Jdeir Formation is unknown.

Hydrocarbon Occurrence

The hydrocarbon accumulations in the northwestern Libyan offshore have mainly been discovered in carbonate reservoirs ranging in age from Late Cretaceous to Early Tertiary.

The Early Eocene nummulitic facies of the Jdeir Formation and the dolomitic facies of the Jirani Formation (Farwah Group) are the main reservoir rocks in the investigated area. A major hydrocarbon accumulation, discovered at the Bouri oil field produces from both the Jdeir Formation and the Jirani Dolomite. The Tellil Group of Middle-Late Eocene age and the Alalgah Formation of Cenomanian age are considered to be the second carbonate reservoirs, particularly in the central and the southern parts of the Libyan offshore.

As yet, all of the hydrocarbon plays were found in structural traps of anticline type. Detailed investigation of facies distribution and the relationship between its environment of deposition and diagenesis will undoubtedly enhance the exploration of the stratigraphic traps at the studied area.

The main source rocks of hydrocarbon at the Libyan offshore are the micritic facies of the Bilal Formation (Farwah Group) and the Maastrichtian-Paleocene Al Jurf Formation. The latter is considered to be mainly gas-borne over all the studied area.

The organic carbon content of the micritic facies of Bilal Formation ranges from 0.5–2.3% of amorphous type. The overall source potential of the Farwah Group corresponds to the zone of oil and gas window. The Farwah Group in the northern parts of the Libyan offshore contains oil-borne organic matter which becomes gradually gas-borne southward where the main Trough of Jifarah is located. This can be explained because in these southern parts the geohydrothermal gradient is high as the Farwah Group occupied deep areas (structurally low land or trough) therefore, the thermal maturation is very high and any oil generated would not be preserved as liquid as the heat would transfer it into a gas or condensate state.

Oil generation in the Libyan offshore basin commenced after the Miocene and is still continuing (Benelli *et al.*, 1985). These authors have distinguished three areas of hydrocarbon generation. In the northern parts, oil generation occurred in the Farwah Group and that of gas and condensate in the Al Jurf Formation of Late Cretaceous-Paleocene age. Only gas and condensate with minor oil were generated by the Al Jurf Formation and Farwah Group in the central southern parts. A third oil-bearing sequence existed in the southeastern part but its source rock is yet not known.

From the diagenetic point of view, the hydrocarbon generation and migration is undoubtedly the last diagenetic stage, which affected the Jdeir Formation. The decreasing of CO_2 during thermal maturation of the organic matter with the source rocks increased the dissolution diagenetic processes and consequently enhanced the formation of the secondary porosity.

SUMMARY AND CONCLUSIONS

Petrographic evidence reveals that diagenesis of the Jdeir Formation was complex and included: the marine phreatic (micritisation and fibrous rim cement), meteoric phreatic (equant sparry calcite, drusy cement, neomorphism, dissolution and syntaxial overgrowth), and burial diagenesis (coarse blocky calcite cement, fractures, stylolites, silicification and hydrocarbon).

The result of different diagenetic histories reflects the variation in the amount and kind of porosity within the formation. Concentration of calcite spar,

fracturing, compaction and pressure solution caused porosity destruction. Porosity in the reservoir is complex and contains primary and secondary types. These different types may have been modified by solution and cementation.

ACKNOWLEDGEMENTS

The author wishes to express his sincere thanks to the Petroleum Research Centre for the Financial support. Thanks are also extended to N.O.C. for the permission to publish this paper. Dr. J.M. Anketell gave helpful advice during the work. He also critically reviewed the first draft of the manuscript and offered many suggestions.

REFERENCES

Bathurst R.G.C., 1964. The replacement of aragonite by calcite in the molluscan shell wall. In: IMBRIE, J. and NEWELL, N.D. (Editors), *approaches to palaeoecology*, Wiley and Sons, New York, p. 357–376.

Bathurst R.G.C., 1966. Boring algae, micrite envelope and lithification of molluscan biosparites. *Geological Journal*, 5: p. 15–32.

Bathurst R.G.C., 1975. *Carbonate sediments and their diagenesis.* Elsevier, Amsterdam, 2nd Edition, 658p.

Becher J.W. and Moore C.H., 1979. The Walker Creek field: a Smackover diagenetic trap. In: Moore, C.H. (Editor), *Geology of carbonate porosity.* Am. Assoc. Petrol. Geologists continuing education, course notes series #11, p. A24–A46.

Benelli F., Mcavaggion M. and El Ashuri O. 1985. *Oil and gas habitat in concession NC41.* Agip N.A.M.E., Tripoli. (Unpublished report).

Bernasconi A., Noguera A.M. and Poliani G., 1984. *Sedimentology, petrography and diagenesis of Metlaoui Formation at the Bouri oil field.* Agip N.A.M.E., Tripoli. (Unpublished report).

Bishop W.F., 1975. Geology of Tunisia and adjacent parts of Algeria and Libya. *Bull. Am. Assoc. Petrol. Geologists*, 59: p. 413–450.

Choquette P.W. and Pray L.C., 1970. Geologic nomenclature and classification of porosity in sedimentary carbonates. *Bull. Am. Assoc. Petrol. Geologists*, 54: p. 207–250.

Dunnington H.V., 1967a. Aspects of diagenesis and shape change in stylolitic limestone reservoirs. *7th world petroleum congress*, 2: 339–352.

Etourbi I.Y., 1989. *Study of the main facies of the Farwah Group (Late Paleocene-Early Middle Eocene) of the Northwestern Libya offshore.*, Unpubl. M.Sc. thesis, University of Manchester.

Flugel E., 1982. *Microfacies analysis of limestones.* Springer-Verlag, Berlin-Heidelburg-New York, 633p.

Folk R.L., 1965. Some aspects of recrystallisation in ancient limestones. *Soc. Econ. Palaeontologists Mineralogists, Spec. Publ.*, 13: p. 14–48.

Folk R.L., 1974. The natural history of crystalline calcium carbonate: effect of magnesium content and salinity. *J. Sediment. Petrol.*, 58: p. 40–53.

Hammuda O.S., Sbeta A.M., Mouzughi A.J. and Eliagoubi B.A., 1985. Stratigraphic Nomenclature of the northwestern offshore of Libya. *The Earth Sciences Society of Libya*, Tarabulus, Libya.

Kendall C.G.St.C. and Skipwith Sir P.A. d'E., 1969. Holocene shallow water carbonates and evaporite sediments of the Khor and Bazam, Abu Dhabi, southwest Persian Gulf. *Bull. Am. Assoc. Petrol. Geologists*, 53: p. 841–870.

Kobluk D.R. and Risk M.J., 1977. Micritisation and carbonate-grain binding by endolithic algae. *Bull. Am. Assoc. Petrol. Geologists*, 61: p. 1069–1082.

Land L.S., 1971. Phreatic versus meteoric diagenesis of limestones: Evidence from a fossil water table in Bermuda. In: Bricker, O.F., (Editor), *Carbonate cements.* John Hopkins Press, Baltimore, MD, pp. 133–136.

Longman M.W., 1980. Carbonate diagenetic textures from near-surface diagenetic environments. *Bull. Am. Assoc. Petrol. Geologists*, 64: p. 461–487.

Longman M.W., 1982. *Carbonate diagenesis as control on stratigraphic traps (with examples from the Williston Basin)*, Education course note series #2. Am. Assoc. Petrol. Geologists, Tulsa, Okla., 159pp.

Nicholas R.A.H., 1967. The sparite complex: Eosparite V. Neosparite. *J. Sediment. Petrol.*, 37: p. 1247–1248.

Sbeta A.M., 1984. *Sedimentology of the Eocene rocks of the offshore-Northwestern Libya.* Internal report, N.O.C., Libya. (Unpublished report).

Schofield K., 1982. *Sedimentology of the Woodale limestone Formation of Derbyshire.* Unpubl. Ph.D. thesis, Univ. Manchester.

Scoffin T.P., 1987. *An introduction to carbonate sediments and rocks.* Chapman and Hall, New York. 274p.

Sultan A.A., 1985. *Petrography, sedimentology, diagenesis and reservoir characteristics of the Shuaiba and Kharaib Formations (Barremian-Mid Aptian) carbonate sediments of Abu Dhabi.* Unpubl. Ph.D. thesis, University of South Carolina.

Wilson J.L., 1975. *Carbonate facies in the geological history.* Springer-Verlag, Berlin-Heidelburg-New York. 471p.

PRJ, Vol. 3 (January 1991); P. 53–56, 4 FIGS, 2 TABLES.

THE COMPARATIVE CATALYTIC ACTIVITIES OF TUNGSTATE AND MOLYBDATE IONS IN THE EPOXIDATION OF MALEIC ANHYDRIDE BY HYDROGEN PEROXIDE

Iftikar Ahmad*, Massod Degam* and Abdel Razak Labib*

دراسة لمقارنة حركية تفاعل انتاج مشتق الأبوكسي من مركب الماليك اللامائي بواسطة فوق أكسيد الهيدروجين في وجود تنجستات الصوديوم ومليبدات الصوديوم كعامل مساعد

د. افتخار أحمد ، مسعود دغيم ، عبد الرزاق لبيب

هذا البحث يتعلق بدراسة مقارنة لحركية تفاعل انتاج مشتق الابوكسي من مركب الماليك اللامائي بواسطة فوق أكسيد الهيدروجين في وجود تنجستات الصوديوم أو موليبدات الصوديوم كعامل مساعد.

درجة التفاعل صفر بالنسبة لتركيز فوق أكسيد الهيدروجين أما بالنسبة للعامل المساعد (سواء تنجستات أو موليبدات الصوديوم) فهو من الدرجة الأولى. التفاعل في وجود التنجستات أسرع منه في حالة استخدام الموليبدات كعامل مساعد.

لقد تم اقتراح معادلة مركبة تربط ما بين سرعة التفاعل وتراكيز مركب الماليك اللامائي والعامل المساعد وفوق أكسيد الهيدروجين. كما تم إقتراح ميكانيكية لكيفية حدوث التفاعل.

ABSTRACT

The comparative kinetics of epoxidation of maleic anhydride by hydrogen peroxide in the presence of sodium tungstate or sodium molybdate as catalyst have been studied. The reaction is zero order with respect to hydrogen peroxide concentration and the reaction is first order with respect to maleic anhydride and catalyst (sodium tungstate or sodium molybdate). Tungstate catalysed epoxidation of maleic anhydride is faster than that of molybdate catalysis. A complex rate equation, describing the dependence of rate on maleic anhydride, catalyst and hydrogen peroxide has been proposed. A reaction mechanism has also been proposed.

INTRODUCTION

Epoxides have shown a growing industrial importance, particularly in the polymer field. The simple epoxides are obtained by aerial oxidation of unsaturated hydrocarbons such as ethylene or propylene over silver catalyst [1–3]. More complex unsaturated substrates are usually converted into their epoxides through the intermediacy of organic peracids [4–6] but the compounds having strong electron withdrawing substituents adjacent to the double bonds are not readily epoxidized by them [7]. More recently hydroperoxides [8–12] are being used for the epoxidation of such alkenes, but these are limited only to nonaqueous medium. In aqueous medium inorganic peracids are often used as specially effective epoxidizing reagents [7]. These inorganic oxidants are usually generated in situ [13] from hydrogen peroxide and a soluble compound of much less common metals as Os, Ti, Zr, Rh, U, Ru, Ta, Cr, Se, W, Mo, V etc. Mugdan and Young [14] made a qualitative comparison of osmic, tungstic, molybdic, selenious, tantalic and titanic acids as catalysts for the direct addition of hydrogen peroxide to ethylenic compounds. The kinetics of the reaction of pertungstic acid with allyl alcohols [15–17] have been reported.

*Petroleum Research Centre, Tripoli, G.S.P.L.A.J.

This paper presents the results of kinetics of the epoxidation of maleic anhydride by hydrogen peroxide in the presence of sodium tungstate and sodium molybdate as catalysts. Maleic anhydride is a petrochemical which can be produced by the oxidation of butane, benzene and butenes [18]. The epoxydicarboxylic acids should be of potential commercial interest because of their easy conversion into tin epoxysuccinates which are important plasticizer-stabilizers for polyvinyl chlorides [19] as well as for cross linkable epoxy containing film-forming polyamides [20].

EXPERIMENTAL

Standardization of the maleic anhydride and hydrogen peroxide solutions were carried out using a bromate-bromide mixture [21] for the former and permanganate [22] for the latter. In kinetic runs, the concentration of hydrogen peroxide was measured colorimetrically [23]. After the reactants had reached thermostat temperature, the reaction was started by addition of the catalyst. The kinetics were followed by examining 5 ml aliquots of the reaction mixture for hydrogen peroxide content. The aliquots were added to 5 ml titanium sulphate solution to stop the reaction. Optical density was measured at 420 nm and the concentration of the hydrogen peroxide was read from a calibration graph. The catalyst concentration was too small to affect the colorimetric estimation of hydrogen peroxide. Every run was followed until the reaction was at least 90% complete.

The epoxysuccinic acid formed in this reaction was measured quantitatively by the pyridinium chloride-pyridine method [24]. Instead of methanolic sodium hydroxide, an aqueous solution was used for titration. Maleic anhydride, at pH 6.0, gave cis-epoxysuccinic acid. No tartaric acid was detected in the reaction mixture above pH 5.0. However, below pH 5.0, the test of tartaric acid [25] was positive and its form was identified by a chromatographic method [26]. The results suggest that maleic anhydride gives a dl form of tartaric acid.

RESULTS AND DISCUSSION

The progress of the reaction was observed by measuring the disappearance of hydrogen peroxide in the presence of high concentration of maleic anhydride. Trial and error plots of the rate data for runs indicate that the reaction is zero order in hydrogen peroxide. The plots of concentration of hydrogen peroxide versus time were straight lines, and their slope yields k_{obsd}. The pseudo zero order rate constants (k_{obsd}) were found to be independent of the concentration of hydrogen peroxide. The results are summarized in Table 1.

Table 1. Pseudo-Zero-Order Rates for the Epoxidation of Maleic Anhydride in the Presence of Catalyst

$[H_2O_2] \times 10^3$ (M)	kobsd $\times 10^7$ (mol lit^{-1} sec^{-1})	
	Sodium tungstate	Sodium molybdate
2.50	5.25	3.50
3.00	5.28	3.49
3.50	5.23	3.52
4.00	5.26	3.51
4.50	5.25	3.49
5.00	5.25	3.50

[Catalyst] $= 1.00 \times 10^{-3}$M; [Maleic anhydride] $= 0.20$M
Temp., 50°C; pH, 6.0

The order of reaction with respect to catalyst (sodium tungstate or sodium molybdate) was determined by varying its concentration and keeping other variables constant. The plot of k_{obsd} against the concentration of catalyst was straight line (Fig. 1)

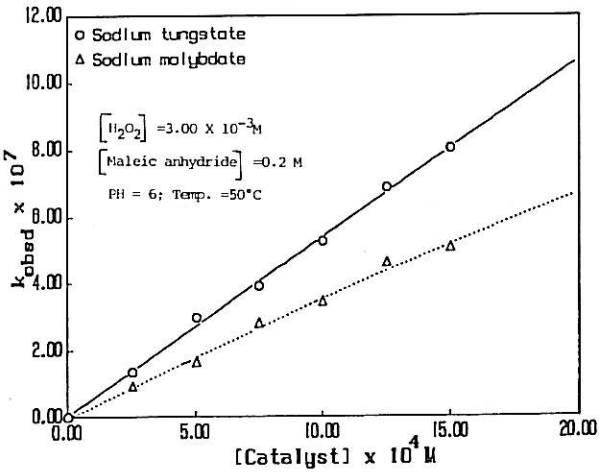


FIG. 1. First order dependence of rate on catalyst concentration.

which passes through the origin for all two catalysts. This confirms first order dependence of rate on catalyst concentration and it also shows that there is no reaction in the absence of catalyst. Similarly, the dependence of rate on maleic anhydride concentration was determined by varying its concentration while keeping all other variables constant. k_{obsd} is directly proportional to the con centration of maleic anhydride in case of all the two catalysts used. This is an indicative of first order dependence of rate on maleic anhydride concentration. The results are presented in Table 2.

Table 2. First Order Dependence of Epoxidation Rate on Maleic Anhydride Concentration

[Maleic anhydride] $\times 10^2$ (M)	kobsd $\times 10^7$ (mol lit^{-1} sec^{-1})	
	Sodium tungstate	Sodium molybdate
20.00	5.25	3.49
30.00	8.20	5.02
40.00	10.51	6.84
50.00	13.54	8.41
60.00	15.87	10.23

[Catalyst] $= 10.00 \times 10^{-4}$M; [H_2O_2] $= 3.00 \times 10^{-3}$M Temp., 50°C; pH, 6.0

In aqueous solutions of tungstate and molybdate gave acid anions by the following equation:

$$MO_4^{2-} + H_2O \rightleftharpoons HMO_4^- + OH^- \quad (1)$$

Where, M is W or Mo.

Preliminary studies have shown that under our experimental conditions, hydrogen peroxide does not bring about epoxidation of maleic anhydride without the catalyst and the catalyst alone (without hydrogen peroxide) as well fails to bring about the epoxidation. These observations suggest that hydrogen peroxide oxidises acid anions into peroxyacid anions which then bring about the epoxidation.

$$HMO_4^- + H_2O_2 \rightarrow HMO_5^- + H_2O \quad (2)$$

It has been reported earlier [27] that the concentration of acid anions are pH dependent. HWO_4^- is maximum around pH 4.7 and $HM_oO_4^-$ is maximum around pH 3.6. The epoxidation rates catalysed by tungstate or molybdate are maximum at the pH at which (HWO_4^-) or ($HMoO_4^-$) are maximum (Figs. 2 and 3).

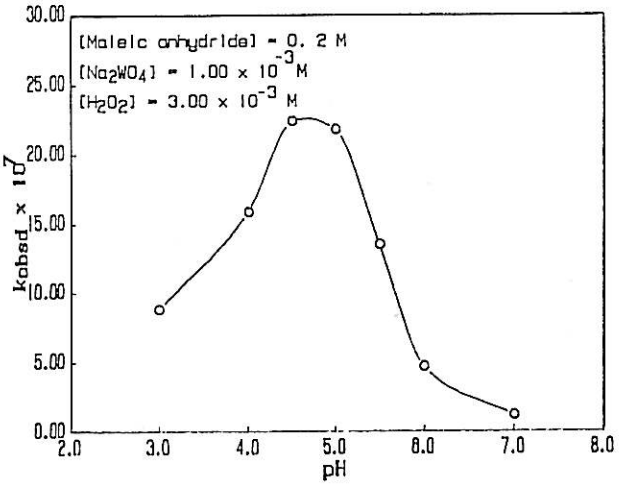


FIG. 2. Tungstate catalyzed epoxidation rate dependence on pH of the medium.

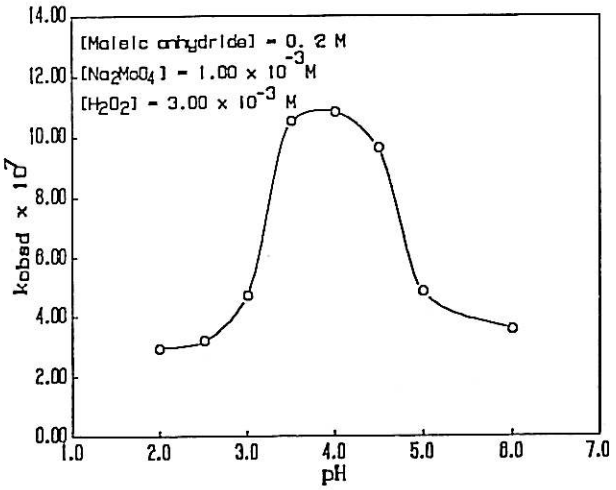


FIG. 3. Molybdate catalyzed epoxidation rate dependence on pH of the medium.

This clearly suggests that the peroxyacid anions are the expoxidizing agents. The most probable mechanism is as follows:

$$MA + HMO_5^- \underset{k2}{\overset{k1}{\rightleftharpoons}} \text{(intermediate complex)} \quad (3)$$

$$\text{(intermediate complex)} \xrightarrow{k3} MAO + HMO_4^- \quad (4)$$

$$\text{Rate of reaction} = k3\ \text{(intermediate complex)} \quad (5)$$

Applying steady-state approximation of the concentration of intermediate complex, we get,

$$k1[MA][HMO_5^-] - k2\ \text{(intermediate complex)} - k3\ \text{(intermediate complex)} = 0 \quad (6)$$

$$\text{or (intermediate complex)} = \frac{k1[MA][HMO_5^-]}{k2 + k3} \quad (7)$$

where MA represents maleic anhydride.

Substituting the concentration of intermediate complex in eqn. 5, we get,

$$\text{Rate of reaction} = k[MA][HMO_5^-] \quad (8)$$

Where,

$$k = \frac{klk3}{k2+k3}$$

since the formation of peroxyacid anions from acid anions is assumed to be instantaneous and complete, eqn. (8) can be written as:

$$\text{Rate of reaction} = k'[MA][Na_2WO_4 \text{ or } Na_2MoO_4] \quad (9)$$

This explains the order of reaction with respect to maleic anhydride, catalyst and hydrogen peroxide. Hence,

$$\text{Rate of reaction} = k_{obsd} \quad (10)$$

Where,

$$k_{obsd} = k'[MA][Na_2WO_4 \text{ or } Na_2MoO_4] \quad (11)$$

Figure 1 shows that among the two catalyst system investigated, the tungstate is the superior catalyst for the epoxidation of maleic anhydride. This may be a reflection of the fact that the formation of the reactive peroxyacid anion of tungstate in situ is comparatively larger, since within the same group of Periodic Table, the stability of peroxyacid anion increases with increasing atomic weight [28]. The proposed transition state of the reaction is shown in Fig. 4.

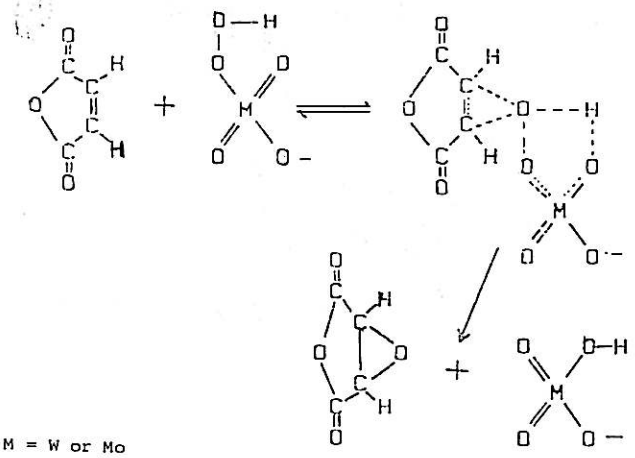


FIG. 4. Mechanism of epoxidation reaction.

ACKNOWLEDGEMENT

The authors are thankful to the management of Petroleum Research Centre for providing facilities to conduct this work.

REFERENCES

[1] Lefort T.E., U.S. Patent Reissues, 20370, 18 May 1937; 22241, 29 December 1942.
[2] Seree I.-Deroch *Bull. Soc. Chi., Fr.*, 1979 (1966).
[3] Weinstein, S. and Henderson, R.D., 1950, Heterocyclic Compounds, Vol. I, edited by R.C. Elderfield, Wiley, New York, pp. 1.
[4] Popescu A. and Croc N., 1967, *Studii Cercetari Chim.*, 15,909.
[5] Takagi T. and Kobayshi M., 1967, Kogyo Kagaku Zasshi, 70,1446.
[6] Takagi T, 1967., *J. Polymer Sci.*, B5, 1031.
[7] Payne G.B., 1959, Fifth Petroleum Congress Proceedings, New York N.Y., Section IV, Paper 16, pp. 185.
[8] Jochsberger T. Miller D., Herman F. and Indicator, 1971, *J. Org. Che.*, 36,4078 (1971).
[9] Howe G.R. and Hiatt R.R., 1971, *J. Org. Chem.*, 36,2493.
[10] Sheng M.N. and Zajacek J.G., 1968, *Adv. Chem. Ser.*, 76,481.
[11] Su C., Reed J.W. and Gould, R.S., 1973, *Inorg. Chem.*, 12,337.
[12] Gould E.S., Hiatt R.R. and Irwin K.C., 1968, *J. Amer. Chem. Soc.*, 90,4573.
[13] Allan G.G., 1964, U.S. Patent, 3156709; 10 Nov.
[14] Mugdan M. and Young D.P., 1949, *J. Chem. Soc.*, 2988.
[15] Raciszewski Z., 1960, *J. Amer. Chem. Soc.*, 82,1267.
[16] Stevens H.C. and Kaman A.J., 1965, *J. Amer. Chem. Soc.*, 87,734.
[17] Sapunov V.M. and Lebedev N.N. 1966, *Zh. Org. Khim.*, 2,272.
[18] Hatch L.F. and Matar S., 1981. From Hydrocarbons to Petrochemicals, Gulf. Pub. Co., pp. 144.
[19] Bavley A. and Knuth C.J., 1961, U.S. Patent, 2972595, Feb. 21.
[20] Campbell, T.W. and McDonald R.N., 1963, *J. Polymer Sci.*, Part A. 1,2525.
[21] Lucas H.J. and Pressman D., 1938, *Ind. Eng. Chem., Anal. Ed.*, 10,140.
[22] Kolthoff I.M., Sandell E.B., Meehan E.J. and Stanley B., 1969, in "Qualitative Chemical Analysis", 4th Ed., pp. 834, Macmillan Co. Collier Macmillan Ltd., London.
[23] Reichert J.S., McNeight S.A. and Rudel H.W., 1939, *Ind. Eng. Chem., Anal Ed.*, 11,194.
[24] Jungnickel J.L., Peters E.D., Polgar A., Weiss F.T., Proskauer E.S. and Weissberger A., 1953, *Organic Analysis*, Wiley (Interscience), New York, Vol. I, pp. 136.
[25] Perkin M.F., 1924, "Qualitative Chemical Analysis", Longmans, Green and Co., New York, N.Y., pp. 219.
[26] Buchan J.C., Dekkar C.A. and Long A.G., 1950, *J. Chem. Soc.*, 3162.
[27] Beg M.A. and Ahmad I, 1975, *J. Catal.*, 39,260.
[28] Melikoff P. and Jelhchaninoff E., 1909, *Chem. Ber.*, 42,2291.

PRJ, Vol. 3 (January 1991); P. 57–62, 9 FIGS, 1 TABLE.

Short Note

SENSITIVITY OF PIPE-LINE STEELS TO HYDROGEN INDUCED CRACKING

Adam Mazur*, Tarek Militti* and Khalifa Abosowa*

حساسية الفولاذ الكربوني للهيدروجين المسبب للتشققات

د. آدم مازور، طارق المليتي، خليفة أبوصوة

تم اختبار عدة أنواع من الفولاذ الكربوني الذي سبق أن تعرض لغاز كبريتيد الهيدروجين المبلل ووجد أن هذا الفولاذ له استجابة للهيدروجين المسبب للتشققات.

بينت الإختبارات الميثالوغرافية وجود عروق من الفسفور وأن الهيدروجين المسبب للتشققات له علاقة بعرض العروق الفسفورية.

INTRODUCTION

According to the technical literature and experience, pipe-steels of the same grade working in almost the same environment containing H_2S have a different sensitivity to hydrogen induced cracking (HIC). Reaction of the wet hydrogen sulfide with iron produces the hydrogen atoms which can be easily absorbed by the iron matrix due to their small diameter and high coefficient of diffusivity at the ambient temperature. In some places as for instance interphase boundaries (Steel matrix-nonmetallic inclusions), the hydrogen atoms are recombining into molecules creating pressure in these sites. After a sufficient pressure build-up in these places, the blisters and stepwise cracks are observed [1]. Sensitivity of pipe-steels to HIC depends on many factors; namely chemical composition, metallurgical and environmental variables [2]. Presence of impurities like sulphur and phosphorous are known to affect the properties of steel adversely if they are not controlled. Presence of MnS inclusion in elongated shape [2] plays a major role in the initiation of HIC.

Effect of sulphur on HIC in steels has been extensively reported in the literature while that of phosphorous on HIC is hardly known. The present note reports some preliminary observations on the effect of phosphorous on HIC.

RESULTS AND DISCUSSION

Hydrogen Induced Cracking (HIC)

The samples were taken from three pipe-lines made of A53 steel grade of chemical composition listed in Table 1. Pipe (D) had 20 inch of diameter, pipes (P) and (E) were 30 inch diameters. Each pipe

Table 1. Chemical Analysis of the Three Steel Pipes

PIPE	CONTENT %									
	C	Mn	Si	S	P	Almet	Cr	Ni	Cu	V
(P)	0.22	1.20	0.37	0.029	0.046	0.02	0.06	Nil	N.T.	Nil
(E)	0.20	1.21	0.30	0.014	0.032	0.04	0.06	Nil	N.T.	Nil
(D)	0.23	0.90	0.35	0.033	0.054	N.T.	0.02	0.0075	0.015	N.T.

N.T. = Not Tested.

*Petroleum Research Centre, P.O. Box 6431, Tripoli, G.S.P.L.A.J.

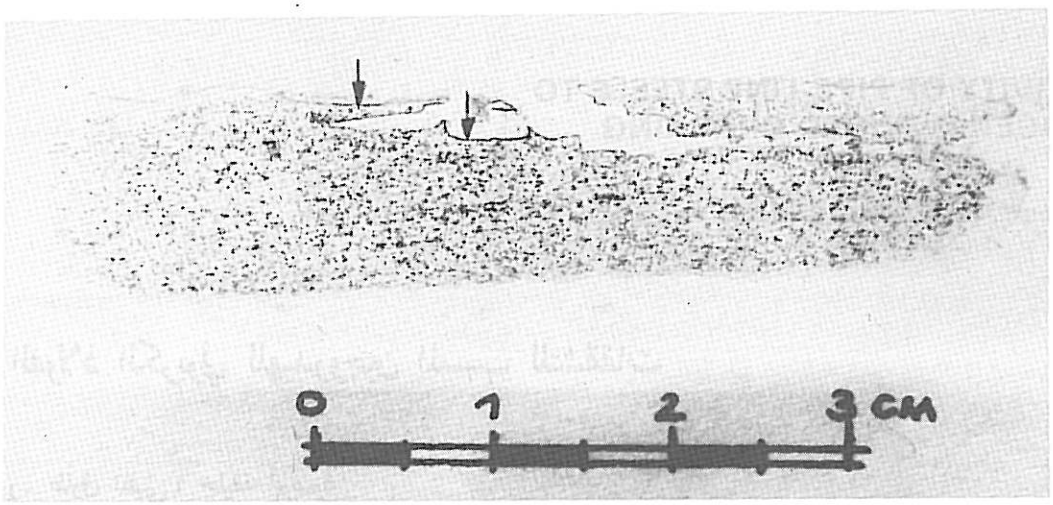


FIG. 1. Sulphur print made from the specimen of steel (P).

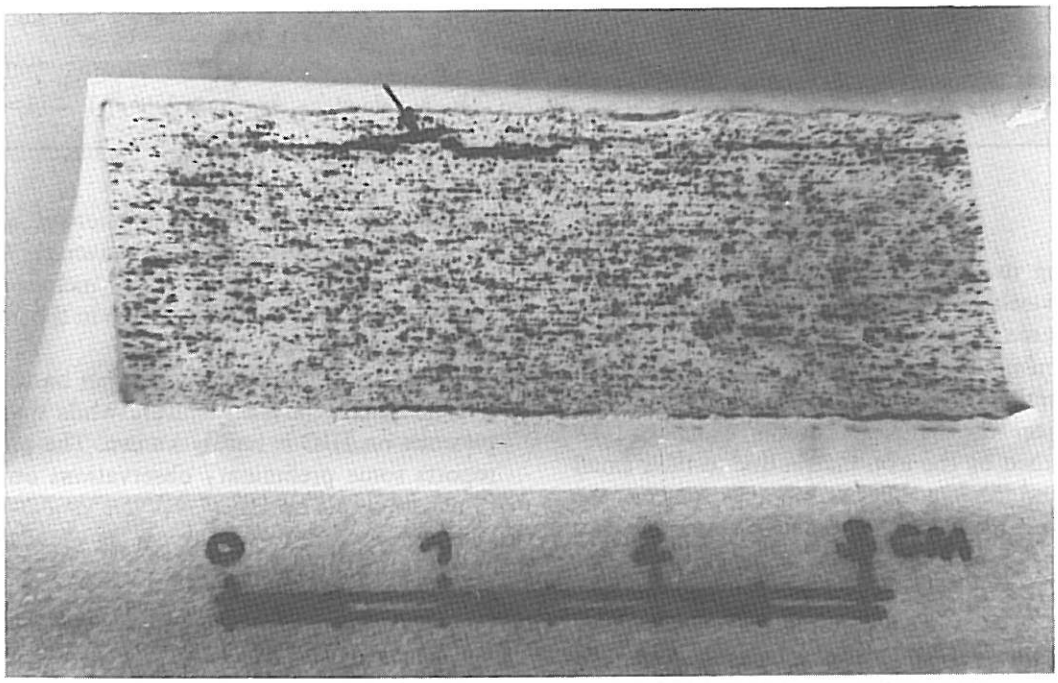


FIG. 2. Sulphur print of Steel (P) with stepwise crack. Dark deposit marked by arrow indicates that the crack had a direct contact with H_2S.

has been in sevice for about 17 years carrying a natural gas containing H_2S in amounts ranging from 500 ppm up to a few thousand ppm depending on the service period and operational circum-stances. The highest concentration up to 1040 ppm of H_2S has been found in pipe (E). The average pressure of the natural gas flowing through all these pipes was about 500 psi.

From each pipe the longitudinal specimens were taken for macro- and micro-observations. All specimens of pipe (P) exhibited many open blisters and inner cracks of lamination type; some of them formed the step wise cracks. Macro-sulphur print in Fig. 1 shows the cracks in the pipe-wall opened in the inner pipe surface. Figure 2 shows sulphur print with stepwise crack situated close to the inner pipe surface. The dark spots indicate the places occupied by non-metallic inclusions (Mn, Fe)S as impurities inherited after metallurgical processing. Black de-posit (FeS) along the cracks (See arrows in Fig. 1 and Fig. 2) are the product of reaction between wet H_2S environment and inner pipe surface. Cathodic reaction is hydrogen ion reduction as illustrated below:

$$\begin{array}{ll} Fe \rightarrow Fe^{++} + 2e^- & \nearrow H + H \rightarrow H_2 \\ H^+ + e^- \rightarrow H \text{ adsorbed} & \longrightarrow H \text{ adsorbed by steel} \end{array}$$

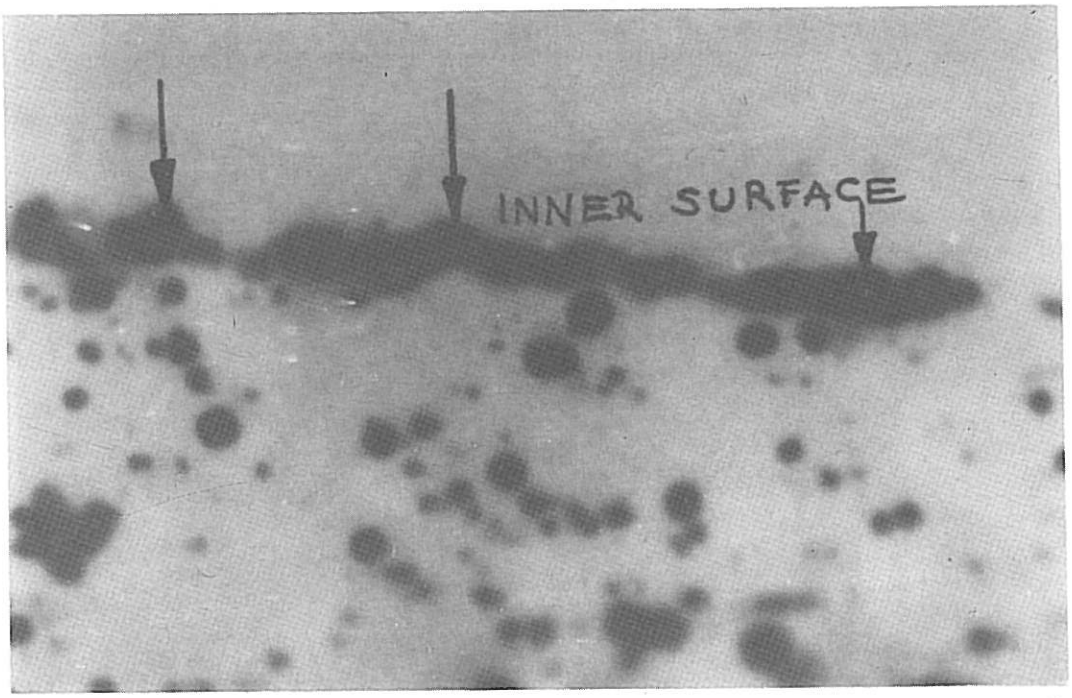


FIG. 3. FeS deposited at the pipe inner surface due to the reaction between H_2S and Fe. Sulphur print magnified 63×.

Part of the hydrogen atoms is absorbed by steel and can diffuse into the iron matrix producing hydrogen induced cracks (Blisters or stepwise cracks), the rest of the atoms recombine into molecules and flow away with the gas stream. This deposit, along the inner surface of the pipe, is shown after magnification in Fig. 3. Samples taken from pipe (E) did not exhibit hydrogen induced cracks in spite of the highest H_2S content in the gas.

Macrophotographs and macro-sulphur prints of samples taken from the pipe (D) are shown in Fig. 4. They are visible in cross-sections with stepwise cracks (see arrows) without black deposit that indicates no direct contact of the cracks with the pipe inner surface.

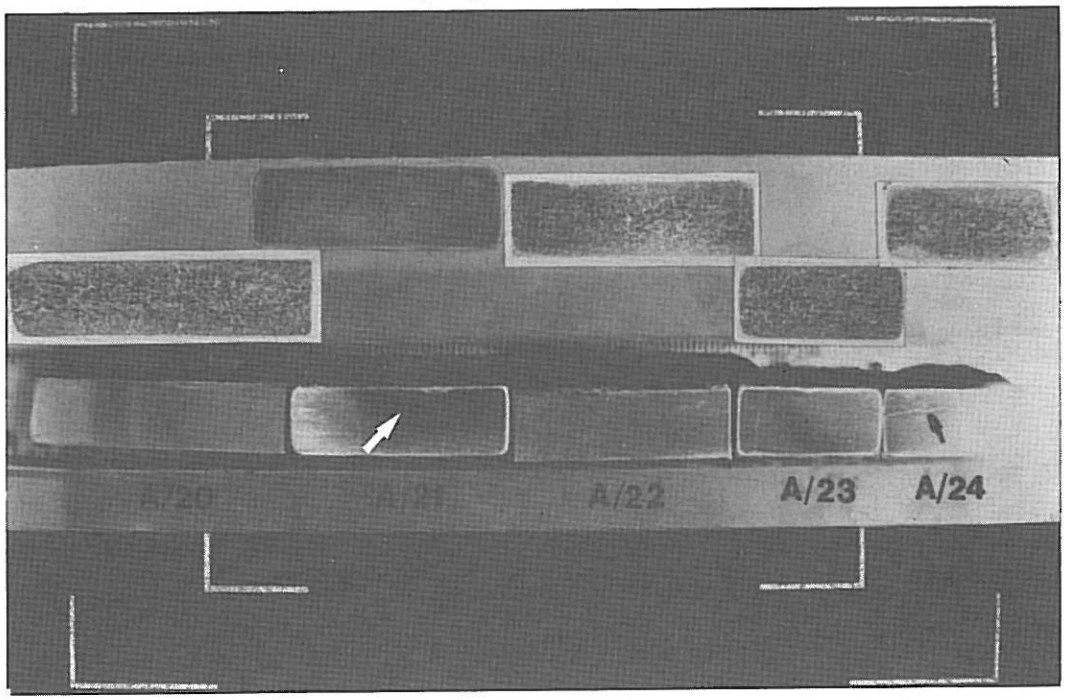


FIG. 4. Samples of A series cut from pipe of (D) type. The arrows are showing stepwise cracks in the section A/21 and A/24. Sulphur prints are showing the (Fe, Mn) S distribution in the cross-section.

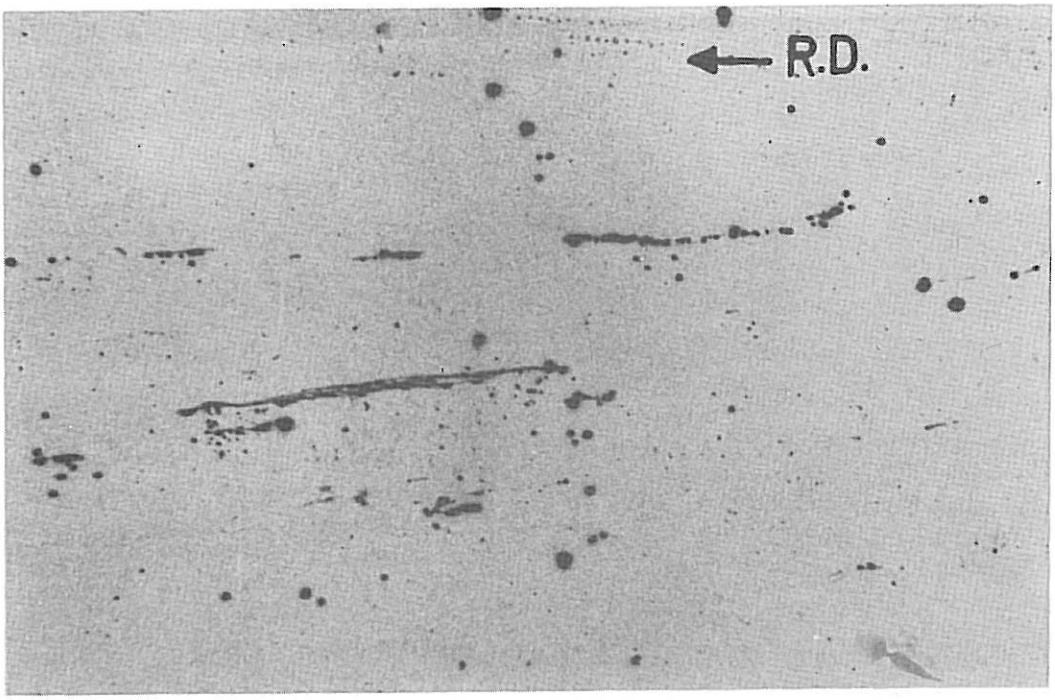


FIG. 5. Elongated non-metallic inclusions due to high deformation stage due to hot rolling. Magnification 130×.

The above observations have revealed a different sensitivity of tested pipes to hydrogen induced cracking. The relationship between phosphorous segregation and the hydrogen induced cracking (HIC) concept has been used, as a hypothesis explaining the above obsevations.

Phosphorous Segregation and HIC

Phosphorous segregation in steel can be easily revealed by using one of the well known etching techniques [3]. For this study Stead's and Oberhoffer's reagents have been used to get better reproducibility of etching results.

The steels used for pipe production have been hot rolled. This operation produced high directionality of structural constituents and non-metallic inclusions. Fig. 5 shows the nonmetallic inclusions elongated towards rolling direction (RD). Similarly, the segregation areas are elongated and form the bands shown for steel (E) in Fig. 6.

The distance between the enriched phosphorous band



FIG. 6. Phosphorous segregation bands following the direction of plastic deformation in steel (E) Steads reagent. Magnification 63×.

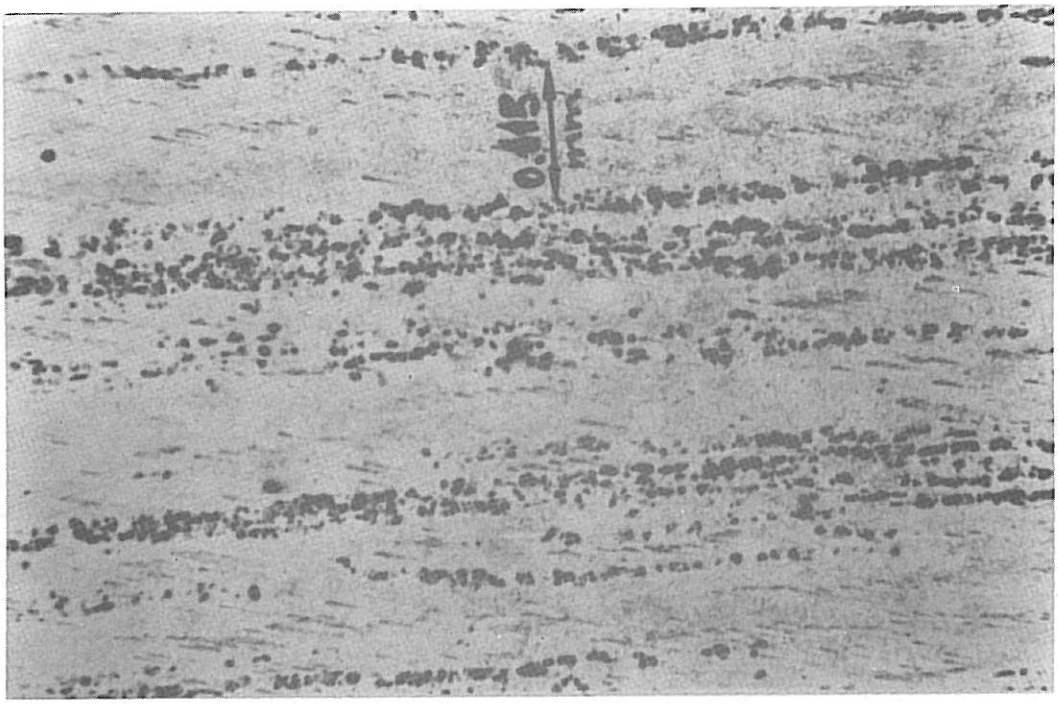


FIG. 7. Phosphorous bands of 0.115 mm of average width (light colour) in steel (P) Stead's reagent. Magnification 130×.

(light colour) and the depleted one (dark colour) for this steel is 0.03 mm. This steel was not sensitive to HIC. Fig. 7 shows for comparison the 0.115 mm wide enriched phosphorous bands in steel (P) that exhibited a great deal of HIC.

The stepwise cracks propagated usually along a wide 0.2 mm band enriched by phosphorous white (or light) bands (see Fig. 8). In the 0.25 mm wide band the stepwise cracks are propagating following the "rolling direction". Fig. 9 shows the two stepwise cracks following wide phosphorous band approaching the area in which 0.3 mm wide segregation bands became narrow and unfavourable for further crack propagation (see arrows). Extremly high forces developed at both crack tips produced deformation of the metallic fibers between these cracks. The above examples illustrate the fact that at the microscale in steel (D) the phosphorous segregation has changed from very

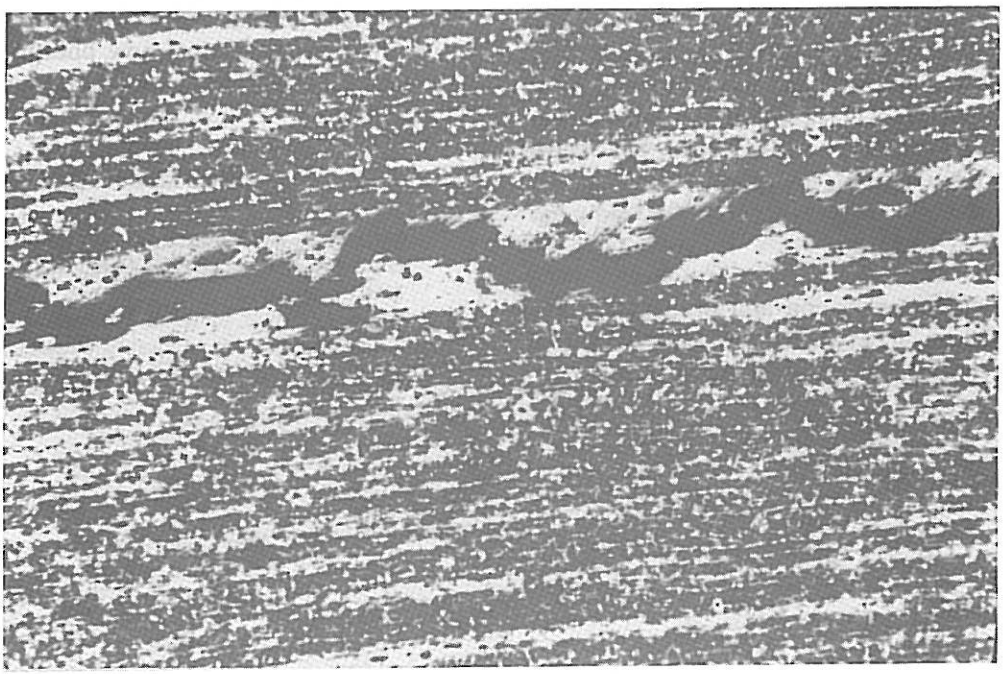


FIG. 8. Stepwise cracks in the 0.25 mm wide phosphorous band. Oberhoffer's reagent. Magnification 130×.

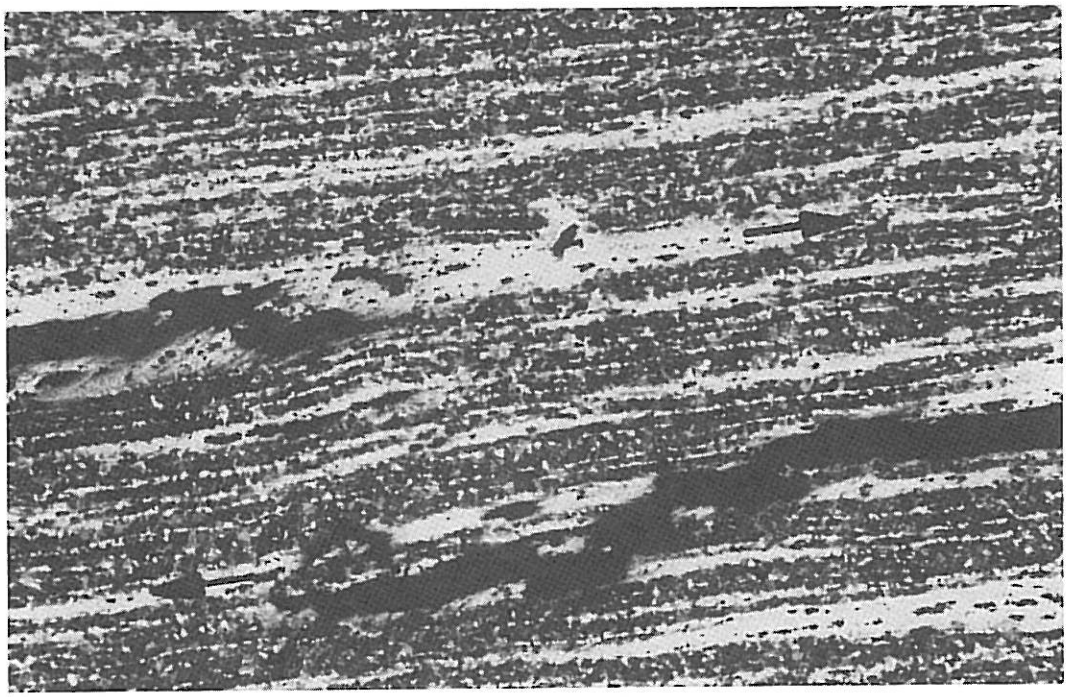


FIG. 9. The situation in the area where two stepwise cracks are arrested due to narrowing (see arrows) the phosphorous bands. Note a plastic deformation of the structure between both cracks ends. Oberhoffer's reagent. Magnification 63 ×.

wide enriched in phosphorous bands, in which many of stepwise cracks have been originated, to very narrow one in which stepwise cracks could not propagate. Probably, the high phosphorous content in this steel exceeded 0.05%, and the uncontrolled solidification process caused such complicated mode of phosphorous segregation and high susceptibility to stepwise cracking of the steel (D). All samples exhibited phosphorous bands wider than 0.1 mm. The steel (P) should be placed in the area of bands over 0.1 mm (measured average band was 0.115 mm). Steel (E) in which stepwise cracks have not been found exhibited bandwidth of about 0.03 mm. The rough estimation of the critical phosphorous segregation bandwidth gave the values between 0.03 mm and 0.1 mm. If the bands are below 0.03 mm the steel should not be sensitive to HIC. The steel is very sensitive to cracks nucleation and propagation due to the presence of H_2S in the natural gas if the phosphorous bands are wider than 0.1 mm.

CONCLUSIONS

(i) Results of metallographic study suggest that sensitivity of low carbon pipe-steel to HIC depends on phosphorous segregation in the pipe-wall cross-section.

(ii) It is believed that if the phosphorous band by width is below 0.03 mm the sensitivity is very small. Over 0.1 mm, the sensitivity is very high.

(iii) The mechanism of how phosphorous segregation affects HIC is not clear and further investigation is needed.

REFERENCES

[1] Tuttle R.N. and Kawe R.D. (Eds), 1981, H_2S Corrosion in Oil and Gas Production, A Compilation of Classic Papers, NACE publication.

[2] Briefer G.J., 1982, Materials Performance, Vol. 21, No. 6.

[3] Kehl G.L., 1949, The Principles of Metallographic Laboratory Practice: McGraw-Hill Book Co.

PRJ, Vol. 3 (January 1991); P. 63–67, 13 FIGS, 2 TABLES.

Short Note

THE ATMOSPHERIC CORROSION OF AUSTENITIC STAINLESS STEEL PNEUMATIC TUBING SYSTEM IN AN OFFSHORE ENVIRONMENT

M.L. Mehta* and K. Abosowa*

ظاهرة تآكل وحدات التشغيل من الفولاذ الأستينيتي 316 في بيئة بحرية

د. م. مهتا ، خليفة أبوصوة

أنابيب وحدات التشغيل قطر 0.25 بوصة من الفولاذ الاستينيتي 316 المستعملة في بيئة بحرية صنفت إلى مجموعتين من حيث المظهر الخارجي لهذه الأنابيب وشدة التآكل. وجد أن معدل التآكل في المجموعة الأولى كان أكثر فاعلية من المجموعة الثانية.
التحليل الكيميائي للعينات أكد أن نوعية المعدن هو الفولاذ الاستينيتي 316. تم معرفة أسباب التآكل واقترحت الحلول المناسبة.

INTRODUCTION

Leaks were reported in the pneumatic stainless steel tubing after about two years in service. The surface of the tubing was exposed to off-shore environment. The tubing system is used for instrumentation purpose. It is reported that the tubing material as per specification is 316 austenitic stainless steel.

OBJECTIVES

(1) To investigate causes for the development of leaks.
(2) To determine chemical composition of the tubing material in order to establish whether the material is according to specificiation.
(3) To examine whether the material used is suitable for the environment encountered.

INVESTIGATION CARRIED OUT

1. Visual observation.
2. Metallographic examination.
3. Chemical composition.

*Petroleum Research Centre, P.O. BOX 6431, Tripoli, G.S.P.L.A.J.

Visual Observation

Among many tube samples received two of them were different in surface appearance and extent of attack. They were marked as ASTM A213 and TP316. These two samples (here after called set (2)) were dull in colour and were lightly pitted in comparison to set (1) of tubes which were bright in surface appearance and have suffered heavy localised corrosion in the form of crevice and pitting corrosion.

Tubes were exposed to marine atmosphere and degree of localized attack varied in different locations. Tube surfaces were in contact among themselves as well as contacting the surface of holding channels. Presence of pollutants such as traces of H_2S in the platform environment appears to exist.

Metallographic Examination

(A) First Set of Tubes

Macroscopic examination:

Localized attack did not take place over the whole tube surface but was confined to a narrow band in the longitudinal direction as illustrated in Figs. 1, 2. Such morphology results from crevice corrosion. Scattered pits as in Fig. 3 were also seen. Figure 4 shows a ring around a cluster of pits indicating the existence of a deposit over these pit sites, which had come off. Figure 4a reveals the growth of adjacent

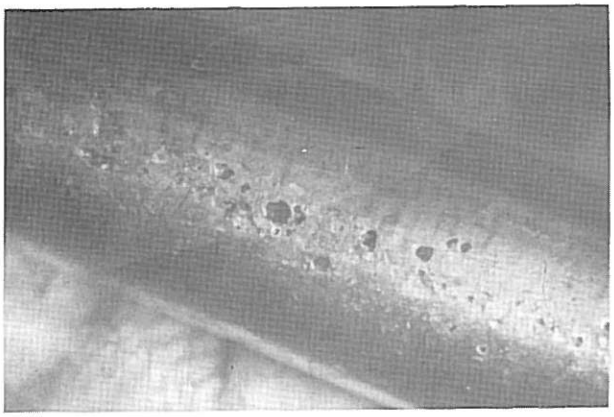


FIG. 1. A band of pits resulting from crevice corrosion × 6.

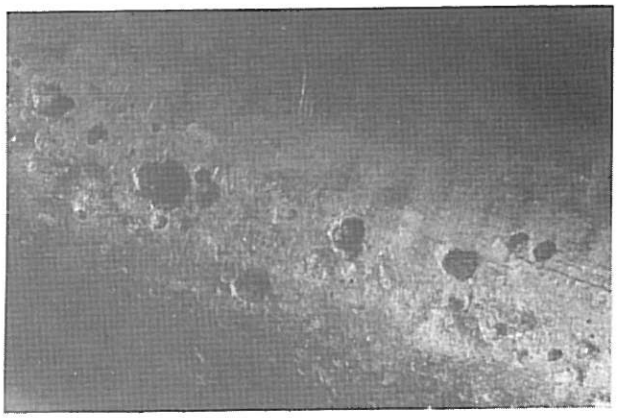


FIG. 2. Another area showing crevice corrosion × 12.

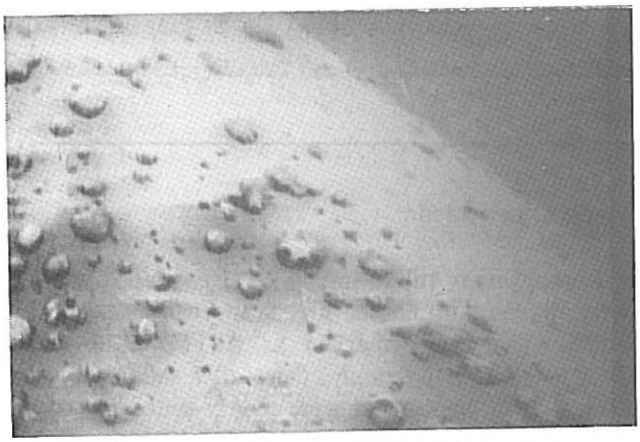


FIG. 3. Scattered pits and particles deposited on tube surface × 64.

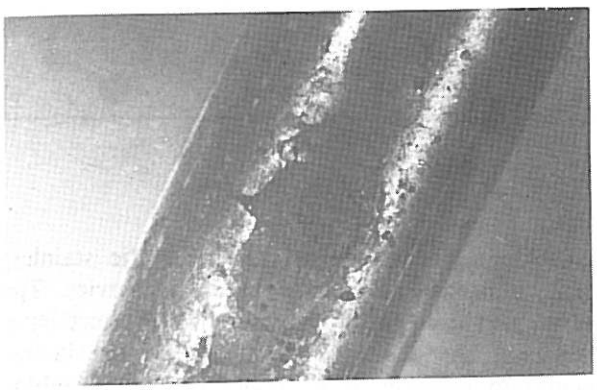


FIG. 4. A ring around a cluster of pits × 6.

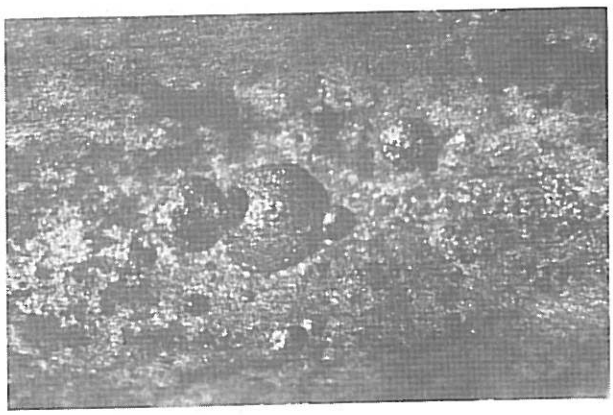


FIG. 4a. Growth of adjacent pits leading to a large pit × 12.

pits till they emerged into one another leading to large pits. Figure 5 illustrates pits under the particle deposits on the tube surface.

Microscopic examination:

This was carried out in the transverse section of the pitted region of the tube. Figure 6 shows the undercut appearance of a pit indicating typical chloride attack. The pit has penetrated about 4/5 of the wall thickness. Figure 7 illustrates another morphology (open pit). Figure 8 shows a pit in the cross-section of the tube which penetrated at an angle to the tube surface. Microstructure was examined in the transverse section of the tube. Figure 9 shows that the tube was not seamless, but it was fabricated through fusion welding and the structure of weld was

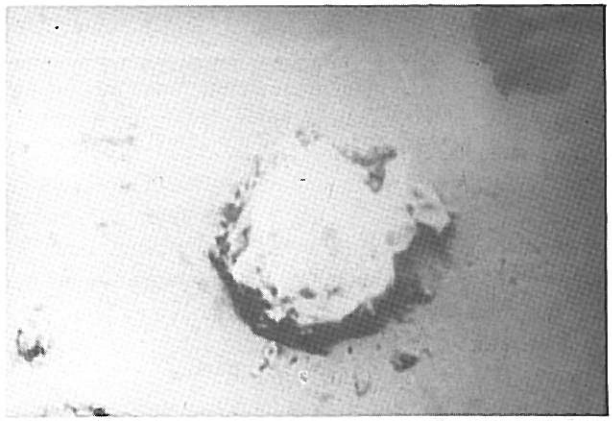


FIG. 5. A pit under the particle deposit × 124.

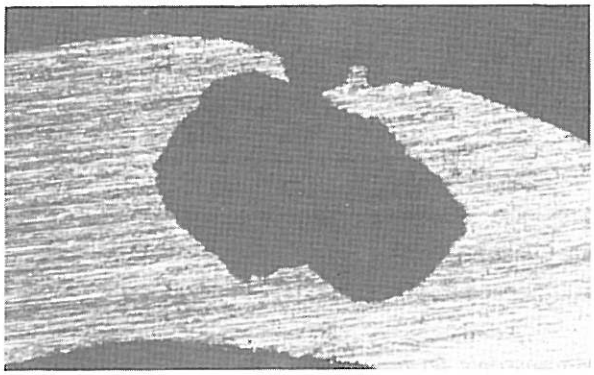


FIG. 6. Under-cut pit typical of chloride attack × 65.

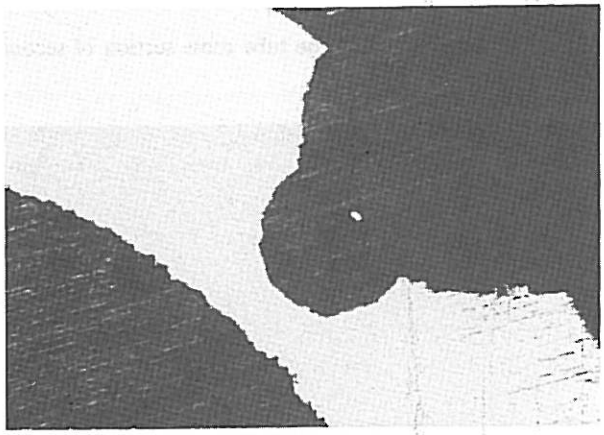


FIG. 7. An open pit × 65.

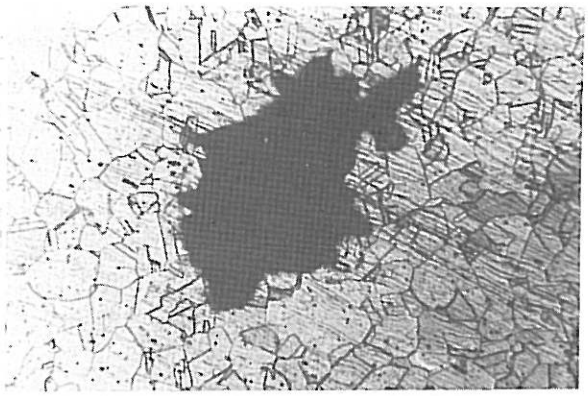


FIG. 8. A pit in the tube cross section × 260.

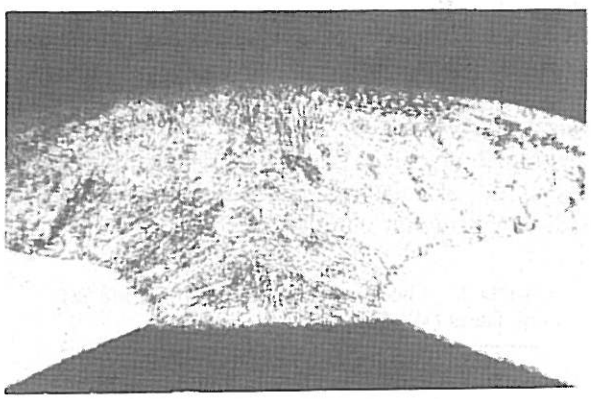


FIG. 9. Fusion weld having dendrite structure × 65.

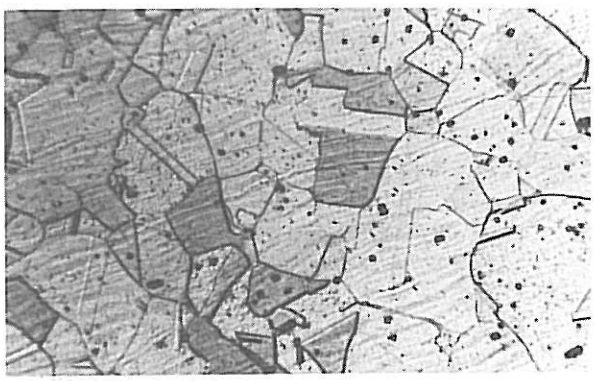


FIG. 10. Microstructure showing grain structure, annealing twins, second phase precipitates and deformation markings × 520.

dendritic. The structure of the base metal as seen in Fig. 10 consists of equiaxed grains, annealing twins, second phase particles and tube has been subjected to slight cold deformation as evident from the presence of deformation markings due to slip.

Chemical Composition:

Table 1 gives the chemical composition of the first set of tube material which corresponds to AISI 316 austenitic stainless steel.

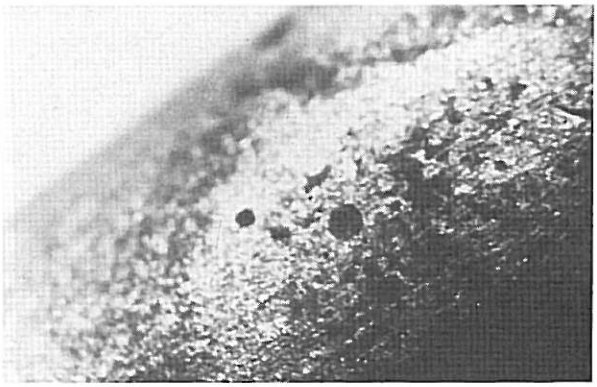
2Table 1. Chemical Composition of First Set of Tubes (Wt. %)

Cr	Ni	Mo	Mn	C
18.5	12.2	2.74	1.71	0.04

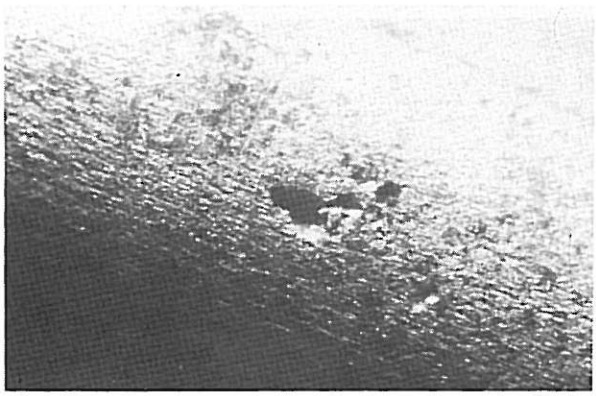
(B) Second Set of Tubes

Macroscopic Examination:

Mild pitting was observed on tubing surface as illustrated in Fig. (11a,b) and had random distribution.



a.



b.

FIG. 11a,b. Show pits in the tube surface of second set of tubes × 6.

Microscopic Examination:

Many cross-sections were examined and only a few shallow pits were seen. Figure 12 shows the undercut pit which penetrated only 1/20 of the wall thickness. Unlike first set of tubing second set of tubing was seamless.

Microstructure consists of equiaxad grain structure showing twining and presence of second phase particles as seen in Fig. 13; quantity being much less than that detected in the first set of tubes.

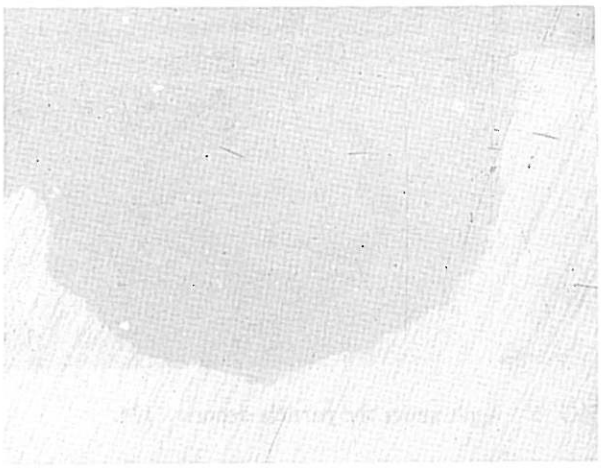


FIG. 12. Shallow pit in the tube cross section of second set of tubes × 130.

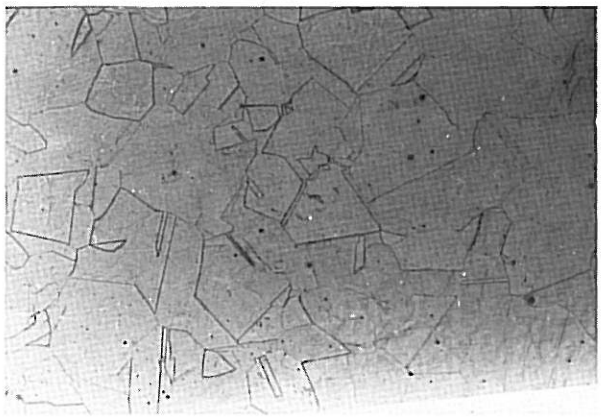


FIG. 13. Microstructure showing less quantity of second phase precipitates × 400.

Chemical Composition:

Table 2 gives the chemical composition of the second set of tube material which corresponds to AISI 316 austenitic stainless steel.

Table 2. Chemical Composition of Second Set of Tubes (Wt. %)

Cr	Ni	Mo	Mn	C
19.1	13.1	2.3	1.2	0.051

DISCUSSION

The present study reveals that the first set of bright tubing, AISI 316 austenitic stainless steel, shows poor resistance to crevice and pitting corrosion in the marine atmosphere, while the second set, also AISI 316 austenitic stainless steel, was also susceptible to pitting corrosion but the extent of pitting was far less.

Localisation of crevice attack to one side of the tubes suggests that the tubes remained in contact with other tubes/holding channels. This contact areas remain shielded from the supply of oxygen creating differential aeration corrosion cells. Salt deposited on the tube surface from marine atmosphere accelerates corrosion activity in corrosion cell [1], causing local break-down of passive film leading to crevice and pitting corrosion.

The difference in behaviour of the two sets of tubes may be due to surface treatment given to the second set of tubing imparting more resistance to pitting corrosion. Further, presence of higher amount of second phase particles as seen in the micro-structure of first set of tubing increases pit initiation [2].

CONCLUDING REMARKS

It is known that 316 austenitic stainless steel does not possess adequate resistance to crevice and pitting corrosion in stagnant chloride bearing aqueous environment. This is also the case in the present study also where tubing surfaces are exposed to marine environment in which a stagnant film of chloride bearing aqueous environment forms on the tube surfaces.

REFERENCES

[1] Mattsson E., 1982, Material Performance; Vol. 21, No 1.
[2] Smialowskal Z.S., 1986, Pitting Corrosion of Metals: NACE, Houston, p. 93.